Università Politecnica delle Marche
Scuola di Laurea Magistrale di Ricerca in Scienze dell’Ingegneria
Curriculum in (specifico nome dell’indirizzo)

What Does the Land - Mediterranean Basin Climate Look Like at 2°C Warming?

Master dissertation of:

Mia Štulić

Advisor:

Prof. Giorgio Passerini

Curriculum supervisor:

Dr. Umberto Rizza

Ancona, 2024.

Università Politecnica delle Marche
Scuola di Laurea Magistrale di Ricerca in Scienze dell'Ingegneria
Curriculum in (nome dello specifico indirizzo)

What Does the Land - Mediterranean Basin Climate Look Like at 2°C Warming?

Master Dissertation of:

Mia Štulić

Advisor:

Prof. Giorgio Passerini

Curriculum supervisor:

Dr. Umberto Rizza

Ancona, 2024.

Università Politecnica delle Marche
Dipartimento di (nome del dipartimento dove la tesi e' stata sviluppata)

Via Brecce Bianche — 60131 - Ancona, Italy

Acknowledgements

First and foremost, I would like to express my sincere gratitude to my advisors, Prof. Giorgio Passerini and Prof. Umberto Rizza, for their invaluable guidance, continuous support, and patience throughout the development of this thesis. Their expertise and encouragement have been essential in helping me complete this project. I wish to thank to entire Marche university staff for the exceptional communication between the students and the institution, the dedication of the professors and their desire to turn students into independent and skilled future engineers and scientists.

Secondly, I would like to give my thanks to the research and technical staff of the NASA NEX-GDDP-CMIP6 database for offering access to the climate model data used in this thesis, as well as the researchers who have studied this topic in the past, thus contributing to the development of the idea for this thesis.

Next, I would like to send my most sincere thanks to those without whom none of my ideas would have been realized, and that would be my family. First of all, thank you for teaching me that anything is possible if you try hard enough, and then for supporting me every time in my decisions, no matter how sudden and frightening they sometimes sounded, such as my move to Italy. To my mother and brother, thank you for being a solid rock to the fragile being that I am, and to my father for giving me an introduction to the profession I chose by connecting me with nature since I was a child. Furthermore, to the Zorić family, thank you for the crazy encouragement and belief, giving me a kick of self-esteem every once and a while. To Dominik, thank you for sharing the same emotions about moving, everyday problems, home-sickness, and many more for two years straight. Your contribution to my degree is unquestionable, thank you for all your selfless acts.

I would like to end my thanks by sending a lot of love to the entire city of Ancona, a city of open-hearted, cheerful and hard-working people who made me feel comfortable in my new environment. Thanks for every opportunity, I hope our story doesn't end here.

Abstract

The Coupled Model Intercomparison Project Phase six (CMIP6) models predict that, if global temperatures keep rising and reach 2 degrees Celsius (3.6 degrees Fahrenheit) above the baseline pre-industrial levels, people worldwide could face multiple impacts of climate change simultaneously, with serious consequences. The study of temperature changes is essential in order to determine and understand how different climate effects might combine. The objective of this master-thesis is to extrapolate the down-scaled climate projections (at 0.25° x 0.25°), provided by the NASA/NEX/GDDP data base on the Mediterranean basin, for the following five key climate variables: the mean near-surface air temperature (tas), precipitation (pr), near-surface relative humidity (hurs), surface downwelling radiation (shortwave: rsds, longwave: rlds). Four of the 35 available models participating to CMPI6, were used in this work to detect the crossing year in two different scenarios compared to the baseline temperature, namely: ACCESS-CM2, CESM2, GFDL-CM4 and EC-Earth3. The Shared Socio-economic Pathway (SSPs) scenarios considered in this study are SSP2-4.5 and SSP5-8.5. The first is an intermediate scenario, in which current climate change trends continue without substantial deviations, leading to a forcing pathway of 4.5 W m^{-2} by 2100 (Park, et al., 2023); the second scenario represents the upper boundary of the range of scenarios described in the

literature with an additional radiative forcing of 8.5 W m^{-2} by the year 2100. Also, the historical (1950-2014) background was used to easily determine the baseline temperature. This thesis, with the box analysis, will provide a time series of the 5 variables in seven selected locations in the Mediterranean Basin and it is going to highlight the urgent need for further studies focused on identifying the Mediterranean hotspots (Giorgi & Francisco, 2000). This may be helpful in suggesting region-specific actionable adaptation and mitigation plans. The baseline temperature over 7 locations was calculated, and it was 286.6750 Kelvin or 13.525 degrees Celsius. With the moving median method in MATLAB, we obtained 2026 as the crossing year for the SSP2-4.5 scenario, and 2025 for the SSP5-8.5 scenario.

Contents

List of Figures

Figure 6 Temperature anomalies time series with the moving median method in the Med Basin.

Figure 7. Time plots of five variables over Algeria; a) temperature anomalies for Algeria b) relative humidity anomalies for Algeria c) precipitation anomalies for Algeria d) surface downwelling shortwave radiation anomalies for Algeria e) surface downwelling longwave radiation anomalies for Algeria.

Figure 8. Time plots of each of five variables over Sardegna, Italy; a) temperature anomalies for Sardegna b) relative humidity anomalies for Sardegna c) precipitation anomalies for Sardegna d) surface downwelling shortwave radiation anomalies for Sardegna e) surface downwelling longwave radiation anomalies for Sardegna.

Figure 9. Time plots of five variables over Milano, Italy; a) temperature anomalies for Milano b) relative humidity anomalies for Milano c) precipitation anomalies for Milano d) surface downwelling shortwave radiation anomalies for Milano e) surface downwelling longwave radiation anomalies for Milano.

Figure 10. Time plots of five variables over Marche region, Italy; a) temperature anomalies for Marche region b) relative humidity anomalies for Marche region c) precipitation anomalies for Marche region d) surface downwelling shortwave radiation anomalies for Marche region e) surface downwelling longwave radiation anomalies for Marche region.

Figure 11. Time plots of five variables over Palermo, Italy; a) temperature anomalies for Palermo b) relative humidity anomalies for Palermo c) precipitation anomalies for Palermo d) surface downwelling shortwave radiation anomalies for Palermo e) surface downwelling longwave radiation anomalies for Palermo.

Figure 12. Time plots of five variables over Zagreb, Croatia; a) temperature anomalies for Zagreb, Croatia b) relative humidity anomalies for Zagreb, Croatia c) precipitation anomalies for Zagreb, Croatia d) surface downwelling shortwave radiation anomalies for Zagreb, Croatia e) surface downwelling longwave radiation anomalies for Zagreb, Croatia.

Figure 13. Time plots of five variables over Bari, Italy; a) temperature anomalies for Bari, Italy b) relative humidity anomalies for Bari, Italy c) precipitation anomalies for Bari, Italy d) surface downwelling shortwave radiation anomalies for Bari, Italy e) surface downwelling longwave radiation anomalies for Bari, Italy.

Figure 14. Time plots of five variables over all the domain used in this thesis, i.e. over the Mediterranean basin.

Figure 15. Climate differences Mediterranean map which includes all of 7 boxes of locations. Map a) is showing SSP5-8.5 scenario represents the upper boundary of the range of scenarios described in the literature with an additional radiative forcing of 8.5 W m-2 by the year 2100 (Park et al., 2023). In a map b) intermediate scenario, in which current climate change trends continue without substantial deviations, leading to a forcing pathway of 4.5 W m-2 by 2100 is shown.

Figure 16. The provided figure consists of two parts, each illustrating different aspects of temperature anomalies, best fit lines a) and their rates of increase b) in the Mediterranean region.

Figure 17. This figure consists of two panels illustrating the relative humidity anomalies (%) in the Mediterranean region for the baseline period (1950-1980) compared to the crossing year centered 30-year mean (2012-2042) under two different SSP (Shared Socioeconomic Pathway) scenarios: SSP5-8.5 and SSP2-4.5. Each panel shows the spatial distribution of these anomalies, with specific locations marked and their respective anomalies listed.

Figure 18. consists of two panels illustrating the relative humidity anomalies (%) in the Mediterranean region using modeled data and their rates of decrease over time; a) Best Fit Lines for Modeled Data, b) Rate of Decrease.

Figure 19. consists of two panels illustrating the precipitation anomalies (mm/year) in the Mediterranean region for the baseline period (1950-1980) compared to the crossing year centered 30-year mean (2012-2042) under two different SSP (Shared Socioeconomic Pathway) scenarios: SSP5-8.5 and SSP2-4.5. Each panel shows the spatial distribution of these anomalies, with specific locations marked and their respective anomalies listed.

Figure 20. consists of two panels illustrating precipitation anomalies (pr in mm/year) in the Mediterranean region using modeled data and their rates of decrease over time; a) Best Fit Lines for Modeled Data, b) Rate of Decrease.

Figure 21. consists of two panels illustrating the anomalies in surface downwelling shortwave radiation (rsds in W/m²) in the Mediterranean region for the baseline period (1950-1980) compared to the crossing year centered 30-year mean (2012-2042) under the SSP5-8.5 scenario.

Figure 22. consists of two panels illustrating the anomalies in surface downwelling shortwave radiation (rsds in W/m²) in the Mediterranean region using modeled data and their rates of increase over time; a) Best Fit Lines for Modeled Data, b) Rate of Decrease.

Figure 23. consists of two panels illustrating the anomalies in surface downwelling longwave radiation (rlds in W/m²) in the Mediterranean region for the baseline period (1950-1980) compared to the crossing year centered 30-year mean (2012-2042) under two different SSP (Shared Socioeconomic Pathway) scenarios: SSP5-8.5 and SSP2-4.5. Each panel shows the spatial distribution of these anomalies, with specific locations marked and their respective anomalies listed; a) SSP5-8.5 Scenario, b) SSP2-4.5 Scenario.

Figure 24. consists of two panels illustrating the anomalies in surface downwelling longwave radiation (rlds in W/m²) in the Mediterranean region using modeled data and their rates of increase over time; a) Best Fit Lines for Modeled Data, b) Rate of Decrease.

List of Tables

Chapter 1.

Introduction

1. Introduction

The climate of planet earth has changed in the last century, and the role of human influence on the climate is unquestionable (Masson-Delmotte et al., 2018). The Coupled Model Intercomparison Project Phase six (CMIP6: https://pcmdi.llnl.gov/CMIP6/) models show that the Earth likely will reach 2°C of global warming by the 2040s without significant policy changes (O' Neill et al., 2016). The 2°C target emerged from scientific consensus, particularly articulated by the Intergovernmental Panel on Climate Change (IPCC: https://www.ipcc.ch/). It may be seen as a threshold beyond which the risks posed by severe climate impacts, such as more frequent and intense heat waves, droughts, storms and sea-level rise increase substantially.

In the 2015 Paris Agreement, nations around the world committed to limiting global warming to well below 2°C above pre-industrial levels, aiming at 1.5°C. This agreement reflects a recognition of the need to avoid the most catastrophic impacts of climate change. Understanding future climatic changes and their spatial heterogeneity at 2°C warming is thus important for policy makers to prepare actionable adaptation and mitigation plans by identifying where and to what extent lives and livelihoods will be impacted (Park, et al., 2022).

This thesis will use the recently released NASA Earth exchange Global Daily Downscaled Projections (NEX-GDDP) CMIP6 data (https://www.nccs.nasa.gov/services/data-collections/land-based-products/nex-gddp-cmip6) to provide a box analysis of projected changes in the Mediterranean Basin for 5 key climate variables at a time when warming exceeds 2°C. The NEX-GDDP-CMIP6 dataset is comprised of global downscaled climate scenarios derived from the General Circulation Models (GCM) runs conducted under the Coupled Model Intercomparison Project Phase 6 (CMIP6) and across all four “Tier 1” greenhouse gas emissions scenarios known as Shared Socio - economic Pathways (SSPs). The CMIP6 GCM runs were developed in support of the Sixth Assessment Report of the Intergovernmental Panel on Climate Change (IPCC,AR6).

The NEX dataset includes downscaled projections from The Scenario Model Intercomparison Project (ScenarioMIP) model runs for which daily scenarios were produced and distributed with the purpose of providing a set of global, high resolution, bias-corrected climate change projections that can be used to evaluate climate change impacts on processes that are sensitive to finer-scale climate gradients and the effects of local topography on climate conditions. This dataset considers all 35 GCMs that have been utilized for the generating the CMIP6 climate projection as depicted in figure 1.

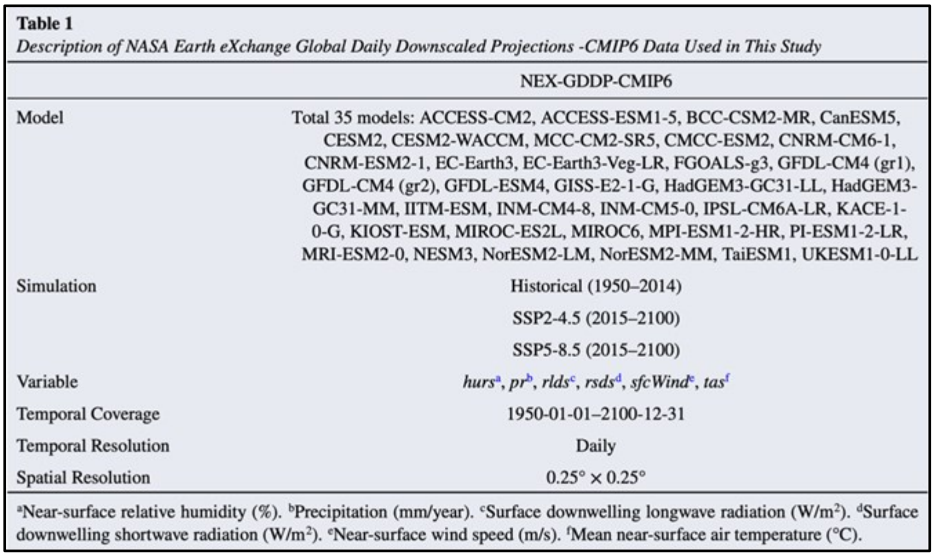

Table 1

Description of NASA Earth eXchange Global Daily Downscaled Projections -CMIP6 Data Used in This Study

	NEX-GDDP-CMIP6
Model	Total 35 models: ACCESS-CM2, ACCESS-ESM1-5, BCC-CSM2-MR, CanESM5, CESM2, CESM2-WACCM, MCC-CM2-SR5, CMCC-ESM2, CNRM-CM6-1, CNRM-ESM2-1, EC-Earth3, EC-Earth3-Veg-LR, FGOALS-g3, GFDL-CM4 (gr1), GFDL-CM4 (gr2), GFDL-ESM4, GISS-E2-1-G, HadGEM3-GC31-LL, HadGEM3-GC31-MM, IITM-ESM, INM-CM4-8, INM-CM5-0, IPSL-CM6A-LR, KACE-1-0-G, KIOST-ESM, MIROC-ES2L, MIROC6, MPI-ESM1-2-HR, PI-ESM1-2-LR, MRI-ESM2-0, NESM3, NorESM2-LM, NorESM2-MM, TaiESM1, UKESM1-0-LL
Simulation	Historical (1950–2014) SSP2-4.5 (2015–2100) SSP5-8.5 (2015–2100)
Variable	*hurs*[a], *pr*[b], *rlds*[c], *rsds*[d], *sfcWind*[e], *tas*[f]
Temporal Coverage	1950-01-01–2100-12-31
Temporal Resolution	Daily
Spatial Resolution	0.25° × 0.25°

[a]Near-surface relative humidity (%). [b]Precipitation (mm/year). [c]Surface downwelling longwave radiation (W/m^2). [d]Surface downwelling shortwave radiation (W/m^2). [e]Near-surface wind speed (m/s). [f]Mean near-surface air temperature (°C).

Figure 1. Description of NASA Earth global daily downscaled projections. Reproduced from Park et al., 2023.

Four of the 35 available models (Figure 1) were used in this paper to detect the crossing year in two different scenarios compared to the baseline temperature, namely: ACCESS-CM2, CESM2, GFDL-CM4 and EC-Earth3, each of these models are explained and referenced in the following Figure1. The Shared Socio-economic Pathway (SSPs) scenarios considered in this study are SSP2-4.5 and SSP5-8.5. SSP2-4.5 is an intermediate scenario, in which current climate change trends continue without substantial deviations, leading to a forcing pathway of 4.5 W m^{-2} by 2100 (Park, et al., 2022). SSP5-8.5 scenario represents the upper boundary of the range of scenarios described in the literature with an additional radiative forcing of 8.5 W m^{-2} by the year 2100. Box coordinate analysis, also known as bounding box analysis, is a method used to summarize and understand the distribution of data points within a defined area or "box" (Rizza et al., 2024). This technique is useful for various applications, including urban planning, environmental studies, and logistics. The area of interest is defined as a rectangular or square "box" on a map. This box can be aligned with natural or administrative boundaries. In this paper the analysis on a 1° squared box was applied.

The World Meteorological Organization considers a thirty-year period to be the minimum required to calculate the average climate, known as a climate normal. Climate normals are updated at the end of every decade (Rigal et al., 2019). According to that, in determining the baseline temperature in this thesis, an average over 31-year period over 7 locations was obtained. For the determination of the crossing year only the mean surface-air temperature (tas) variable was used. To determine the crossing year the data was normalized by coupling the multi model data, per scenario, to the historical data and recalculating the values using four different methods of which moving median method was chosen for further calculations.

Chapter 2.

Capitolo 2

2. Materials and methods

For the determination of the crossing year, only the mean surface-air temperature (tas) variable was used. A baseline temperature was compared with the yearly averaged, calculated on 7 locations and multi-model averaged Shared Socio-economic Pathways (SSP2-4.5 and SSP5-8.5) data (2015 - 2100), to determine the temperature anomaly across the timespan, and crossing year when the temperature anomaly reaches 2 °C (1.75 °C from our baseline period of 1950 - 1980) (Park, et al., 2022). To determine the crossing year the data was normalized by coupling the multi-model data, per scenario, to the historical data and recalculating the values using a moving median with a 30-year window, to add larger weights to older data within the window, to both minimize the effects of the increasing rate of heating and decreasing the modeled data's rising inaccuracy while going further into the future. Next in the paragraph, figure 2 presents the conceptual framework for analyzing climate projections in the Mediterranean Basin, focusing on several key components. It illustrates the use of multiple climate projection models, specifically ACCESS-CM2, CESM2, GFDL-CM4, and EC-Earth3, derived from the NASA NEX-GDDP-CMIP6 database. This study considers two Shared Socio-economic Pathway (SSP) scenarios—SSP2-4.5 and SSP5-8.5—alongside essential climate variables such as mean near-surface air temperature, relative humidity, precipitation, and surface downwelling radiation. Analysis is performed on seven representative locations within the Mediterranean, including Bou Saada (Algeria), Sardegna, Milano, Marche, Palermo (Italy), Zagreb (Croatia), and Bari (Italy). The outcomes of this analysis will highlight the crossing years for temperature anomalies and provide insights into how climate variables are expected to change in this region.

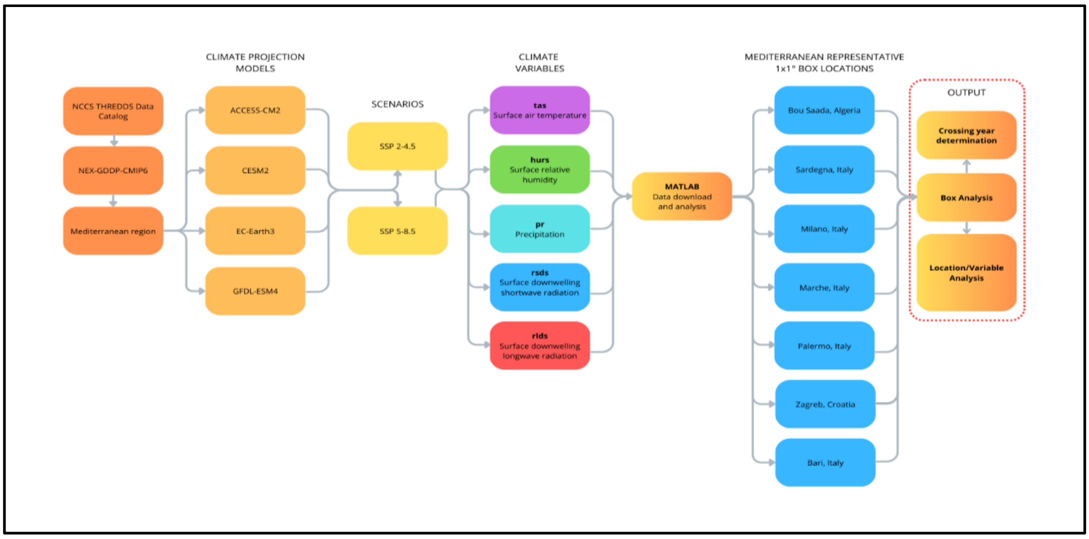

Figure 2. Flow-chart of the workflow.

2.1. NEX-GDDP CMIP6 data download with MATLAB

The NEX-GDDP-CMIP6 datasets offer downscaled climate projections derived from CMIP6 GCM simulations across four SSP scenarios: SSP1-2.6, SSP2-4.5, SSP3-7.0, and SSP5-8.5. With a spatial resolution of 0.25° × 0.25° (~ 25×25 km), these datasets provide high-resolution, bias-corrected, and seamless daily climate projections over land. The period covered includes a retrospective run from 1950 to 2014 and a prospective run from 2015 to 2100, blending ground observations with native GCM results (Thrasher et al., 2022). This methodology enhances the CMIP6 simulations from large-scale to regional-to-local scales without altering long-term trends (Thrasher et al., 2012). Each downscaled projection features nine climate variables (for details, see Thrasher et al., 2022). This thesis employs four GCMs and focuses on five key climate variables: mean near-surface air temperature (tas), precipitation (pr), near-surface relative humidity (hurs) and surface downwelling radiation (shortwave: rsds, longwave: rlds) (see Table 1.). Our analysis includes two future SSP scenarios: SSP2-4.5 and SSP5-8.5 (O'Neill et al., 2016).

Table 1. NEX-GDDP CMIP6 GCM		
MODELS	DESCRIPTION	REFERENCES
ACCESS-CM2	Australian Community Climate and Earth system simulator - Coupled Model 2 (features improved fluid dynamics and a microphysical aerosol scheme)	Zeih, et al., 2022.
CESM2	Community System Model 2 is developed by the National Center for Atmospheric Research (NCAR), is a widely used Earth system model that integrates various components of the Earth's climate system to simulate past, present, and future climate conditions.	Gettelman, et al., 2019.
EC-Earth3	Model is developed by the European Consortium for High-Resolution Earth System Modelling (EC-Earth), is a comprehensive Earth system model used for climate research and forecasting.	Döscher, et al., 2021.

GFDL-ESM4	Earth system model developed by the Geophysical Fluid Dynamics Laboratory (GFDL), a research laboratory of the National Oceanic and Atmospheric Administration (NOAA) located in the United States. It is designed to simulate the behavior of the Earth's climate system and its interactions with the atmosphere, ocean, land surface, and cryosphere.	Dunne, et al., 2020.
SIMULATION	DESCRIPTION	REFERENCES
historical	Data obtained through the history between 1950 – 2014	Park, et al., 2023.
SSP2-4.5	Intermediate scenario, in which current climate change trends continue without substantial deviations, leading to a forcing pathway of 4.5 W m^{-2} by 2100.	Park, et al., 2023.
SSP5-8.5	This scenario represents the upper boundary of the range of scenarios described in the literature with an additional radiative forcing of 8.5 W m^{-2} by the year 2100.	Park, et al., 2023.
SPATIAL RESOLUTION	0.25° × 0.25° (~ 25 x 25 km)	Park, et al., 2023.

TEMPORAL RESOLUTION	Daily	Park, et al., 2023.

Table 1. Description of NASA Earth global daily downscaled projections used in this paper.

On the open-source NASA's NCCS THREDDS data catalog (https://ds.nccs.nasa.gov/thredds/catalog/AMES/NEX/GDDP-CMIP6/catalog.html) the desired model should be selected, followed by the selection of the variable of interest and the appropriate coordinates (min and max lat-lon).

Table 1 describes the models that we have considered for the analysis performed in this thesis. The data was downloaded year by year, with the input coordinates of the Mediterranean basin, with the horizontal, vertical and time stride fixed at 1, in netCDF (nc4) format. The bounding box (in decimal degrees) necessary to select a subset of the whole dataset is: lon [-10W:30E] and lat [30N:50N] (figure 3c). At the bottom of the NASA's NCCS THREDDS page (https://ds.nccs.nasa.gov/thredds/catalog/AMES/NEX/GDDP-CMIP6/catalog.htm) a URL will be displayed that directly leads to the desired file. Figure 3. (below) shows the necessary steps in downloading data from the aforementioned NASA Thredds Catalog.

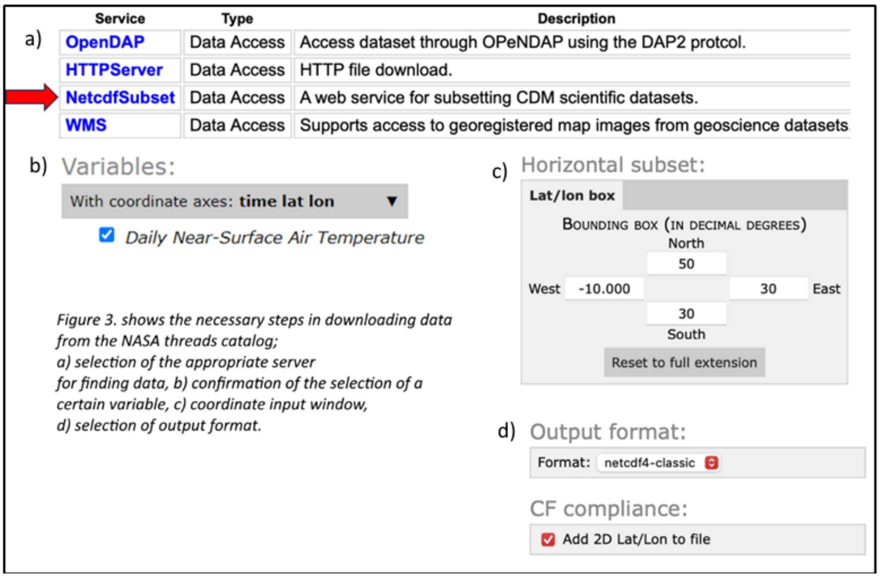

a)

Service	Type	Description
OpenDAP	Data Access	Access dataset through OPeNDAP using the DAP2 protcol.
HTTPServer	Data Access	HTTP file download.
NetcdfSubset	Data Access	A web service for subsetting CDM scientific datasets.
WMS	Data Access	Supports access to georegistered map images from geoscience datasets

b) Variables:

With coordinate axes: **time lat lon** ▼

☑ *Daily Near-Surface Air Temperature*

c) Horizontal subset:

Lat/lon box

Bounding box (in decimal degrees)

North: 50

West: -10.000

East: 30

South: 30

Reset to full extension

d) Output format:

Format: netcdf4-classic

CF compliance:

☑ Add 2D Lat/Lon to file

Figure 3. shows the necessary steps in downloading data from the NASA threads catalog; a) selection of the appropriate server for finding data, b) confirmation of the selection of a certain variable, c) coordinate input window, d) selection of output format.

A script was created in MATLAB that iterates the variable name and the year for every scenario and every model and it downloads the overall time-series in that file. In the following text there is an example of the code used for downloading the data. So, the code given below contains instructions for downloading one specific model (CESM2), which indicates that when downloading data from other models, certain lines of code must be replaced. In the first line, the selected model and scenario are defined, indicating that the name of the model as well as the name of the scenario must be changed manually. Following the changes in the code, we also change the settings on the website that contains our data (https://www.nccs.nasa.gov/services/data-collections/land-based-products/nex-gddp-cmip6). Initially, the script defines the base URL, which points to the location of the data files on the NASA server. The URL structure is critical, as it specifies the exact directory for the chosen model and scenario. For instance, the base URL for CESM2 in the SSP2-4.5 scenario is as follows: "`baseURL = 'https://ds.nccs.nasa.gov/thredds/ncss/grid/AMES/NEX/GDDP-CMIP6/CESM2/ssp245/r4i1p1f1/';`".

To adapt the script for different models or scenarios, users must change the model name (in this case, "CESM2") and the scenario name (here, "ssp245") in the URL. The specific variables of interest, such as near-surface relative humidity (hurs), precipitation (pr), longwave radiation (rlds), shortwave radiation (rsds), surface wind (sfcWind), and near-surface air temperature (tas), are then defined.

Last, we need to define the destination folder in which we want to save our files, and we construct the file name in the desired format.

```
%CESM 245
% Define the base URL where the files are located
baseURL =
'https://ds.nccs.nasa.gov/thredds/ncss/grid/AMES/NEX/GDDP-
CMIP6/CESM2/ssp245/r4i1p1f1/';
% Define the variables you want to download
variables = {'hurs','pr', 'rlds', 'rsds', 'sfcWind', 'tas'};
% Define the years you want to download
years = 2015:2100;
```

```
% Define the destination folder where you want to save the
files
destinationFolder =
'C:\Users\Mia\Documents\ZAVRSNI\NEX_data\CESM2_data\ssp245_da
ta';
% Set timeout value (in seconds)
timeoutValue = 30;

% Loop through each variable
for var_idx = 1:length(variables)
    % Get the current variable
    variable = variables{var_idx};

    % Define the URL for the current variable
    variableURL = [baseURL, variable, '/', variable,
'_day_CESM2_ssp245_r4i1p1f1_gn_'];

    % Loop through each year
    for year = years
        % Construct the filename for the file of the current
year and variable
        filename =
sprintf('%s_day_CESM2_ssp245_r4i1p1f1_gn_%d.nc.nc4',
variable, year);

        % Construct the full URL for the file
        fileURL = [variableURL, num2str(year), '.nc?var=',
variable, '&north=50&west=-
10&east=30&south=30&horizStride=1&time_start=',
```

```
num2str(year), '-01-01T12:00:00Z&time_end=', num2str(year),
'-12-31T12:00:00Z&timeStride=1&vertStride=1&accept=netcdf4-
classic&addLatLon=true'];

        % Download the file using websave with timeout
        websave(fullfile(destinationFolder, variable,
filename), fileURL, weboptions('Timeout', timeoutValue));
    end
end
```

2.2. Box analysis on selected locations

Box coordinates analysis, often referred to in geographical and spatial analysis, is a method used to summarize and understand the distribution of data points within a defined squared area or "box." This technique is useful for various applications, including urban planning, environmental studies, and logistics. The area of interest is defined as a rectangular or square "box" on a map. This box can be aligned with natural or administrative boundaries. In this paper box analysis on a 1° scale was applied (≈100 x 100 km). Box analysis on a 1° scale involves dividing a geographic area into grid cells, each measuring 1 degree of latitude by 1 degree of longitude. A box is typically defined by its minimum and maximum latitude and longitude (e.g., (lat_min, lon_min) to (lat_max, lon_max)). This method is often used in spatial analysis to study large-scale spatial patterns and distributions (Rizza et al., 2024). For each selected location one box was superimposed. In the following text, parts of the script from MATLAB is reported, which is showing how the boxes were defined using coordinates.

```
longitude_al = 364.0000; % input-->lon+360 ; dx->0.25 x0-->.00, .25, .50, .75
lattitude_al = 35.1250; %input-->lat ; dy->0.25 y0-->.125, .375, .625, .875
longitude_cr = 375.2500;
lattitude_cr = 45.1250;
longitude_ba = 376.5000;
lattitude_ba = 40.6250;
longitude_pa = 373.7500;
lattitude_pa = 37.6250;
longitude_ma = 373.0000;
lattitude_ma = 43.1250;
longitude_mi = 369.2500;
lattitude_mi = 45.3750;
longitude_sa = 369.0000;
lattitude_sa = 40.125;
```

Longitude coordinates should be corrected by adding 360° to real longitude, this is needed as MATLAB …..

In the MATLAB script, geographical coordinates for various Mediterranean locations are defined in a specific format to ensure compatibility with the analyzed data. The longitudes require correction by adding 360° to values that would otherwise be outside the standard range, allowing for representation in degrees from 0° to 360°. For instance, the longitude for Bou-Saada, Algeria, is given as 364.0, which effectively corresponds to 4° east (since 364° - 360° = 4°). In contrast, latitude values, such as 35.1250 for Bou-Saada, are straightforward, indicating degrees north of the Equator without any transformations. The comments in the code indicate that coordinates are incremented by 0.25 degrees, enhancing precision in geographic representation. This systematic approach ensures accurate calculations of temperature averages and other climate variables within defined geographic boxes, thereby facilitating a thorough analysis of climate change impacts across selected locations. Overall, the chosen coordinate format is essential for aligning with the dataset and enabling precise data extraction and analysis in the context of climate modeling.

Later in the script, code designed to calculate the yearly average temperature within a specific geographic box based on climate model data was created.

```
% Calculate yearly average and store it
indx_al = lon==longitude_al; %ordinal number of node
corresponding to longitude
indy_al = lat==lattitude_al; %ordinal number of node
corresponding to lattitude
```

```
nlonpoint_al=find(any(indx_al>0,2)); %numerical value of the
lon node
nlatpoint_al=find(any(indy_al>0,2)); %numerical value of the
lat node
```

“indx_al” and “indy_al” identify the indices in the longitude and latitude arrays that match the specified coordinates (longitude_al and latitude_al). “nlonpoint_al” and “nlatpoint_al” find the exact numerical positions of these indices.

```
nlon_al = [nlonpoint_al - 2, nlonpoint_al - 1, nlonpoint_al,
nlonpoint_al + 1, nlonpoint_al + 2];
nlat_al = [nlatpoint_al - 2, nlatpoint_al - 1, nlatpoint_al,
nlatpoint_al + 1, nlatpoint_al + 2];
```

Last two of the previous lines create a list of indices representing a box centered around the specified point, extending 2 units in all directions.

```
%reducing dimensions of variable array,  x and y-->1,
coordinate specific variable/time array
ACCES245_varData_al = squeeze(ACCES245_data(nlon_al, nlat_al,
:)); %daily temperatures at specific box
ACCES245_tasyearavg_al= nanmean(ACCES245_varData_al,
'all');%yearly average at box/one value
```

“squeeze” reduces the dimensions of the data array, isolating the data for the specific geographic box.

“nanmean” calculates the mean temperature, ignoring any NaN values, to find the yearly average for the specified box.

```
ACCES585_varData_al = squeeze(ACCES585_data(nlon_al, nlat_al,
:));
ACCES585_tasyearavg_al = nanmean(ACCES585_varData_al, 'all');
CESM245_varData_al = squeeze(CESM245_data(nlon_al, nlat_al,
:));
CESM245_tasyearavg_al = nanmean(CESM245_varData_al, 'all');
CESM585_varData_al = squeeze(CESM585_data(nlon_al, nlat_al,
:));
CESM585_tasyearavg_al = nanmean(CESM585_varData_al, 'all');
ECE3245_varData_al = squeeze(ECE3245_data(nlon_al, nlat_al,
:));
ECE3245_tasyearavg_al = nanmean(ECE3245_varData_al, 'all');
ECE3585_varData_al = squeeze(ECE3585_data(nlon_al, nlat_al,
:));
ECE3585_tasyearavg_al = nanmean(ECE3585_varData_al, 'all');
GFDLESM4245_varData_al = squeeze(GFDLESM4245_data(nlon_al,
nlat_al, :));
GFDLESM4245_tasyearavg_al = nanmean(GFDLESM4245_varData_al,
'all');
GFDLESM4585_varData_al = squeeze(GFDLESM4585_data(nlon_al,
nlat_al, :));
GFDLESM4585_tasyearavg_al = nanmean(GFDLESM4585_varData_al,
'all');
```

Previous section repeats the extraction and averaging process for various climate model datasets, allowing for comparison between different scenarios (e.g., different emission scenarios or different climate models).

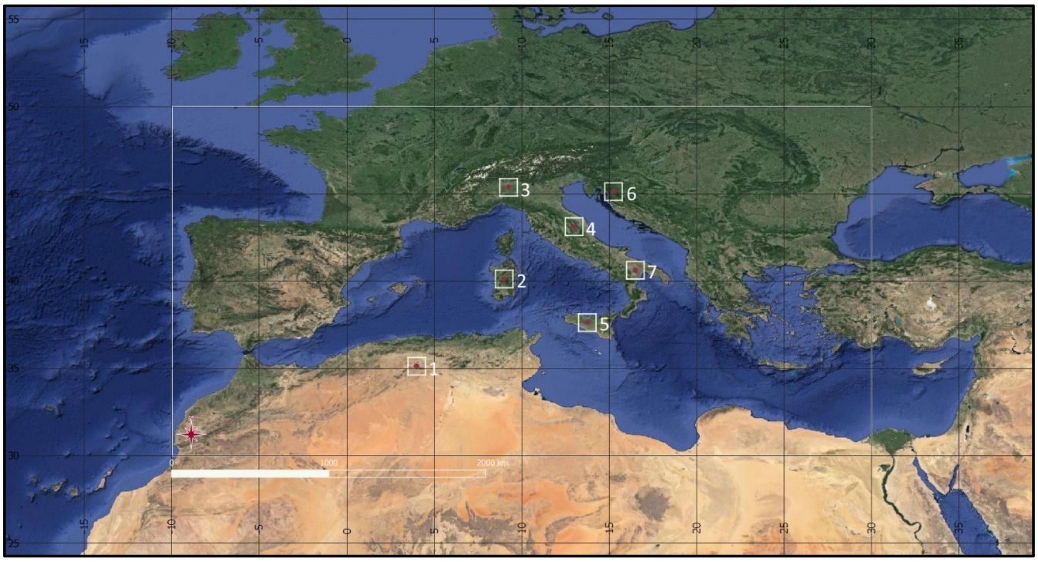

Figure 4. Analysis domain and location of boxes. From Google Satellite imagery processed in QGIS using doc.csv file.

As depicted in figure 4, seven box locations are visible, and it is clear that for this analysis Italy was processed in the most detail (with 5 box locations within the country), and the rest of the Mediterranean is rounded out by box locations in Croatia and one in Northern Sahara Desert (Bou-Saada, Algeria). This methodology allows us to determine the time series of each variable in each box in order to be able to record individual changes in certain locations.

Location	Latitude (°)	Longitude (°)	Corner
1 Bou-Saada desert, Algeria	35.625	4.50	NW
	34.625	4.5	SW
	34.625	3.5	SE
	35.625	3.5	NE
Center coordinate	35.125	4.00	
2 Sardegna, Italy	40.625	9.5	NW
	39.625	9.5	SW
	39.625	8.5	SE
	40.625	8.5	NE
Center coordinate	40.125	9.00	

3 Milano, Italy	45.875	9.75	NW
	44.875	9.75	SW
	44.875	8.75	SE
	45.875	8.75	NE
Center coordinate	45.375	9.25	
4 Marche region, Italy	43.625	13.5	NW
	42.625	13.5	SW
	42.625	12.5	SE
	43.625	12.5	NE
Center coordinate	43.125	13.00	
5 Palermo, Italy	38.125	14.25	NW
	37.125	14.25	SW

	37.125	13.25	SE
	38.125	13.25	NE
Center coordinate	37.625	13.75	
6 Zagreb, Croatia	45.625	15.75	NW
	44.625	15.75	SW
	44.625	14.75	SE
	45.625	14.75	NE
Center coordinate	45.125	15.25	
7 Bari, Italy	41.125	17	NW
	40.125	17	SW
	40.125	16	SE
	41.125	16.00	NE

Center coordinate	40.625	16.5	
Mediterranean basin	50	-10.00	NW
	30	-10.00	SW
	30	30.00	SE
	50	30.00	NE

Table 2. Box coordinates for each of 7 locations and for the whole domain. The Center coordinates of each box are highlighted in yellow.

2.3. Determination of the baseline temperature

For determining the baseline temperature, an average over a 31-year (1950 - 1980) period over 7 locations was obtained. The World Meteorological Organization considers a thirty-year period to be the minimum required to calculate the average climate, known as a climate normal (Morice et al., 2021). Climate normals are updated at the end of every decade (Rigal et al., 2019). This kind of calculation is important in order to be able to include extremes that do not repeat every year, as well as to make it easier to follow seasonal changes. This way of determining climate also covers deviations in climatic variables such as volcanic eruptions, floods. To determine the baseline temperature the historical temperature data was uploaded into the MATLAB environment. Data from 1950 - 1980 was used (31-year period/31 files). For each year/file a yearly average per node was made (161x81x365 becomes 161x81x1) and then we averaged all the 31 years/files. From the 31-year average for all nodes in the Mediterranean basin 7 locations are extracted using the indices of coordinates that are shown in Table 2. Next step was extracting the modeled data. For each model/scenario all the files are read and all the days are averaged to obtain yearly averages. This data is stored in matrices for every scenario/model (8 matrices) which contain all the yearly averages of 86 years. Out of every of these matrices nodes corresponding to the 7 locations were extracted. Now for every model/scenario the average of locations is done to obtain a scenario time plot of 86 years (2015-2100). The following text contains the MATLAB code used to calculate the baseline temperature, in reality the code was coupled with the box coordinates of all locations and was used to determine the crossing year; that code will be shown in its entirety in the next paragraph. The code shown in this section has been edited to show lines needed for determining only the baseline temperature.

```
histplot_prefix = 'tas_day_ACCESS-
CM2_historical_r1i1p1f1_gn_';

histplot_start_year = 1950;

histplot_end_year = 2014;
```

```
% Initialize arrays to store yearly averages for historical
data

hist_yearly_averages = zeros(hist_end_year - hist_start_year
+ 1, 1);

hist_years = hist_start_year:hist_end_year;

hyears = abs(hist_years);

% Initialize matrices to store yearly averages for specific
locations for

% historical data

hist_yearly_averages_al = zeros(hist_end_year -
hist_start_year + 1, 1);

hist_yearly_averages_cr = zeros(hist_end_year -
hist_start_year + 1, 1);

hist_yearly_averages_ba = zeros(hist_end_year -
hist_start_year + 1, 1);

hist_yearly_averages_pa = zeros(hist_end_year -
hist_start_year + 1, 1);

hist_yearly_averages_ma = zeros(hist_end_year -
hist_start_year + 1, 1);

hist_yearly_averages_mi = zeros(hist_end_year -
hist_start_year + 1, 1);

hist_yearly_averages_sa = zeros(hist_end_year -
hist_start_year + 1, 1);

% Loop over each year FOR HISTORICAL DATA

for j = 1:length(hyears)

% Construct filename for the current year
```

```
hist_filename = sprintf('%s%d%s', hist_prefix, hyears(j),
hist_suffix);

% Read data from the current file

hist_data = ncread(hist_filename, var);

%reducing dimensions of variable array,  x and y-->1,
coordinate specific variable/time array

hist_varData_al = squeeze(hist_data(nlon_al, nlat_al, :));

hist_tasyearavg_al= nanmean(hist_varData_al,
'all');%numerical value/yearly average of box

hist_varData_cr = squeeze(hist_data(nlon_cr, nlat_cr, :));

hist_tasyearavg_cr= nanmean(hist_varData_cr, 'all');

hist_varData_ba = squeeze(hist_data(nlon_ba, nlat_ba, :));

hist_tasyearavg_ba= nanmean(hist_varData_ba, 'all');

hist_varData_pa = squeeze(hist_data(nlon_pa, nlat_pa, :));

hist_tasyearavg_pa= nanmean(hist_varData_pa, 'all');

hist_varData_ma = squeeze(hist_data(nlon_ma, nlat_ma, :));

hist_tasyearavg_ma= nanmean(hist_varData_ma, 'all');

hist_varData_mi = squeeze(hist_data(nlon_mi, nlat_mi, :));

hist_tasyearavg_mi= nanmean(hist_varData_mi, 'all');

hist_varData_sa = squeeze(hist_data(nlon_sa, nlat_sa, :));

hist_tasyearavg_sa= nanmean(hist_varData_sa, 'all');

% Store yearly averages in matrices

hist_yearly_averages_al(j) = hist_tasyearavg_al;
```

```
hist_yearly_averages_cr(j) = hist_tasyearavg_cr;

hist_yearly_averages_ba(j) = hist_tasyearavg_ba;

hist_yearly_averages_pa(j) = hist_tasyearavg_pa;

hist_yearly_averages_ma(j) = hist_tasyearavg_ma;

hist_yearly_averages_mi(j) = hist_tasyearavg_mi;

hist_yearly_averages_sa(j) = hist_tasyearavg_sa;

end

% historical data Calculate the average along each row to
create timepolot

% of yearly averages

hist_yearly_averages_avg = mean(hist_yearly_averages, 2);

histplot_yearly_averages_avg = mean(histplot_yearly_averages,
2);

%baseline temperature per location

baseline_al = mean(hist_yearly_averages_al)

baseline_cr = mean(hist_yearly_averages_cr)

baseline_ba = mean(hist_yearly_averages_ba)

baseline_pa = mean(hist_yearly_averages_pa)

baseline_ma = mean(hist_yearly_averages_ma)

baseline_mi = mean(hist_yearly_averages_mi)

baseline_sa = mean(hist_yearly_averages_sa)

%baseline temperature medditerranean
```

```
baseline = mean(hist_yearly_averages_avg)

% historical data Calculate the average along each row to
create timepolot

% of yearly averages

hist_yearly_averages_avg = mean(hist_yearly_averages, 2);

histplot_yearly_averages_avg = mean(histplot_yearly_averages,
2);

%baseline temperature per location

baseline_al = mean(hist_yearly_averages_al)

baseline_cr = mean(hist_yearly_averages_cr)

baseline_ba = mean(hist_yearly_averages_ba)

baseline_pa = mean(hist_yearly_averages_pa)

baseline_ma = mean(hist_yearly_averages_ma)

baseline_mi = mean(hist_yearly_averages_mi)

baseline_sa = mean(hist_yearly_averages_sa)

%baseline temperature medditerranean

baseline = mean(hist_yearly_averages_avg)
```

2.4. Determination of the crossing year

For the determination of the crossing year only the mean surface-air temperature (tas) variable was used. A baseline temperature was compared with the yearly average over the 7 locations and multi-model scenario (SSP2-4.5 and SSP5-8.5) data (2015-2100), to determine the temperature anomaly across the timespan, and crossing year when the temperature anomaly reaches 2ºC (1.75ºC from our baseline period of 1950-1980, Park, et al.,2022). To determine the crossing year the data was normalized by coupling the multi model data, per scenario, to the historical data and recalculating the values using four different methods; the "moving mean" with a 30-year window and the "square root moving mean" method with a 15-year window, to add larger weights to older data within the window, to both minimize the effects of the increasing rate of heating and decreasing the modeled data's rising inaccuracy while going further into the future. Then, the "moving mean" method using a 30-year window but this time by taking into account pure arithmetic mean - predicts too early years and does not match reality due to the influence of the increasing growth rate that raises the temperature. Finally, the last method was the "moving median" with a 30-year window, which we used in the further analysis because it matches the modeled temperature best. In the following text the part of the MATLAB code for determination of the crossing year is given. The code includes all analyzed models and scenarios, contains all coordinates for all seven locations, and its results will be presented further in this paper.

```
% Apply a moving average filter with moving mean method
Historical_anomaly_smoothedmedian =
movmedian(Historical_combined_matrix,window_size);
```

```
SSP245combined_anomaly_smoothedmedian =
movmedian(SSP245combined_matrix,window_size);
SSP585combined_anomaly_smoothedmedian =
movmedian(SSP585combined_matrix,window_size);
```

By establishing a moving median from the historical combined matrix (that contained total historical data), for the SSP2-4.5 scenario and SSP5-8.5 scenario in the same way. This created the three matrices that contain the main data from the plotting of the crossing year.

```
% Find the index of the first value exceeding 1.75°C in
SSP245combined_anomaly_smoothed
index_SSP245median =
find(SSP245combined_anomaly_smoothedmedian > 1.75, 1,
'first');
% Find the index of the first value exceeding 1.75°C in
SSP585combined_anomaly_smoothed
index_SSP585median =
find(SSP585combined_anomaly_smoothedmedian > 1.75, 1,
'first');
```

To define the crossing year the first index in the matrices SSP2-4.5 and SSP5-8.5 individually, where the temperature exceeds 1.75 Celsius degrees.

```
% Find the value in totalyears corresponding to index_SSP245
value_SSP245median = totalyears(index_SSP245median);
% Find the value in totalyears corresponding to index_SSP585
value_SSP585median = totalyears(index_SSP585median);
```

The index of the exceeding value was then located in the total year matrix to identify the year associated with the exceeding value and was displayed as text in the next two commands.

```
% Display the results
disp(['Value in totalyears corresponding to index_SSP245
using moving median: ', num2str(value_SSP245median)]);
disp(['Value in totalyears corresponding to index_SSP585
using moving median: ', num2str(value_SSP585median)]);
```

To plot the data the three matrices containing the moving median of all four models were plotted against the total year (1950-2100) in corresponding colors. The matrices containing the raw data were also plotted against time to give sense of variability and the range of the data.

```
% Plotting moving median method
figure;
hold on;
% Plot Historical_anomaly_raw data
plot(historical_years, Historical_combined_matrix (1:66), 'k-
', 'LineWidth', 1.5);
% Plot SSP245_anomaly_raw data
plot(future_years, SSP245combined_matrix(66:end), 'c-',
'LineWidth', 1.5);
% Plot SSP585_anomaly_raw data
plot(future_years, SSP585combined_matrix(66:end), 'm-',
'LineWidth', 1.5);
% Plot Historical_anomaly_smoothed
plot(historical_years, Historical_anomaly_smoothedmedian
(1:66), 'k-', 'LineWidth', 1.5);
% Plot SSP245_anomaly_smoothed
plot(future_years,
SSP245combined_anomaly_smoothedmedian(66:end), 'b-',
'LineWidth', 1.5);
% Plot SSP585_anomaly_smoothed
plot(future_years,
SSP585combined_anomaly_smoothedmedian(66:end), 'r-',
'LineWidth', 1.5);
% Add a horizontal line at 1.75 degrees Celsius
```

```
line([1950, 2100], [1.75, 1.75], 'Color', 'g', 'LineStyle',
'--', 'LineWidth', 1.5);
ylim([min_value, max_value]);
% Set plot title and labels
title('Mediterranean Temperature Anomalies - Moving Median
method');
xlabel('Year');
ylabel('Temperature Anomaly (°C)');
% Set x-axis limit to span from 1950 to 2100
xlim([1950, 2100]);
```

Here, minimum and maximum values for the y-axis are set to ensure that the plot displays the temperature anomalies within a specified range. Also, it labels the y-axis as "Temperature Anomaly (°C)", indicating that the vertical axis represents temperature anomalies measured in degrees Celsius.

```
% Add legend
legend('Historical Raw Data', ('SSP245 Raw Data'), ('SSP585
Raw Data'), ...
    'Historical Moving Median', ...
    ['SSP245  Moving Median(' num2str(value_SSP245mean) ')'],
...
    ['SSP585  Moving Median(' num2str(value_SSP585mean) ')'],
...
    'Location', 'northwest');
grid on;
hold off;
```

2.5. Variable analysis

For every variable a baseline value was determined (1950-1980), by averaging over the selected locations. This methodology is the same as that we have utilized in t determining the crossing year. The daily data was averaged for every year (model data 2015-2100, historical data 1950-2014), except for precipitation where the daily data in mm/s was summed up and multiplied by 86400 to achieve yearly value in mm/year.

Averaging daily data for each year is commonly used for most variables (like temperature or humidity). For precipitation, the approach differs slightly. For precipitation data, it's common to sum up daily values rather than averaging them, since precipitation represents cumulative amounts over time. Multiplying daily precipitation data by 86,400 (the number of seconds in a day) to convert from mm/s to mm/day is standard practice in climate modeling, as models often report precipitation in mm/s. Climate models often report precipitation as a flux (rate), which is typically in mm/s. To calculate the total yearly precipitation, you need to convert the daily flux into a more understandable unit. Multiplying by 86,400 converts from a rate (mm/s) into a daily amount (mm/day). Then, summing the daily values over a year gives you the total precipitation for that year in mm/year. This method ensures that the data is properly scaled to represent real-world precipitation over time.

Then the data corresponding to the 7 locations was extracted and averaged to determine an average value for the Mediterranean for every analyzed model and scenario, including the historical data. All of the data was subtracted by the baseline value to get the values of the anomalies. Again, a mean anomaly was determined for each scenario by averaging the four models. A time plot was created including the historical data, mean modeled anomaly and ranges of models within the scenario. A map of the mean anomaly that was averaged over a 31-year period around the crossing year was created for both scenarios. A graph was created containing a boxplot for each scenario and model, plotting the anomalies at different locations, highlighting the variability between models/scenarios. Time plots are made for the entire Mediterranean and for each location separately. Each time plot contains an average curve for each scenario, ranges values from each scenario and are interpolated with the "moving median" method to show the deviations between individual locations and the entire Mediterranean, and for the Mediterranean time plot to show the deviations of the different models and visually show the approximation method. Again, in the following text the MATLAB code used for the analysis of variables is presented. In the first two lines of the input parameters section variable name should be changed and corresponding to the variable unit should be changed, too. In continuation it is possible to manipulate the location of the legend. The script contains the previously written names of the variables, as well as their units of measurement, contains the box coordinates of all 7 locations, but also the coordinates of the Mediterranean that were agreed upon in the previous paragraphs. The code script was made for four variables (hurs, tas, rsds, rlds and separately, pr), separate script was made for the fifth variable, i.e. precipitation, and only the part that is different from the code presented below will be delivered at the very end of this paragraph.

All the files associated with the chosen variable were iteratively opened with data from chosen boxes extracted from these files by connecting the value of longitude and latitude with their index in the format ".nc4" files.

```
for i = 1:length(years)

   % Construct filename for the current year
   ACCES245_filename = sprintf('%s%d%s', ACCES245_prefix,
years(i), ACCES245_suffix);
   ACCES585_filename = sprintf('%s%d%s', ACCES585_prefix,
years(i), suffix);
   CESM245_filename = sprintf('%s%d%s', CESM245_prefix,
years(i), suffix);
   ...
lon = ncread(ACCES245_filename,'lon'); %read longitude vector
lat = ncread(ACCES245_filename,'lat'); %read lattitude vector
time = ncread(ACCES245_filename,'time'); % read time vector
   % Read data from the current file
   ACCES245_data = ncread(ACCES245_filename, var);
   ACCES585_data = ncread(ACCES585_filename, var);
   CESM245_data = ncread(CESM245_filename, var);
   ...

   % Calculate yearly average and store it
indx_al = lon==longitude_al; %ordinal number of node
corresponding to longitude
indy_al = lat==lattitude_al; %ordinal number of node
corresponding to lattitude
nlonpoint_al=find(any(indx_al>0,2)); %numerical value of the
lon node
nlatpoint_al=find(any(indy_al>0,2)); %numerical value of the
lat node
nlon_al = [nlonpoint_al - 2, nlonpoint_al - 1, nlonpoint_al,
nlonpoint_al + 1, nlonpoint_al + 2];
nlat_al = [nlatpoint_al - 2, nlatpoint_al - 1, nlatpoint_al,
nlatpoint_al + 1, nlatpoint_al + 2];
%reducing dimensions of variable array,  x and y-->1,
coordinate specific variable/time array
```

```
ACCES245_varData_al = squeeze(ACCES245_data(nlon_al, nlat_al,
:)); %daily temperatures at specific node
ACCES245_tasyearavg_al= nanmean(ACCES245_varData_al,
'all');%yearly average at node/one value
ACCES585_varData_al = squeeze(ACCES585_data(nlon_al, nlat_al,
:));
ACCES585_tasyearavg_al = nanmean(ACCES585_varData_al, 'all');
CESM245_varData_al = squeeze(CESM245_data(nlon_al, nlat_al,
:));
CESM245_tasyearavg_al = nanmean(CESM245_varData_al, 'all');
...
%baseline temperature per location
baseline_al = mean(hist_yearly_averages_al);
baseline_cr = mean(hist_yearly_averages_cr);
baseline_ba = mean(hist_yearly_averages_ba);
baseline_pa = mean(hist_yearly_averages_pa);
baseline_ma = mean(hist_yearly_averages_ma);
baseline_mi = mean(hist_yearly_averages_mi);
baseline_sa = mean(hist_yearly_averages_sa);
%baseline temperature medditerranean
baseline = mean(hist_yearly_averages_avg)
```

A baseline value for each location and the overall baseline value has been calculated to illustrate the magnitude of anomaly.

```
% Define the input matrices for SSP245 and SSP585
SSP245_matrices = [ACCES245_anomaly, CESM245_anomaly,
ECE3245_anomaly, GFDLESM4245_anomaly];
SSP585_matrices = [ACCES585_anomaly, CESM585_anomaly,
ECE3585_anomaly, GFDLESM4585_anomaly];
```

For each scenario the data from all models was collected.

```
%variable anomaly value at crossing year
% Define the offset
offset = -15:15;
% Calculate the mean of values with the specified index range
```

```
varvalue245 = mean(SSP245combined_matrix(index_SSP245sq +
offset));
varvalue585 = mean(SSP585combined_matrix(index_SSP585sq +
offset));
```

An averaged value of the variable is calculated over a 30 year window, to minimize irregularities.

```
window_size = 30;
% Apply a moving average filter with square root method
Historical_anomaly_smoothedmedian =
movmedian(Historical_combined_matrix,window_size);
SSP245combined_anomaly_smoothedmedian =
movmedian(SSP245combined_matrix,window_size);
SSP585combined_anomaly_smoothedmedian =
movmedian(SSP585combined_matrix,window_size);
%%%%%%%%Plotting senario averages and ranges%%%%%%%%%%%
figure;
hold on;
% Fill the area between the curves
fill([totalyears, fliplr(totalyears)], [SSP245combined_max1,
fliplr(SSP245combined_min1)], 'b', 'EdgeColor', 'none',
'FaceAlpha', 0.2, 'LineWidth', 0.01);
fill([totalyears, fliplr(totalyears)], [SSP585combined_max1,
fliplr(SSP585combined_min1)], 'r', 'EdgeColor', 'none',
'FaceAlpha', 0.3, 'LineWidth', 0.01);
```

A moving median is performed upon the datasets of scenarios, SSP2-4.5 and SSP5-8.5 with a 30 year window. The ranges are plotted for each scenario by filling the area between the maximal and minimal data points from all models within a scenario. Later, raw data and moving median data was plotted as well. The same has been done for the Mediterranean and for each location, with the only difference being that more specific data points were used, corresponding to a certain geographic location.

To plot differences in maps, a mean crossing year was decided to be able to visually compare maps from the same period.

```
mean_crossing_year = round(mean([Crossingyear_SSP245,
Crossingyear_SSP585]));
% Calculate the anomaly map for 245
Anomaly_map245 = Crossingyear_map245 - Historical_map;
% Calculate the anomaly map for 585
Anomaly_map585 = Crossingyear_map585 - Historical_map;
pcolor(lon_grid1, lat_grid1, Anomaly_map245');
colorbar('Limits', [min_value, max_value]);
colormap('jet');
%colormap(flipud(jet));
caxis([min_value, max_value]); % Set colormap
limitsxlabel('Longitude');
ylabel('Latitude');
title(['Mediterranean ' var ' (' unit ') Anomaly/Difference
for Averaged SSP2-4.5 Scenarios, Between Periods: 1950-1980
and 30-year Average, Centered at Mean Crossing Year = '
num2str(mean_crossing_year)]);
shading interp; % Interpolate colors between grid points
axis equal;
```

The map is simply a 2D matrix, containing 30year average values of the variable for each longitude, latitude pair. it is plotted with the “pcolor” function.

```
% Add points to the plot
hold on;
scatter(lon(nlonpoint_al), lat(nlatpoint_al), 75, 'ro',
'filled', 'DisplayName', ['Bou-Saada,AL: ',
num2str(nanmean(Anomaly_map245(nlon_al, nlat_al),'all'))]);
scatter(lon(nlonpoint_ba), lat(nlatpoint_ba), 75, 'rs',
'filled', 'DisplayName', ['Bari,IT: ',
num2str(nanmean(Anomaly_map245(nlon_ba, nlat_ba),'all'))]);
scatter(lon(nlonpoint_cr), lat(nlatpoint_cr), 75, 'bo',
'filled', 'DisplayName', ['Zagreb,CR: ',
num2str(nanmean(Anomaly_map245(nlon_cr, nlat_cr),'all'))]);
scatter(lon(nlonpoint_ma), lat(nlatpoint_ma), 75, 'bs',
'filled', 'DisplayName', ['Marche,IT: ',
num2str(nanmean(Anomaly_map245(nlon_ma, nlat_ma),'all'))]);
scatter(lon(nlonpoint_mi), lat(nlatpoint_mi), 75, 'ko',
'filled', 'DisplayName', ['Milano,IT: ',
num2str(nanmean(Anomaly_map245(nlon_mi, nlat_mi),'all'))]);
scatter(lon(nlonpoint_pa), lat(nlatpoint_pa), 75, 'ks',
'filled', 'DisplayName', ['Palermo,IT: ',
num2str(nanmean(Anomaly_map245(nlon_pa, nlat_pa),'all'))]);
scatter(lon(nlonpoint_sa), lat(nlatpoint_sa), 75, 'm^',
'filled', 'DisplayName', ['Sardegna,IT: ',
num2str(nanmean(Anomaly_map245(nlon_sa, nlat_sa),'all'))]);
% Define the coordinates of the nodes
x_nodes = [lon(nlonpoint_al); lon(nlonpoint_ba);
lon(nlonpoint_cr);lon(nlonpoint_ma);lon(nlonpoint_mi);lon(nlo
npoint_pa);lon(nlonpoint_sa)]; % Center nodes
y_nodes = [lat(nlatpoint_al); lat(nlatpoint_ba);
lat(nlatpoint_cr); lat(nlatpoint_ma); lat(nlatpoint_mi);
lat(nlatpoint_pa);lat(nlatpoint_sa)]; % Example nodes
% Calculate the width and height of the rectangle
width = 1; % width
height = 1; % height
% Plot the rectangles around the nodes
hold on;
for i = 1:numel(x_nodes)
   rectangle('Position', [x_nodes(i)-width/2, y_nodes(i)-
height/2, width, height], 'EdgeColor', 'k', 'LineWidth', 1);
end
hold off;
% Display legend
legend('Location',  'northwest');
h = legend;
```

```
h.String{1} = ['Anomaly per location (', unit, '):'];
% Adjust the y-axis limits to reduce empty space
ymin1 = min(lat(:));
ymax1 = max(lat(:));
axis([min(lon(:)) max(lon(:)) ymin1 ymax1]);
```

Center points and their corresponding boxes are added to the graph as well as the averaged variable values at location in the legend.

Chapter 3.

Concluding Remarks

3. Results

The results indicate that in the "extreme" scenario (SSP5-8.5), which gave results for the year 2025 as a crossing year, the projected anomalies are generally slightly smaller than those in the SSP2-4.5 scenario, which projects conditions for the year 2028. For instance, temperature anomalies in Bou-Saada, Algeria, and several regions in Italy show higher values under SSP2-4.5 (Table 3). This trend is also evident in relative humidity and shortwave radiation anomalies, where the SSP2-4.5 scenario consistently exhibits larger deviations compared to SSP5-8.5. Despite SSP5-8.5 representing a higher greenhouse gas concentration pathway, the earlier crossing year of 2025 compared to 2028 for SSP2-4.5 likely accounts for these differences. This suggests that while SSP5-8.5 projects more immediate impacts, the long-term anomalies may be more pronounced under SSP2-4.5 as the effects of climate change continue to intensify over a longer period.

For the SSP5-8.5 scenario, the crossing year is 2025, while for the SSP2-4.5 scenario, it is 2028. The values presented for these scenarios correspond to the exact data points from the respective years in the model, reflecting the temperature or precipitation anomaly for that specific year. In contrast, the values shown on the maps represent the mean anomaly averaged over a 30-year period centered around the crossing year. This approach ensures that the maps provide a more comprehensive, smoothed representation of the long-term climate impacts, rather than focusing on a single year's data, which might be subject to short-term variability.

Variable	Tas Anomaly (°C)		Pr Anomaly (mm/y)		Hurs Anomaly (%)		Rsds Anomaly (W/m²)		Rlds Anomaly (W/m²)	
Location	SSP 2-4.5	SSP 5-8.5	SSP 2-4.5	SSP 5-8.5	SSP 2-4.5	SSP 5-8.5	SSP 2-4.5	SSP 5-8.5	SSP 2-4.5	SSP 5-8.5
Bou-Saada, Algeria (AL)	2.00	1.94	-20.46	-7.31	-1.27	-0.88	2.37	1.48	9.44	9.50
Sardegna, Italy (IT)	1.61	1.55	-2.37	-17.65	-0.21	-0.35	4.93	4.56	7.62	7.25

Milano, Italy (IT)	1.99	1.89	85.67	87.46	-0.89	-0.98	4.57	4.60	8.57	7.92
Marche, Italy (IT)	1.92	1.89	17.60	17.68	-1.04	-1.14	5.59	5.29	7.68	7.32
Palermo, Italy (IT)	1.61	1.54	-7.17	-19.51	-0.12	-0.15	4.53	3.94	8.38	8.07
Zagreb, Croatia (CR)	2.05	2.00	61.19	71.35	-1.53	-1.58	6.70	6.37	8.30	7.91
Bari, Italy (IT)	1.82	1.75	-3.62	2.32	-0.70	-0.56	5.65	4.72	7.91	7.76
Mediterranean Region	1.86	1.79	18.69	19.2	-0.21	-0.26	4.91	4.42	8.27	7.96

Table 3 Table 3 provides a comprehensive overview of the projected climate anomalies under two different Shared Socioeconomic Pathway (SSP) scenarios: SSP2-4.5 and SSP5-8.5, for several locations within the Mediterranean basin. This includes temperature anomalies (Tas), precipitation anomalies (Pr), relative humidity anomalies (Hurs), shortwave radiation anomalies (Rsds), and longwave radiation anomalies (Rlds).

For Bou-Saada, Algeria (AL), the temperature anomaly is analyzed to be higher under SSP2-4.5 compared to SSP5-8.5. Precipitation anomalies are the same for both scenarios, indicating a significant decrease in rainfall. The relative humidity anomalies show a larger decrease under SSP2-4.5 compared to SSP5-8.5. Shortwave radiation anomalies are higher under SSP2-4.5, while longwave radiation anomalies are almost the same for both scenarios.

In Sardegna, Italy (IT), temperature anomalies are slightly higher under SSP2-4.5. Precipitation anomalies remain consistent across both scenarios, showing a decrease in rainfall. Relative humidity anomalies show a small decrease, with SSP2-4.5 being marginally higher. Shortwave radiation anomalies are higher under SSP2-4.5, whereas longwave radiation anomalies are lower under SSP5-8.5.

Milano, Italy (IT) shows similar temperature anomalies across both scenarios, with a slight decrease under SSP5-8.5. Precipitation anomalies indicate a consistent decrease in rainfall. Relative humidity anomalies are slightly higher under SSP2-4.5. Shortwave radiation anomalies are higher under SSP2-4.5, while longwave radiation anomalies are slightly lower under SSP5-8.5.

For Marche, Italy (IT), temperature anomalies are consistent across both scenarios. Precipitation anomalies show a moderate decrease. Relative humidity anomalies are slightly higher under SSP2-4.5. Shortwave radiation anomalies are higher under SSP2-4.5, whereas longwave radiation anomalies are lower under SSP5-8.5.

Palermo, Italy (IT) shows similar temperature anomalies across both scenarios. Precipitation anomalies indicate a decrease in rainfall. Relative humidity anomalies are slightly higher under SSP2-4.5. Shortwave radiation anomalies are higher under SSP2-4.5, while longwave radiation anomalies are lower under SSP5-8.5.

Zagreb, Croatia (CR) shows a slight increase in precipitation anomalies, which is unique compared to other locations. Temperature anomalies are consistent across both scenarios. Relative humidity anomalies are slightly higher under SSP2-4.5. Shortwave radiation anomalies are higher under SSP2-4.5, while longwave radiation anomalies are lower under SSP5-8.5.

Bari, Italy (IT) shows consistent temperature anomalies across both scenarios. Precipitation anomalies indicate a slight decrease in rainfall. Relative humidity anomalies are slightly higher under SSP2-4.5. Shortwave radiation anomalies are higher under SSP2-4.5, whereas longwave radiation anomalies are lower under SSP5-8.5.

The overall Mediterranean Region shows consistent temperature anomalies across both scenarios. Precipitation anomalies show an increase under SSP5-8.5. Relative humidity anomalies are slightly higher under SSP2-4.5. Shortwave radiation anomalies are higher under SSP2-4.5, while longwave radiation anomalies are lower under SSP5-8.5. Precise data obtained throughout this thesis will be shown and explained in detail, in paragraph “3.3. Analysis of variables on selected locations”.

3.1. Determination of the baseline temperature

The baseline temperature, was calculated as a spatial-temporal average over a 31-year (1950 - 1980) period and over the seven locations. These two averages provided the following value:
Tbase = 286.6750 Kelvin (13.525 degrees Celsius).

3.2. Determination of the crossing year

The following analysis reveals the crossing years for temperature anomalies using various methods and under two different SSP (Shared

Socioeconomic Pathway) scenarios, with the baseline temperature defined above.

Method	SSP245 Crossing Year	SSP585 Crossing Year
Square Root Method	2038	2036
Moving Mean Method	2026	2025
Raw Data Method	2019	2019
Moving Median Method	2028	2025

Table 4 This table is summarizing the crossing years for temperature anomalies using various methods under SSP2-4.5 and SSP5-8.5 scenarios.

The data used in this analysis was obtained from climate model projections and downloaded through MATLAB, following adjustments based on the specific model and scenario. The data was downloaded from the NASA NEX-GDDP-CMIP6 database, accessed via the appropriate URL, which was customized to reflect the chosen model and scenario. The downloaded data was processed using several statistical methods to determine the crossing year, a key point in climate projections. Among the methods tested, the "Moving Median Method", highlighted in yellow in Table 4, was chosen for further analysis due to its robustness in smoothing the data while retaining the most important trends. The “Moving Median Method” is highlighted in yellow because this method was used in the further analysis (Table 4).

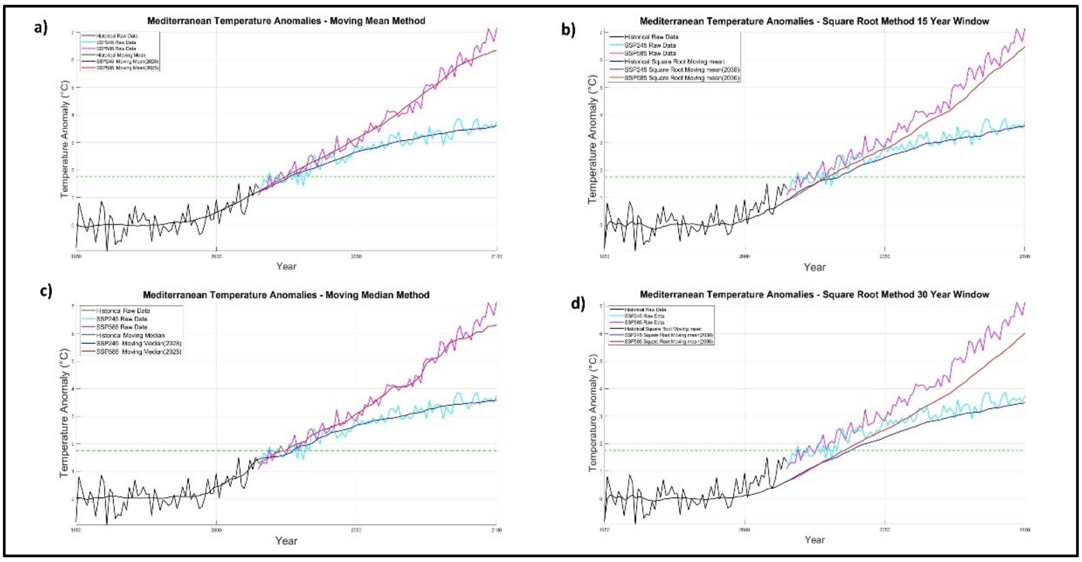

Figure 5: This figure shows all four methods used to determine the crossing year; a) Moving Mean Method b) Square Root Method with a 15-year window c) Moving Median Method d) Square Root Method with a 30-year window

Figure 5a shows the Mediterranean temperature anomalies using the “Moving Mean Method”. The black line represents the historical temperature anomalies, while the colored lines represent the projected anomalies under different SSP scenarios: SSP2-4.5 (blue line) projects a gradual increase in temperature anomalies. SSP5-8.5 (pink line) indicates a more significant increase in temperature anomalies. Figure 5b illustrates the Mediterranean temperature anomalies using the “Square Root Method” with a 15-year window. Similar to panel a, the black line represents historical data, and the colored lines show future projections: SSP2-4.5 (blue line) projects an increase in temperature anomalies. SSP5-8.5 (pink line) shows a steeper increase in temperature anomalies. Figure 4c reports the Mediterranean temperature anomalies using the “Moving Median Method”. The black line shows historical temperature anomalies, while the colored lines represent future projections: SSP2-4.5 (blue line) projects a steady increase in temperature anomalies. SSP5-8.5 (pink line) indicates a substantial rise in temperature anomalies. Figure 5d shows the Mediterranean temperature anomalies using the “Square Root Method” with a 30-year window. The black line represents historical data, and the colored lines show future projections: SSP2-4.5 (blue line) projects an increase in temperature anomalies. SSP5-8.5 (pink line) indicates a significant rise in temperature anomalies.

In the graphs presented in Figure 5a-d, the green dotted line represents the 2° C temperature anomaly threshold above pre-industrial levels. This threshold is significant as it marks the point where the global temperature increase reaches 2° C, a critical benchmark in climate change studies.

Exceeding this threshold is associated with severe and potentially irreversible impacts on global ecosystems, human societies, and weather patterns. The green dotted line serves as a visual reference across all the methods, allowing for comparison of when the temperature anomaly crosses this critical limit under different models and methods.

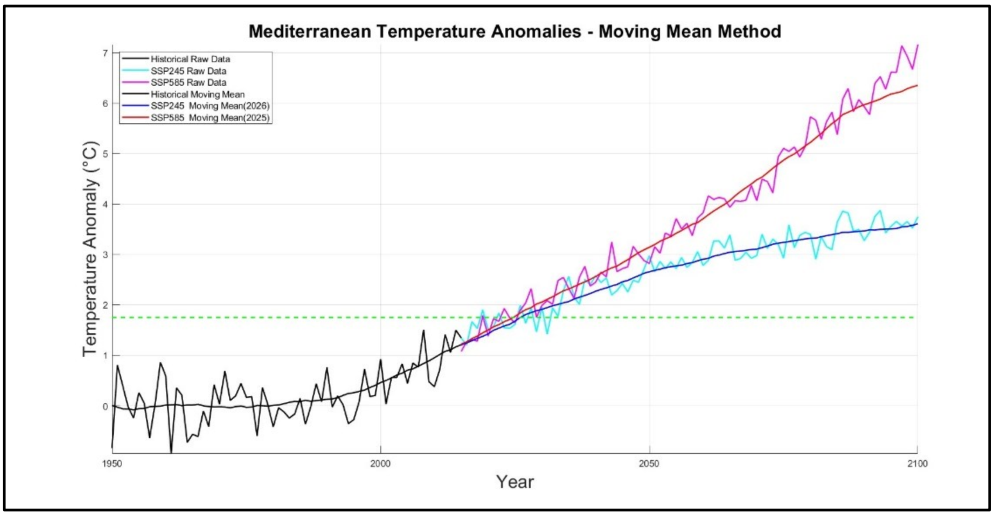

Figure 6 Temperature anomalies time series with the moving median method in the Med Basin.

With this method, we obtained 2028 as the crossing year for the SSP2-4.5 scenario, and 2025 for the SSP5-8.5 scenario.

3.3. Analysis of variables on selected locations

The Mediterranean basin is a climatic hotspot, it is characterized by different climate and ecological zones, making it particularly sensitive to the impacts of climate change. This thesis analyses the projected climate anomalies under two different Shared Socioeconomic Pathway (SSP) scenarios: SSP2-4.5, which projects conditions for the crossing year on 2028 and the SSP5-8.5 scenario with the relative crossing year on 2025. By analyzing key climate variables—mean daily temperature (Tas), precipitation (Pr), relative humidity (Hurs), shortwave radiation (Rsds), and longwave radiation (Rlds)—across various locations within the region, we aim to understand the potential future changes and their spatial implications. The chosen locations include Bou-Saada in Algeria, and several regions in Italy such as Sardegna, Milano, Marche, Palermo, as well as Zagreb in Croatia, and the broader Mediterranean basin. The analysis reveals that, despite SSP5-8.5 representing a higher greenhouse gas concentration pathway, the projected anomalies for 2025 are generally slightly smaller than those for 2028 under SSP2-4.5. This counterintuitive result likely arises from the difference in the crossing years, suggesting that while SSP5-8.5 shows more immediate impacts, SSP2-4.5 may exhibit more pronounced long-term anomalies as climate change continues to progress. Each location displays unique responses to the changing climate, influenced by local geographical and environmental conditions.

3.3.1. Algeria

In the following figure 7, it is reported the time series for the anomalies of the above mentioned five variables.

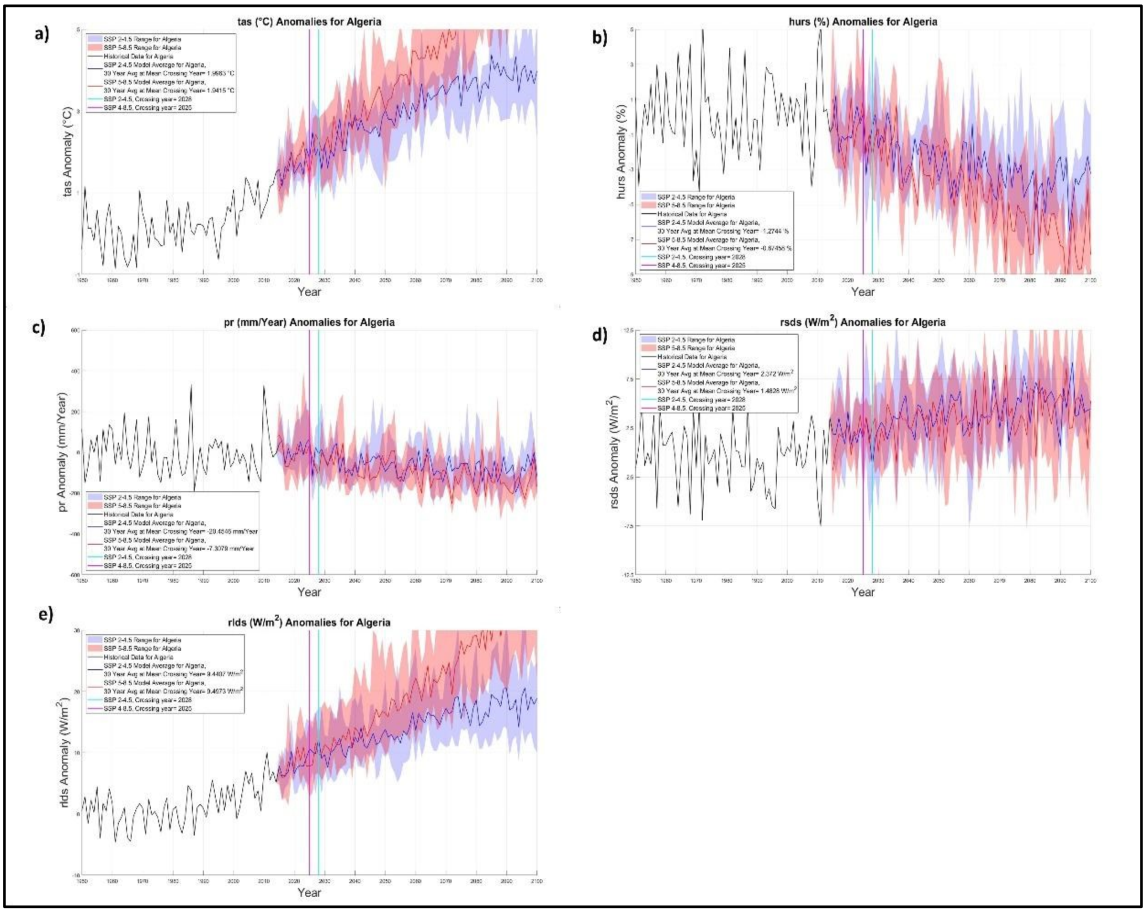

Figure 7 Anomalies: Time plots of five variables over Algeria; a) temperature, b) relative humidity, c) precipitation, d) surface downwelling shortwave radiation, e) surface downwelling longwave radiation.

Figure 7 presents time plots for five climate variables over Algeria, comparing anomalies under two scenarios: SSP2-4.5 and SSP5-8.5. The ranges on the graphs are consistent across different locations, though they may vary slightly depending on the specific climate variable and geographic conditions. For temperature anomalies (tas) (fig. 7a), the y-axis typically spans from -1°C to +5°C across all locations, as temperature changes in the Mediterranean region tend to follow a similar pattern. Relative humidity anomalies (hurs) (fig. 7b) are represented on a y-axis ranging from -7% to +7%, a uniform range reflecting the typical fluctuations in humidity. Precipitation anomalies (pr) (fig. 7c) generally range from -400 mm/year to +400 mm/year, though local precipitation variability may cause slight differences between locations. Shortwave radiation anomalies (rsds) (fig. 7d) are shown on a y-axis ranging from -7.5 W/m² to +17.5 W/m², indicating a consistent increase in solar radiation across all locations. Lastly, longwave radiation anomalies (rlds) (Fig. 7e) are depicted on a y-axis that spans from -10 W/m² to +30 W/m², reflecting the intensified greenhouse effect. The anomalies increase after 2020, particularly in the SSP5-8.5 scenario, reflecting the enhanced greenhouse effect. Overall, Figure 7 illustrates that Algeria will likely experience more extreme warming, drier conditions, and increased radiation under SSP5-8.5 compared to SSP2-4.5.

For the mean near-surface air temperature (tas: panel 7a), anomaly values of 1.9963 °C for SSP2-4.5, and 1.9415 °C for SSP5-8.5 were obtained compared to the baseline period. In panel 5b it is shown the near-surface relative humidity (hurs) anomaly of the 30-year average centered on the crossing year for the SSP2-4.5 scenario of -1.27 %, and for the SSP5-8.5 of -0. 87 %. The time plot of precipitation (pr) is shown in Fig. 7c, where the precipitation time plot over Algeria gives results for the SSP2-4.5 scenario of -20.4546 mm/Year, and for the SSP5-8.5 scenario, an anomaly of -7.3079 mm/Year is captured compared to the baseline period. In panel 7d the shortwave surface downwelling radiation is shown (rsds). Anomaly of rsds is obtained, for SSP2-4.5 is 2.37 W/m^2, and for SSP5-8.5 is 1.48 W/m^2. For longwave surface downwelling radiation (rlds) variable (panel 7e) anomaly at crossing year, in SSP2-4.5 a value of 9.44 W/m^2 is obtained, and for SSP5-8.5 a value of 9.45 W/m^2, both compared to the baseline period.

3.3.2. Sardegna

In this paragraph five variable over Sardegna were analyzed.

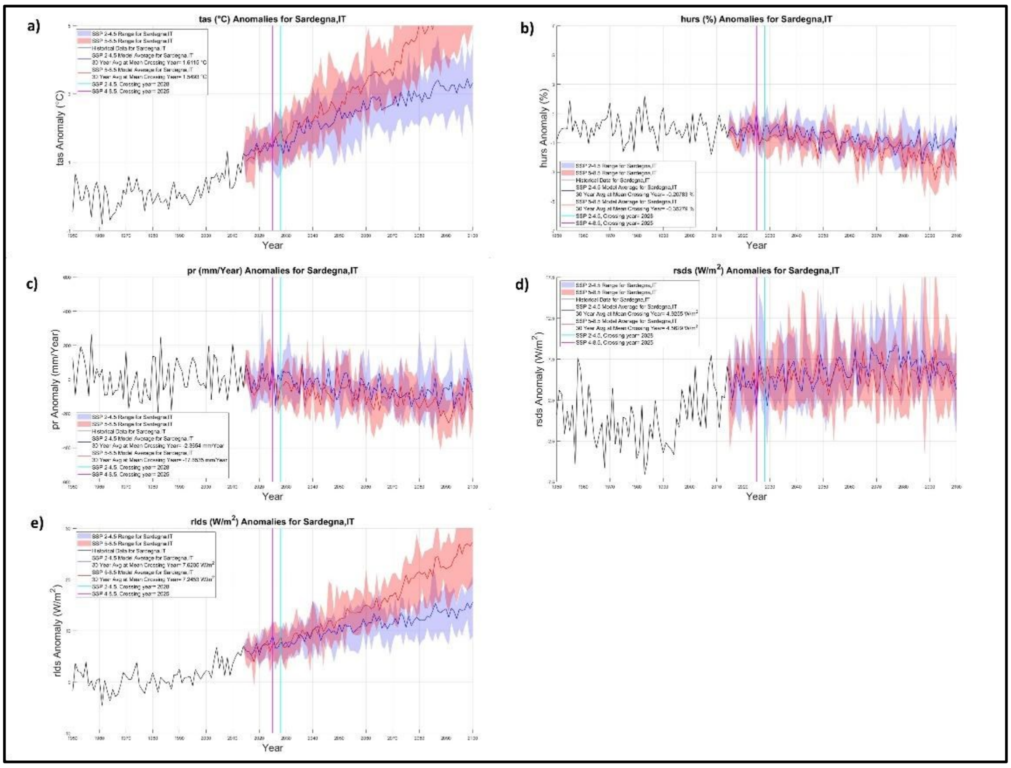

Figure 8 Time plots of each of five variables over Sardegna, Italy; a) temperature anomalies for Sardegna b) relative humidity anomalies for Sardegna c) precipitation anomalies for Sardegna d) surface downwelling shortwave radiation anomalies for Sardegna e) surface downwelling longwave radiation anomalies for Sardegna.

Figure 8 presents time plots for five climate variables over Sardegna, Italy, comparing anomalies under two scenarios: SSP2-4.5 and SSP5-8.5.

Overall, Figure 8 demonstrates that Sardegna, like Algeria, is likely to experience more extreme warming, drier conditions, and increased radiation under the SSP5-8.5 scenario compared to SSP2-4.5.

The historical baseline temperature is represented by the black line. For future projections, SSP2-4.5, shown in blue, projects a gradual increase in temperature anomalies, with a 30-year average centered at the crossing year of 2028 being 1.86 °C. The minimal and maximal anomalies at the mean crossing year of 2025 are 1.30 °C and 2.39 °C, respectively. SSP5-8.5, shown in red, indicates a more significant increase in temperature anomalies, with an average at the crossing year of 2025 being 1.79 °C. The minimal and maximal anomalies at the mean crossing year of 2025 are 1.33 °C and 2.54 °C, respectively. The shaded areas represent the range of uncertainties for both SSP scenarios. The crossing years are identified as 2028 for SSP2-4.5 and 2025 for SSP5-8.5 using the moving median method. Panel 8b depicts relative humidity anomalies (%) over time. The black line shows historical relative humidity. For future projections, SSP2-4.5, indicated in blue, shows a slight decline in relative humidity, with a 30-year average centered at the crossing year of 2028 being -0.82 %. The minimal and maximal anomalies at this crossing year are -2.36 % and 0.90 %, respectively. SSP5-8.5, shown in red, suggests a more pronounced decrease, with an average at the crossing year of 2025 being -0.81 %. The minimal and maximal anomalies at this crossing year are -2.48 % and 0.89 %, respectively. Shaded areas represent the uncertainty range for both SSP scenarios, with crossing years indicated similarly to panel 8a. Panel 8c illustrates precipitation anomalies (mm/year) over time. Historical data is shown with the black line. For future projections, SSP2-4.5, indicated in blue, shows variability in future precipitation anomalies, with a 30-year average centered at the crossing year of 2028 being 18.69 mm/year. The minimal and maximal anomalies at this crossing year are -104.36 mm/year and 229.16 mm/year, respectively. SSP5-8.5, shown in red, also shows significant variability but with a different pattern, averaging 19.19 mm/year at the crossing year of 2025. The minimal and maximal anomalies at this crossing year are -97.06 mm/year and 232.93 mm/year, respectively. Shaded areas highlight the range of uncertainties. Figure 8d shows anomalies in surface downwelling shortwave radiation (W/m^2) over time. Historical baseline is depicted with the black line. For future projections, SSP2-4.5, shown in blue, projects anomalies with a 30-year average centered at the crossing year of 2028 being +4.91 W/m^2. The minimal and maximal anomalies at this crossing year are -2.5712 W/m^2 and +7.83 W/m^2, respectively. SSP5-8.5, shown in red, indicates more pronounced increases, averaging +4.42 W/m^2 at the crossing year of 2025. The minimal and maximal anomalies at this crossing year are -2.75 W/m^2 and 8.22 W/m^2, respectively. Shaded areas indicate uncertainty ranges.

Figure 8e depicts anomalies in surface downwelling longwave radiation (W/m^2) over time. Historical data is shown with the black line. For future projections, SSP2-4.5, shown in blue, projects anomalies with a 30-year average centered at the crossing year of 2028 being 8.27 W/m^2. The minimal and maximal anomalies at this crossing year are 4.40 W/m² and 15.12 W/m², respectively. SSP5-8.5, shown in red, indicates higher increases in anomalies, averaging 7.96 W/m² at the crossing year of 2025. The minimal and maximal anomalies at this crossing year are 4.72 W/m² and 15.97 W/m², respectively. Shaded areas highlight the uncertainties for future projections.

Key remarks include the consistent increase in temperature anomalies for both scenarios, with SSP5-8.5 showing a more significant rise compared to SSP2-4.5. Relative humidity is projected to decline under both scenarios, with a more substantial decrease under SSP5-8.5. Precipitation projections show high variability, with both increases and decreases in different periods and scenarios. Both shortwave and longwave radiation anomalies are projected to increase, with SSP5-8.5 showing higher anomalies than SSP2-4.5.

3.3.3. Milano

In figure 9 we have reported the analysis in a box centered around Milano metropolitan area.

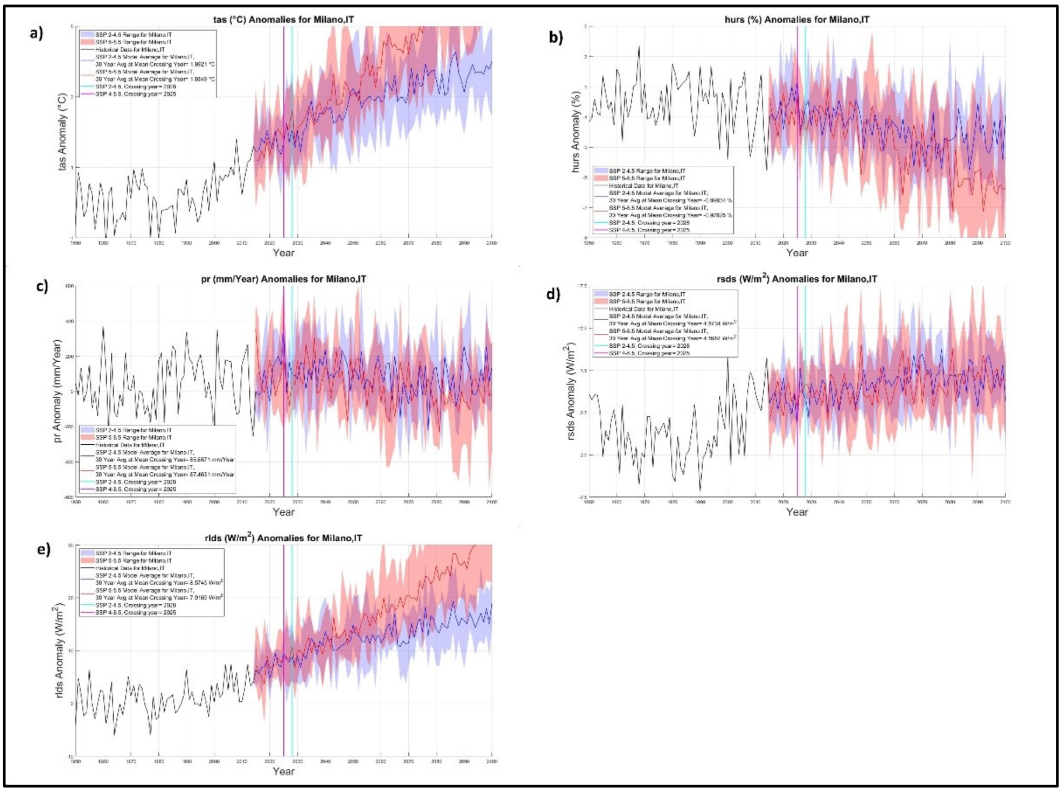

Figure 9: Anomalies time plots of five variables over Milano, Italy; a) temperature; b) relative humidity; c) precipitation; d) surface downwelling shortwave radiation; e) surface downwelling longwave radiation.

Figure 9a shows the near-surface air temperature anomalies (°C) over time. The historical baseline temperature is represented by the black line. For future projections, SSP2-4.5, shown in blue, projects a gradual increase in temperature anomalies with a 30-year average centered at the crossing year of 2028 being 1.86 °C. The minimal and maximal anomalies at the mean crossing year of 2025 are 1.30 °C and 2.39 °C, respectively. SSP5-8.5, shown in red, indicates a more significant increase in temperature anomalies with an average at the crossing year of 2025 being 1.79 °C. The minimal and maximal anomalies at the mean crossing year of 2025 are 1.33 °C and 2.54 °C, respectively. The shaded areas represent the range of uncertainties for both SSP scenarios. The crossing years are identified as 2028 for SSP2-4.5 and 2025 for SSP5-8.5 using the moving median method.

Figure 9b depicts relative humidity anomalies (%) over time. The black line shows historical relative humidity. For future projections, SSP2-4.5, indicated in blue, shows a slight decline in relative humidity, with a 30-year average centered at the crossing year of 2028 being -0.82 %. The minimal and maximal anomalies at this crossing year are -2.36 % and 0.90 %, respectively. SSP5-8.5, shown in red, suggests a more pronounced decrease, with an average at the crossing year of 2025 being -0.81 %. The minimal and maximal anomalies at this crossing year are -2.48 % and 0.89 %, respectively. Shaded areas represent the uncertainty range for both SSP scenarios for precipitation anomalies (mm/year) over time (fig.9c). Historical data is shown with the black line. For future projections, SSP2-4.5, indicated in blue, shows variability in future precipitation anomalies, with a 30-year average centered at the crossing year of 2028 being +18.69 mm/year. The minimal and maximal anomalies at this crossing year are -104.36 mm/year and 229.16

mm/year, respectively. SSP5-8.5, shown in red, also shows significant variability but with a different pattern, averaging +19.1923 mm/year at the crossing year of 2025. The minimal and maximal anomalies at this crossing year are -97.06 mm/year and 232.93 mm/year, respectively. Shaded areas highlight the range of uncertainties. Figure 7d shows anomalies in surface downwelling shortwave radiation (W/m²) over time. The historical baseline is depicted with the black line. For future projections, SSP2-4.5, shown in blue, projects anomalies with a 30-year average centered at the crossing year of 2028 being 4.91 W/m². The minimal and maximal anomalies at this crossing year are -2.57 W/m² and 7.83 W/m², respectively. SSP5-8.5, shown in red, indicates more pronounced increases, averaging 4.42 W/m² at the crossing year of 2025. The minimal and maximal anomalies at this crossing year are -2.75 W/m² and 8.22 W/m², respectively. Shaded areas indicate uncertainty ranges. Panel 9. e) presents anomalies in surface downwelling longwave radiation (W/m²) over time. Historical data is shown with the black line. For future projections, SSP2-4.5, shown in blue, projects anomalies with a 30-year average centered at the crossing year of 2028 being 8.27 W/m². The minimal and maximal anomalies at this crossing year are 4.39 W/m² and 15.13 W/m², respectively. SSP5-8.5, shown in red, indicates higher increases in anomalies, averaging 7.96 W/m² at the crossing year of 2025. The minimal and maximal anomalies at this crossing year are 4.72 W/m² and 15.97 W/m², respectively. Shaded areas highlight the uncertainties for future projections.

3.3.4. Marche Region

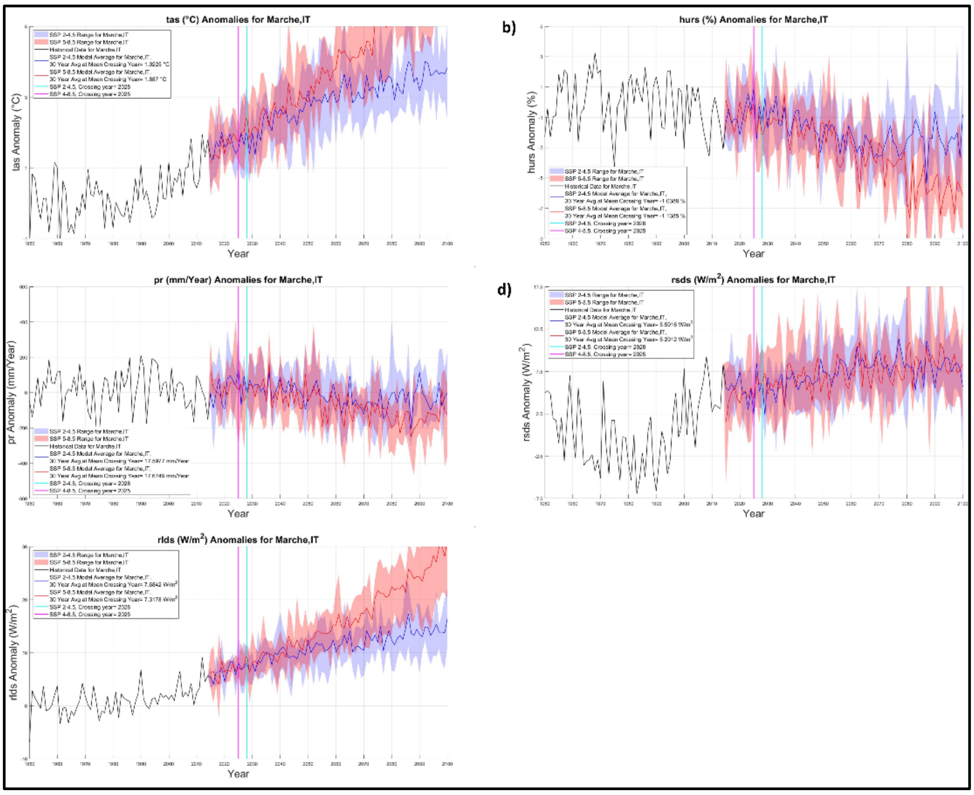

Figure 10: Anomalies time plots of five variables over Marche region, Italy; a) temperature; b) relative humidity; c) precipitation; d) surface downwelling shortwave radiation; e) surface downwelling longwave radiation.

Figure 10 consists of five panels showing climate anomalies for different variables over Marche, Italy, under two SSP (Shared Socioeconomic Pathway) scenarios: SSP2-4.5 and SSP5-8.5.

The five panels of figure 10 present historical data up to the present and future projections with uncertainty ranges. Panel 10a presents the near-surface air temperature anomalies (°C) over time. The historical baseline temperature is represented by the black line. For future projections, SSP2-4.5, shown in blue, projects a gradual increase in temperature anomalies with a 30-year average centered at the crossing year of 2028 being 1.86 °C. The minimal and maximal anomalies at the mean crossing year of 2025 are 1.30 °C and 2.39 °C, respectively. SSP5-8.5, shown in red, indicates a more significant increase in temperature anomalies with an average at the crossing year of 2025 being 1.79 °C. The minimal and maximal anomalies at the mean crossing year of 2025 are 1.33 °C and 2.54 °C, respectively. The shaded areas represent the range of uncertainties for both SSP scenarios. The crossing years are identified as 2028 for SSP2-4.5 and 2025 for SSP5-8.5 using the moving median method. Panel 10b shows relative humidity anomalies (%) over time. The black line represents historical relative humidity. For future projections, SSP2-4.5, indicated in blue, shows a slight decline in relative humidity, with a 30-year average centered at the crossing year of 2028 being -0.82 %. The minimal and maximal anomalies at this crossing year are -2.36 % and 0.90 %, respectively. SSP5-8.5, shown in red, suggests a more pronounced decrease, with an average at the crossing year of 2025 being -0.81 %. The minimal and maximal anomalies at this crossing year are -2.48 % and 0.89 %, respectively. Shaded areas represent the uncertainty range for both SSP scenarios, with crossing years indicated similarly to panel 10a.

Panel 10c presents precipitation anomalies (mm/year) over time. Historical data is shown with the black line. For future projections, SSP2-4.5, indicated in blue, shows variability in future precipitation anomalies, with a 30-year average centered at the crossing year of 2028 being +18.69 mm/year. The minimal and maximal anomalies at this crossing year are -104.36 mm/year and +229.16 mm/year, respectively. SSP5-8.5, shown in red, also shows significant variability but with a different pattern, averaging +19.19 mm/year at the crossing year of 2025. The minimal and maximal anomalies at this crossing year are -97.06 mm/year and +232.93 mm/year, respectively. Shaded areas highlight the range of uncertainties. Figure 10d shows anomalies in surface downwelling shortwave radiation (W/m²) over time. The historical baseline is depicted with the black line. For future projections, SSP2-4.5, shown in blue, projects anomalies with a 30-year average centered at the crossing year of 2028 being +4.91 W/m². The minimal and maximal anomalies at this crossing year are -2.57 W/m² and +7.83 W/m², respectively. SSP5-8.5, shown in red, indicates more pronounced increases, averaging +4.42 W/m² at the crossing year of 2025. The minimal and maximal anomalies at this crossing year are -2.75 W/m² and +8.22 W/m², respectively. Shaded areas indicate uncertainty ranges. Figure 10e presents anomalies in surface downwelling longwave radiation (W/m²) over time. Historical data is shown with the black line. For future projections, SSP2-4.5, shown in blue, projects anomalies with a 30-year average centered at the crossing year of 2028 being 8.27 W/m². The minimal and maximal anomalies at this crossing year are 4.40 W/m² and +15.12 W/m², respectively. SSP5-8.5, shown in red, indicates higher increases in anomalies, averaging +7.96 W/m² at the crossing year of 2025. The minimal and maximal anomalies at this crossing year are +4.7174 W/m² and +15.9732 W/m², respectively. Shaded areas highlight the uncertainties for future projections.

3.3.5. Palermo

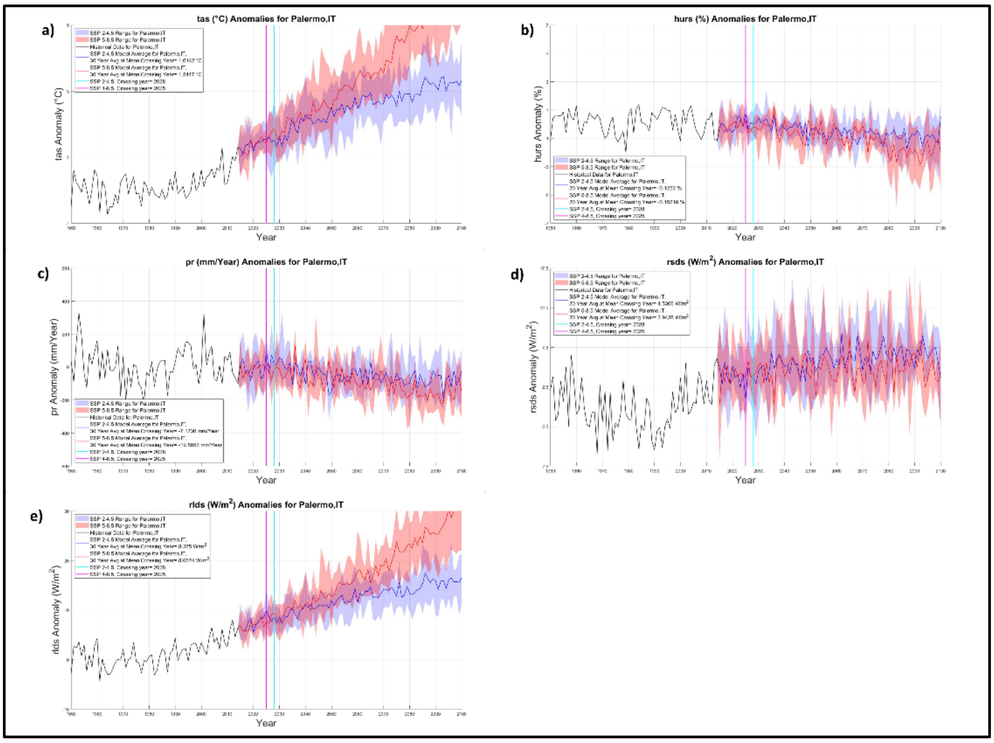

Figure 11 Time plots of five variables over Palermo, Italy; a) temperature anomalies for Palermo b) relative humidity anomalies for Palermo c) precipitation anomalies for Palermo d) surface downwelling shortwave radiation anomalies for Palermo e) surface downwelling longwave radiation anomalies for Palermo.

Figure 11 consists of five panels showing climate anomalies for different variables over Palermo, Italy, under two SSP (Shared Socioeconomic Pathway) scenarios: SSP2-4.5 and SSP5-8.5.

Panel 11a presents the near-surface air temperature anomalies (°C) over time. The historical baseline temperature is represented by the black line. For future projections, SSP2-4.5, shown in blue, projects a gradual increase in temperature anomalies with a 30-year average centered at the crossing year of 2028 being 1.86 °C. The minimal and maximal anomalies at the mean crossing year of 2025 are 1.30 °C and 2.40 °C, respectively. SSP5-8.5, shown in red, indicates a more significant increase in temperature anomalies with an average at the crossing year of 2025 being 1.80 °C. The minimal and maximal anomalies at the mean crossing year of 2025 are 1.33 °C and 2.54 °C, respectively. The shaded areas represent the range of uncertainties for both SSP scenarios. The crossing years are identified as 2028 for SSP2-4.5 and 2025 for SSP5-8.5 using the moving median method.

Panel 11b shows relative humidity anomalies (%) over time. The black line represents historical relative humidity. For future projections, SSP2-4.5, indicated in blue, shows a slight decline in relative humidity, with a 30-year average centered at the crossing year of 2028 being -0.8227 %. The minimal and maximal anomalies at this crossing year are -2.36 % and 0.90 %, respectively. SSP5-8.5, shown in red, suggests a more pronounced decrease, with an average at the crossing year of 2025 being -0.81 %. The minimal and maximal anomalies at this crossing year are -2.49 % and 0.88715 %, respectively. Shaded areas represent the uncertainty range for both SSP scenarios, with crossing years indicated similarly to panel 11a.

Panel 11c presents precipitation anomalies (mm/year) over time. Historical data is shown with the black line. For future projections, SSP2-4.5, indicated in blue, shows variability in future precipitation anomalies, with a 30-year average centered at the crossing year of 2028 being +18.69 mm/year. The minimal and maximal anomalies at this crossing year are -104.36 mm/year and +229.16 mm/year, respectively. SSP5-8.5, shown in red, also shows significant variability but with a different pattern, averaging +19.19 mm/year at the crossing year of 2025. The minimal and maximal anomalies at this crossing year are -97.06 mm/year and +232.93 mm/year, respectively. Shaded areas highlight the range of uncertainties. Figure 11 d) shows anomalies in surface downwelling shortwave radiation (W/m^2) over time. The historical baseline is depicted with the black line. For future projections, SSP2-4.5, shown in blue, projects anomalies with a 30-year average centered at the crossing year of 2028 being +4.91 W/m^2. The minimal and maximal anomalies at this crossing year are -2.57 W/m^2 and +7.83 W/m^2, respectively. SSP5-8.5, shown in red, indicates more pronounced increases, averaging 4.42 W/m^2 at the crossing year of 2025. The minimal and maximal anomalies at this crossing year are -2.75 W/m^2 and +8.22 W/m^2, respectively. Shaded areas indicate uncertainty ranges. Figure 11e presents anomalies in surface downwelling longwave radiation (W/m^2) over time. Historical data is shown with the black line. For future projections, SSP2-4.5, shown in blue, projects anomalies with a 30-year average centered at the crossing year of 2028 being +8.27 W/m^2. The minimal and maximal anomalies at this crossing year are +4.40 W/m^2 and 15.12 W/m^2, respectively. SSP5-8.5, shown in red, indicates higher increases in anomalies, averaging +7.96 W/m^2 at the crossing year of 2025. The minimal and maximal anomalies at this crossing year are +4.71 W/m^2 and +15.97 W/m^2, respectively. Shaded areas highlight the uncertainties for future projections.

3.3.6. Croatia

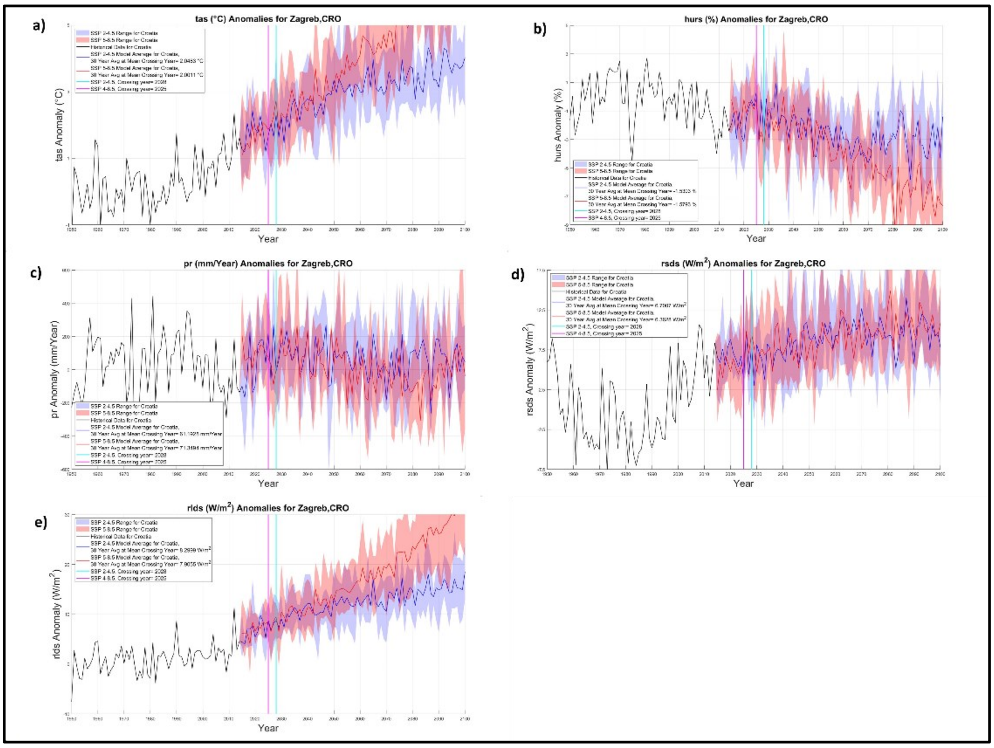

Figure 12 Time plots of five variables over Zagreb, Croatia; a) temperature anomalies for Zagreb, Croatia b) relative humidity anomalies for Zagreb, Croatia c) precipitation anomalies for Zagreb, Croatia d) surface downwelling shortwave radiation anomalies for Zagreb, Croatia e) surface downwelling longwave radiation anomalies for Zagreb, Croatia.

Figure 12 consists of five panels showing climate anomalies for different variables over Zagreb, Croatia, under two SSP (Shared Socioeconomic Pathway) scenarios: SSP2-4.5 and SSP5-8.5.

Panel 12a presents the near-surface air temperature anomalies (°C) over time. The historical baseline temperature is represented by the black line. For future projections, SSP2-4.5, shown in blue, projects a gradual increase in temperature anomalies with a 30-year average centered at the crossing year of 2028 being 1.86 °C. The minimal and maximal anomalies at the mean crossing year of 2025 are 1.30 °C and 2.3905 °C, respectively. SSP5-8.5, shown in red, indicates a more significant increase in temperature anomalies with an average at the crossing year of 2025 being 1.79 °C. The minimal and maximal anomalies at the mean crossing year of 2025 are 1.33 °C and 2.54 °C, respectively. The shaded areas represent the range of uncertainties for both SSP scenarios. The crossing years are identified as 2028 for SSP2-4.5 and 2025 for SSP5-8.5 using the moving median method. Panel 12b shows relative humidity anomalies (%) over time. The black line represents historical relative humidity. For future projections, SSP2-4.5, indicated in blue, shows a slight decline in relative humidity, with a 30-year average centered at the crossing year of 2028 being -0.82 %. The minimal and maximal anomalies at this crossing year are -2.36 % and 0.90 %, respectively. SSP5-8.5, shown in red, suggests a more pronounced decrease, with an average at the crossing year of 2025 being -0.80 %. The minimal and maximal anomalies at this crossing year are -2.48 % and 0.89 %, respectively. Shaded areas represent the uncertainty range for both SSP scenarios, with crossing years indicated similarly to panel 12a.

Panel 12c presents precipitation anomalies (mm/year) over time. Historical data is shown with the black line. For future projections, SSP2-4.5, indicated in blue, shows variability in future precipitation anomalies, with a 30-year average centered at the crossing year of 2028 being 18.69 mm/year. The minimal and maximal anomalies at this crossing year are -104.36 mm/year and 229.16 mm/year, respectively. SSP5-8.5, shown in red, also shows significant variability but with a different pattern, averaging 19.19 mm/year at the crossing year of 2025. The minimal and maximal anomalies at this crossing year are -97.06 mm/year and 232.93 mm/year, respectively. Shaded areas highlight the range of uncertainties. Panel 12d shows anomalies in surface downwelling shortwave radiation (W/m^2) over time. The historical baseline is depicted with the black line. For future projections, SSP2-4.5, shown in blue, projects anomalies with a 30-year average centered at the crossing year of 2028 being 4.91 W/m^2. The minimal and maximal anomalies at this crossing year are -2.57 W/m^2 and 7.83 W/m^2, respectively. SSP5-8.5, shown in red, indicates more pronounced increases, averaging 4.42 W/m^2 at the crossing year of 2025. The minimal and maximal anomalies at this crossing year are -2.75 W/m^2 and 8.22 W/m^2, respectively. Shaded areas indicate uncertainty ranges. Panel 10e presents anomalies in surface downwelling longwave radiation (W/m^2) over time. Historical data is shown with the black line. For future projections, SSP2-4.5, shown in blue, projects anomalies with a 30-year average centered at the crossing year of 2028 being 8.26 W/m². The minimal and maximal anomalies at this crossing year are 4.3993 W/m² and 15.12 W/m², respectively. SSP5-8.5, shown in red, indicates higher increases in anomalies, averaging 7.9582 W/m² at the crossing year of 2025. The minimal and maximal anomalies at this crossing year are 4.72 W/m² and 15.97 W/m², respectively. Shaded areas highlight the uncertainties for future projections.

3.3.7. Bari

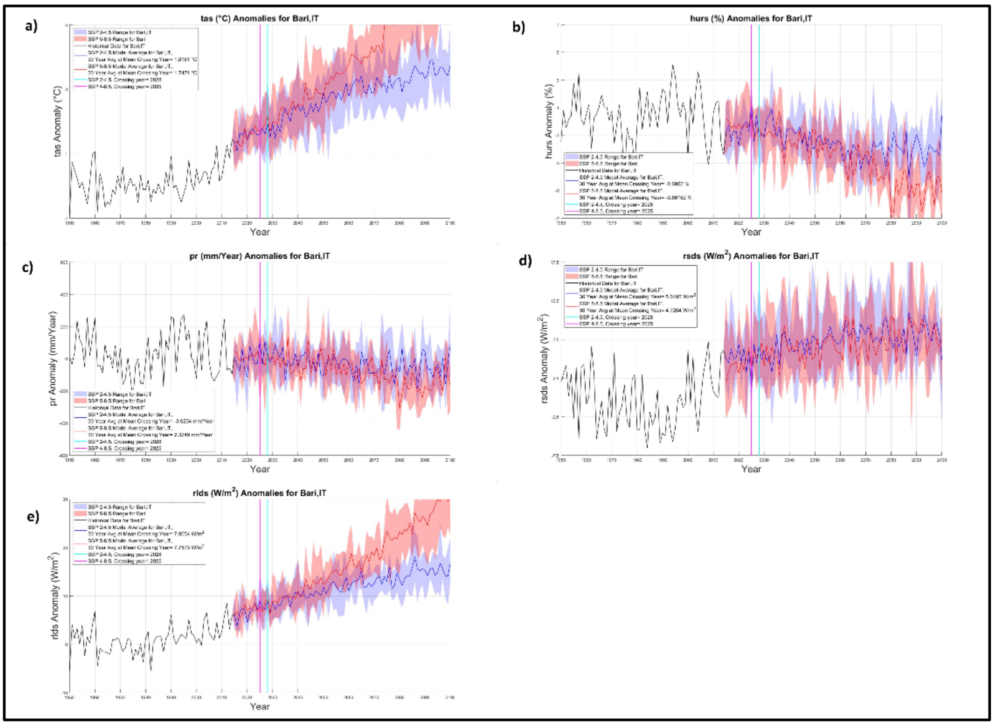

Figure 13 Time plots of five variables over Bari, Italy; a) temperature anomalies for Bari, Italy b) relative humidity anomalies for Bari, Italy c) precipitation anomalies for Bari, Italy d) surface downwelling shortwave radiation anomalies for Bari, Italy e) surface downwelling longwave radiation anomalies for Bari, Italy.

Figure 13 consists of five panels showing climate anomalies for different variables over Bari, Italy, under two SSP (Shared Socioeconomic Pathway) scenarios: SSP2-4.5 and SSP5-8.5.

Panel 13a presents the near-surface air temperature anomalies (°C) over time. The historical baseline temperature is represented by the black line. For future projections, SSP2-4.5, shown in blue, projects a gradual increase in temperature anomalies with a 30-year average centered at the crossing year of 2028 being 1.86 °C. The minimal and maximal anomalies at the mean crossing year of 2025 are 1.30 °C and 2.39 °C, respectively. SSP5-8.5, shown in red, indicates a more significant increase in temperature anomalies with an average at the crossing year of 2025 being 1.79 °C. The minimal and maximal anomalies at the mean crossing year of 2025 are 1.33 °C and 2.54 °C, respectively. The shaded areas represent the range of uncertainties for both SSP scenarios. The crossing years are identified as 2028 for SSP2-4.5 and 2025 for SSP5-8.5 using the moving median method. Panel 13b shows relative humidity anomalies (%) over time. The black line represents historical relative humidity. For future projections, SSP2-4.5, indicated in blue, shows a slight decline in relative humidity, with a 30-year average centered at the crossing year of 2028 being -0.82 %. The minimal and maximal anomalies at this crossing year are -2.36 % and 0.90 %, respectively. SSP5-8.5, shown in red, suggests a more pronounced decrease, with an average at the crossing year of 2025 being -0.81 %. The minimal and maximal anomalies at this crossing year are -2.48 % and 0.89 %, respectively. Shaded areas represent the uncertainty range for both SSP scenarios, with crossing years indicated similarly to panel 13a.

Panel 13c presents precipitation anomalies (mm/year) over time. Historical data is shown with the black line. For future projections, SSP2-4.5, indicated in blue, shows variability in future precipitation anomalies, with a 30-year average centered at the crossing year of 2028 being 18.69 mm/year. The minimal and maximal anomalies at this crossing year are -104.3604 mm/year and 229.16 mm/year, respectively. SSP5-8.5, shown in red, also shows significant variability but with a different pattern, averaging 19.19 mm/year at the crossing year of 2025. The minimal and maximal anomalies at this crossing year are -97.06 mm/year and 232.93 mm/year, respectively. Shaded areas highlight the range of uncertainties. Panel 13d shows anomalies in surface downwelling shortwave radiation (W/m^2) over time. The historical baseline is depicted with the black line. For future projections, SSP2-4.5, shown in blue, projects anomalies with a 30-year average centered at the crossing year of 2028 being 4.91 W/m^2. The minimal and maximal anomalies at this crossing year are -2.57 W/m^2 and 7.83 W/m^2, respectively. SSP5-8.5, shown in red, indicates more pronounced increases, averaging 4.42 W/m^2 at the crossing year of 2025. The minimal and maximal anomalies at this crossing year are -2.75 W/m^2 and 8.22 W/m^2, respectively. Shaded areas indicate uncertainty ranges. Panel 13e presents anomalies in surface downwelling longwave radiation (W/m^2) over time. Historical data is shown with the black line. For future projections, SSP2-4.5, shown in blue, projects anomalies with a 30-year average centered at the crossing year of 2028 being 8.27 W/m^2. The minimal and maximal anomalies at this crossing year are 4.40

W/m² and 15.12 W/m², respectively. SSP5-8.5, shown in red, indicates higher increases in anomalies, averaging 7.96 W/m² at the crossing year of 2025. The minimal and maximal anomalies at this crossing year are 4.71 W/m² and 15.97 W/m², respectively. Shaded areas highlight the uncertainties for future projections.

3.3.8. Mediterranean basin

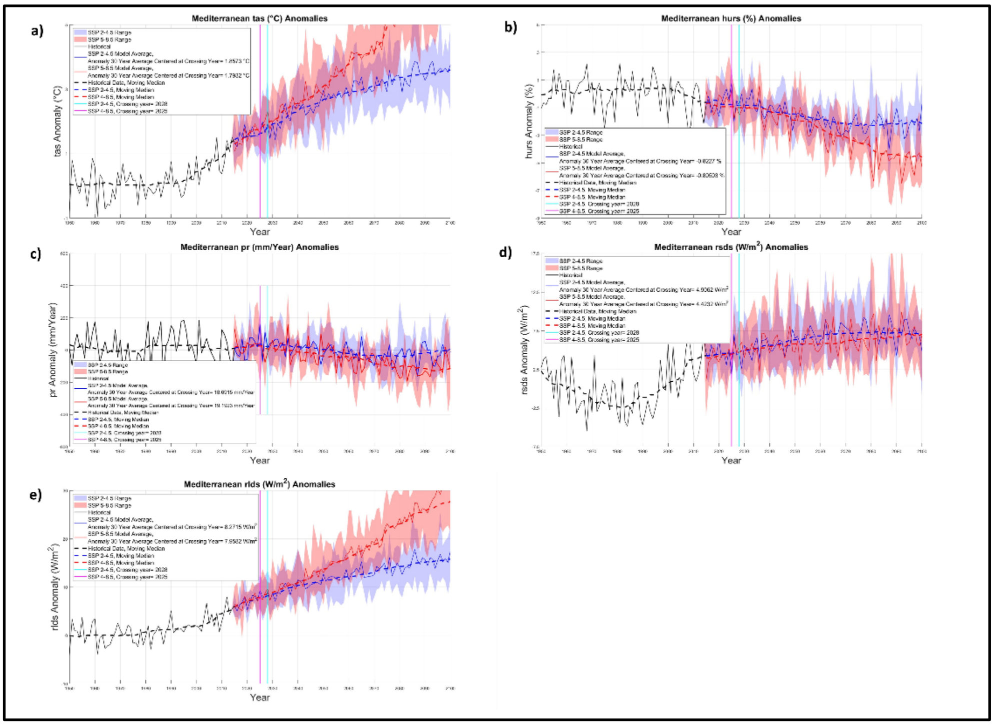

Figure 14 Time plots of the five variables averaged over the selected points.

The figure 14 consists of multiple panels illustrating the anomalies of various climate variables in the Mediterranean basin

These panels show historical data and future projections under two different SSP (Shared Socioeconomic Pathway) scenarios. Panel 14 a) depicts the Mediterranean temperature anomalies (tas in °C) over time. The historical baseline temperature is 286.6750°C. For SSP2-4.5, the temperature anomaly averaged at 7 locations with a 30-year average centered at the crossing year of 2028 is 1.86 °C. The minimal and maximal anomalies at the mean crossing year of 2025 are 1.30 °C and 2.39 °C, respectively. For SSP5-8.5, the anomaly averaged at the crossing year of 2025 is 1.79 °C, with minimal and maximal anomalies at the mean crossing year of 2025 being 1.33 °C and 2.54 °C, respectively. The historical data is represented by the black line, while the colored lines and shaded areas indicate the projected anomalies and their uncertainties under different SSP scenarios. Both scenarios show an increasing trend in temperature anomalies, with SSP5-8.5 indicating higher warming compared to SSP2-4.5. Panel 14 b) illustrates the Mediterranean relative humidity (hurs) anomalies over time. The historical baseline relative humidity is 73.98 %. For SSP2-4.5, the relative humidity anomaly averaged at 7 locations with a 30-year average centered at the crossing year of 2028 is

-0.82 %. The minimal and maximal anomalies at this crossing year are -2.36 % and 0.91 %, respectively. For SSP5-8.5, the anomaly averaged at the crossing year of 2025 is -0.81%, with minimal and maximal anomalies at this crossing year being -2.48 % and 0.89 %, respectively. Historical data is shown in black, and future projections are depicted for SSP2-4.5 in blue and SSP5-8.5 in red, with shaded uncertainty ranges. The relative humidity anomalies exhibit more variability than temperature anomalies, with both scenarios suggesting a potential decrease in relative humidity in the future. SSP5-8.5 shows a more significant decline. Panel 14. c) presents the Mediterranean precipitation (pr) anomalies (in mm/year) over time. The historical baseline precipitation is 781.10 mm/year. For SSP2-4.5, the precipitation anomaly averaged at 7 locations with a 30-year average centered at the crossing year of 2028 is 18.69 mm/year. The relatively high baseline precipitation value of 781.10 mm/year reflects the cumulative nature of precipitation data averaged over the selected locations, some of which may experience wetter conditions. Additionally, the baseline period (1950-1980) might have included regions with naturally higher rainfall, contributing to the overall high value. The precipitation anomaly of 18.69 mm/year under SSP2-4.5, centered around the crossing year of 2028, can be attributed to regional variations in climate response, where some areas may experience increased rainfall even in moderate climate change scenarios.

The minimal and maximal anomalies at this crossing year are -104.3604 mm/year and 229.16 mm/year, respectively. For SSP5-8.5, the anomaly averaged at the crossing year of 2025 is 19.19 mm/year, with minimal and maximal anomalies at this crossing year being -97.06 mm/year and 232.93 mm/year, respectively. The black line represents historical precipitation data, while future scenarios are shown in blue for SSP2-4.5 and red for SSP5-8.5, with shaded areas indicating uncertainties. Precipitation anomalies display considerable variability, with projections showing a mix of increases and decreases. There is a slight tendency towards more variability under SSP5-8.5. Panel 14. d) shows the surface downwelling shortwave radiation (rsds) anomalies (in W/m^2) over time. The historical baseline rsds is 197.07 W/m^2. For SSP2-4.5, the rsds anomaly averaged at 7 locations with a 30-year average centered at the crossing year of 2028 is 4.91 W/m^2. The minimal and maximal anomalies at this crossing year are -2.57 W/m^2 and 7.83 W/m^2, respectively. For SSP5-8.5, the anomaly averaged at the crossing year of 2025 is 4.42 W/m^2, with minimal and maximal anomalies at this crossing year being -2.75 W/m^2 and 8.22 W/m^2, respectively. Historical data is represented in black, with future projections for SSP2-4.5 shown in blue and for SSP5-8.5 shown in red, with their uncertainties shaded. Both scenarios indicate an increase in rsds anomalies, with SSP5-8.5 projecting a more pronounced increase, suggesting higher incoming shortwave radiation under this scenario. Panel 14. e) depicts the surface downwelling longwave radiation (rlds) anomalies (in W/m^2) over time. The historical baseline rlds is 311.5917 W/m^2. For SSP2-4.5, the rlds anomaly averaged at 7 locations with a 30-year average centered at the crossing year of 2028 is 8.27 W/m^2. The minimal and maximal anomalies at this crossing year are 4.40 W/m² and 15.12 W/m², respectively. For SSP5-8.5, the anomaly averaged at the crossing year of 2025 is 7.96 W/m², with minimal and maximal anomalies at this crossing year being 4.72 W/m² and 15.97 W/m², respectively. The historical data is shown in black, with future scenarios depicted in blue for SSP2-4.5 and red for SSP5-8.5, along with shaded uncertainty ranges. The anomalies in rlds show an increasing trend, with SSP5-8.5 projecting a higher increase in longwave radiation compared to SSP2-4.5. Overall, each panel highlights the differences in climate projections between SSP2-4.5 and SSP5-8.5. SSP5-8.5 generally shows more extreme changes in all variables, indicating a higher impact of the higher emission scenario. Understanding these anomalies is crucial for climate impact assessments and developing strategies to mitigate and adapt to climate change in the Mediterranean region.

Next figure (15) consists of two maps showing temperature anomalies in the Mediterranean region. These panels show historical data and future projections under two different SSP (Shared Socioeconomic Pathway) scenarios.

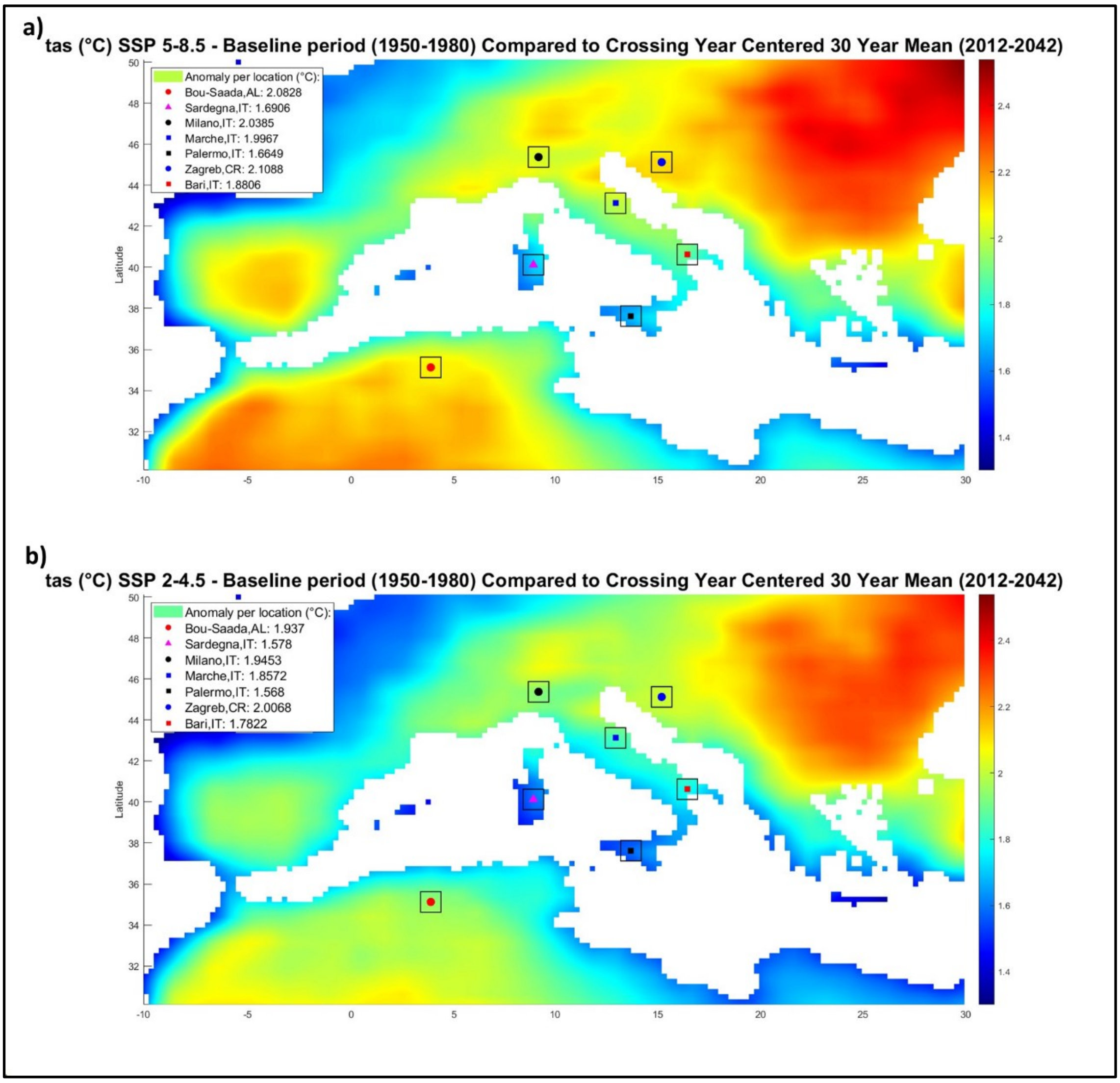

Figure 15 Climate differences Mediterranean map which includes all of 7 boxes of locations. Panel a irepresents the SSP5-8.5 scenario represents the upper boundary of the range of scenarios

described in the literature with an additional radiative forcing of 8.5 W m^{-2} by the year 2100 (Park et al., 2023). Panel b represents the intermediate scenario, in which current climate change trends continue without substantial deviations, leading to a forcing pathway of 4.5 W m^{-2} by 2100 is shown.

Figure 15 figure consists of two maps showing temperature anomalies in the Mediterranean region. The temperature anomalies shown in figure 15 for the Mediterranean region are calculated by comparing future temperature projections with a defined baseline period. Specifically, the baseline average temperature was established from the years 1950 to 1980, serving as a reference point. Climate models are then utilized to simulate future conditions under two different Shared Socioeconomic Pathways (SSPs): SSP 5-8.5, which represents a high greenhouse gas concentration scenario with a radiative forcing of 8.5 W/m^2 by 2100, and SSP 2-4.5, a moderate pathway leading to a forcing of 4.5 W/m^2. For each scenario, the projected average temperature for the crossing year centered 30-year mean (2012-2042) is calculated. The temperature anomalies are determined by subtracting the baseline average from the future average, resulting in values that indicate how much warmer (or cooler) temperatures are expected under the different scenarios. These anomalies are then mapped spatially across the Mediterranean region, using color scales to visually represent the magnitude of temperature changes, with blue indicating lower anomalies and red signifying higher anomalies. These maps compare the baseline period (1950-1980) to the crossing year centered 30-year mean (2012-2042) under two different SSP (Shared Socioeconomic Pathway) scenarios. The map on figure 15a uses the SSP 5-8.5 scenario, which is the highest greenhouse gas concentration pathway. The color scale represents temperature anomalies in degrees Celsius. The anomalies range from around 1.4°C (blue) to over 2.4°C (red). Specific locations are marked with symbols, and their respective temperature anomalies are listed in the legend. In the map of figure 15b the SSP 2-4.5 scenario, which is a moderate greenhouse gas concentration pathway is shown. The anomalies for the same locations are different from those in the SSP 5-8.5 scenario, reflecting the different impacts of the two pathways, anomalies in this case range from around 1.4°C (blue) to over 2.4°C (red).

Figure 16 shows the modeled temperature data (tas) for various locations in the Mediterranean from 2010 to 2100, and highlights geographical variations in the rate of temperature increase. Locations with larger bubbles are experiencing faster rates of warming.

a)

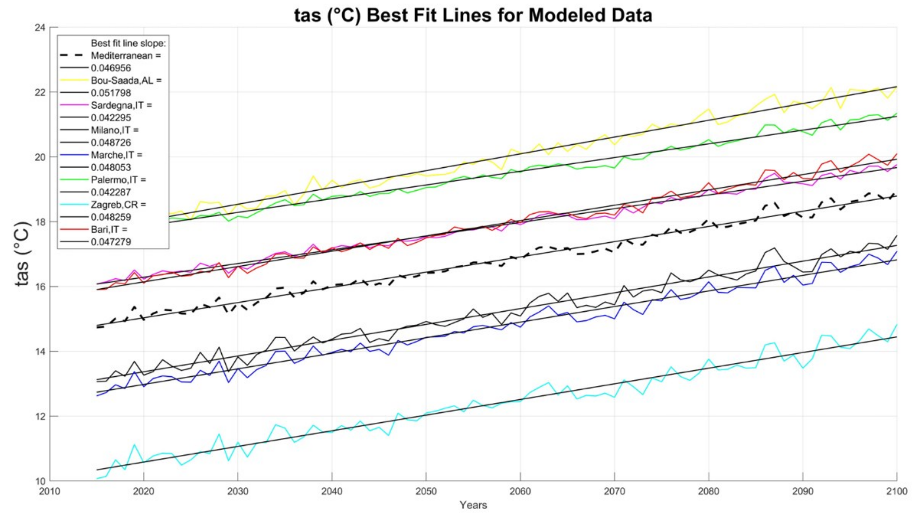

b)

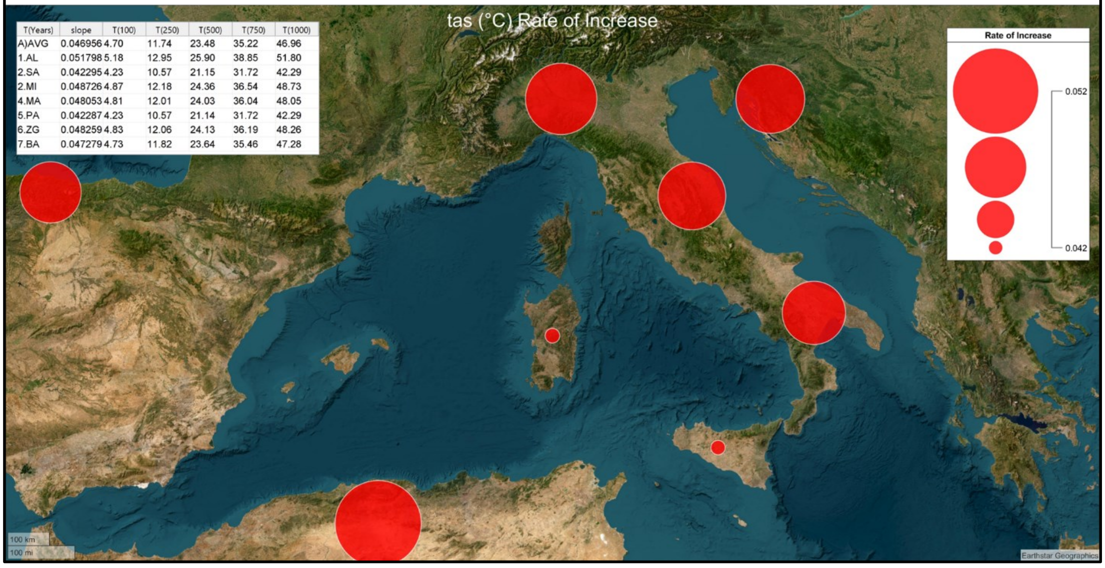

T(Years)	slope	T(100)	T(250)	T(500)	T(750)	T(1000)
A)AVG	0.046956	4.70	11.74	23.48	35.22	46.96
1.AL	0.051798	5.18	12.95	25.90	38.85	51.80
2.SA	0.042295	4.23	10.57	21.15	31.72	42.29
2.MI	0.048726	4.87	12.18	24.36	36.54	48.73
4.MA	0.048053	4.81	12.01	24.03	36.04	48.05
5.PA	0.042287	4.23	10.57	21.14	31.72	42.29
6.ZG	0.048259	4.83	12.06	24.13	36.19	48.26
7.BA	0.047279	4.73	11.82	23.64	35.46	47.28

Figure 16 The provided figure consists of two parts, each illustrating different aspects of temperature anomalies, best fit lines a) and their rates of increase b) in the Mediterranean region.

Figure 16a shows the modeled temperature data (tas) for various locations in the Mediterranean from 2010 to 2100. Each line represents a best fit for the temperature trend over this period. The legend provides the slope values for each location, indicating the rate of temperature increase per year. The slopes in the legend indicate the annual increase in temperature for each location. For instance, Bou-Saada, Algeria is showing a higher slope, implying a faster rate of temperature increase compared to other locations. The linear rate in figure 16a shows a clear upward trend in temperatures for all locations, with varying rates of increase. The Mediterranean average (black dashed line) provides a benchmark for comparing individual locations. Figure 16b) highlights geographical variations in the rate of temperature increase. Locations with larger bubbles are experiencing faster rates of warming. This visual representation helps identify hotspots of climate change impact within the region. The combination of best fit lines and bubble maps offers a comprehensive view of both temporal and spatial variations in temperature anomalies.

Figure 17, next in the paragraph shows the relative humidity anomalies under the SSP5-8.5 scenario, which represents a high greenhouse gas concentration pathway. The color scale represents relative humidity anomalies, with red indicating a more significant decrease and blue indicating an increase.

a)

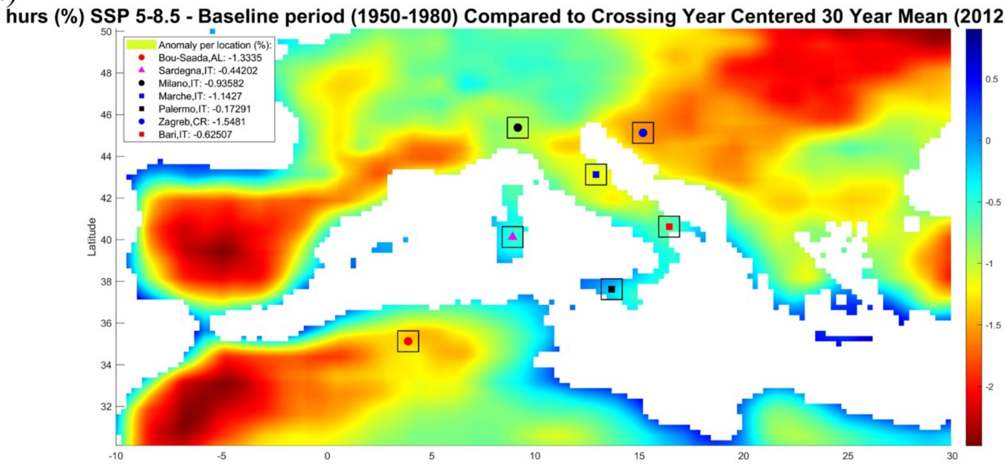
hurs (%) SSP 5-8.5 - Baseline period (1950-1980) Compared to Crossing Year Centered 30 Year Mean (2012-2042)
Anomaly per location (%):
Bou-Saada,AL: -1.3335
Sardegna,IT: -0.44202
Milano,IT: -0.93582
Marche,IT: -1.1427
Palermo,IT: -0.17291
Zagreb,CR: -1.5481
Bari,IT: -0.62507
Latitude
50
48
46
44
42
40
38
36
34
32
-10
-5
0
5
10
15
20
25
30
0.5
0
-0.5
-1
-1.5
-2

b)

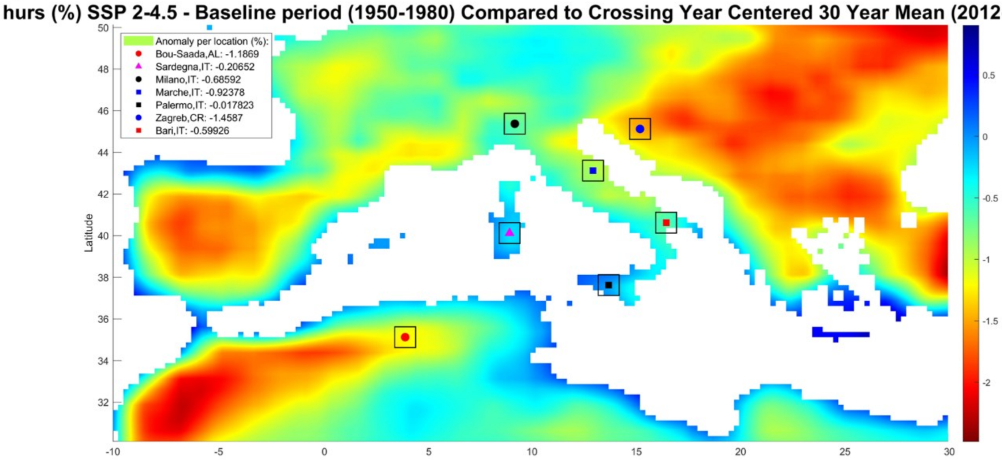
hurs (%) SSP 2-4.5 - Baseline period (1950-1980) Compared to Crossing Year Centered 30 Year Mean (2012-2042)
Anomaly per location (%):
Bou-Saada,AL: -1.1869
Sardegna,IT: -0.20652
Milano,IT: -0.68592
Marche,IT: -0.92378
Palermo,IT: -0.017823
Zagreb,CR: -1.4587
Bari,IT: -0.59926
Latitude
50
48
46
44
42
40
38
36
34
32
-10
-5
0
5
10
15
20
25
30
0.5
0
-0.5
-1
-1.5
-2

Figure 17 This figure consists of two panels illustrating the relative humidity anomalies (%) in the Mediterranean region for the baseline period (1950-1980) compared to the crossing year centered 30-year mean (2012-2042) under two different SSP (Shared Socioeconomic Pathway) scenarios: SSP5-8.5 and SSP2-4.5. Each panel shows the spatial distribution of these anomalies, with specific locations marked and their respective anomalies listed.

The relative humidity anomalies presented in Figure 17 are calculated by comparing future projections of relative humidity (hurs) to a defined baseline period (1950-1980). First, the average relative humidity for the baseline period is established using historical climate data. Climate models then simulate future conditions under two Shared Socioeconomic Pathways SSP5-8.5 and SSP2-4.5. For the future years centered around 30-year means (2012-2042), relative humidity data is generated, allowing for the calculation of anomalies using the formula: *Anomaly = hurs_future - hurs_baseline.* This calculation is performed for each grid point across the Mediterranean region, where specific locations are marked on the map. The resulting anomalies are mapped spatially, revealing areas of significant decrease (indicated in red) or increase (indicated in blue) in relative humidity, with the magnitude of changes represented by a color scale. Figure 17a shows the relative humidity anomalies under the SSP5-8.5 scenario. The color scale represents relative humidity anomalies. The range of anomalies is from -2.0% to +0.5%. Specific locations and their respective anomalies are Bou-Saada, Algeria with -1.43 %, Sardegna (Italy) with -0.40 %, Milano (Italy) with -1.25 %, Marche (Italy) with -0.94 %, Palermo (Italy) with -1.07 %, Zagreb (Croatia) with -1.17 %, and Bari (Italy) with -0.33 %. The map shows that most of the Mediterranean region, especially the areas marked with specific locations, is projected to experience a decrease in relative humidity under the SSP5-8.5 scenario. Panel 17b presents the relative humidity anomalies under SSP2-4.5. The color scale is the same as in panel a, representing relative humidity anomalies ranging from -2.0 % to +0.5 %. Specific locations and their respective anomalies are Bou-Saada, Algeria with -1.17 %, Sardegna with -0.10 %, Milano with -0.66 %, Marche with -0.38 %, Palermo with -0.61 %, Zagreb with -1.15 %, and Bari with -0.60 %. The map indicates that under the SSP2-4.5 scenario, the Mediterranean region is also projected to experience a decrease in relative humidity, though the anomalies are generally less pronounced compared to the SSP5-8.5 scenario. Both scenarios show a general trend of decreasing relative humidity across the Mediterranean region, with SSP5-8.5 showing more significant decreases compared to SSP2-4.5. There is spatial variability in the magnitude of relative humidity anomalies, with some areas experiencing larger decreases than others. Decreasing relative humidity can have significant impacts on agriculture, water resources, and ecosystem health in the Mediterranean region. The more pronounced decreases under SSP5-8.5 highlight the greater potential impact of higher greenhouse gas emissions. These observations emphasize the importance of considering different emission scenarios in climate projections and the need for adaptive strategies to mitigate the impacts of decreased relative humidity in the Mediterranean region.

In figure 18 (next in the paragraph) the relative humidity anomalies (%) in the Mediterranean region are presented, providing insights into the projected changes in humidity levels over time using modeled data.

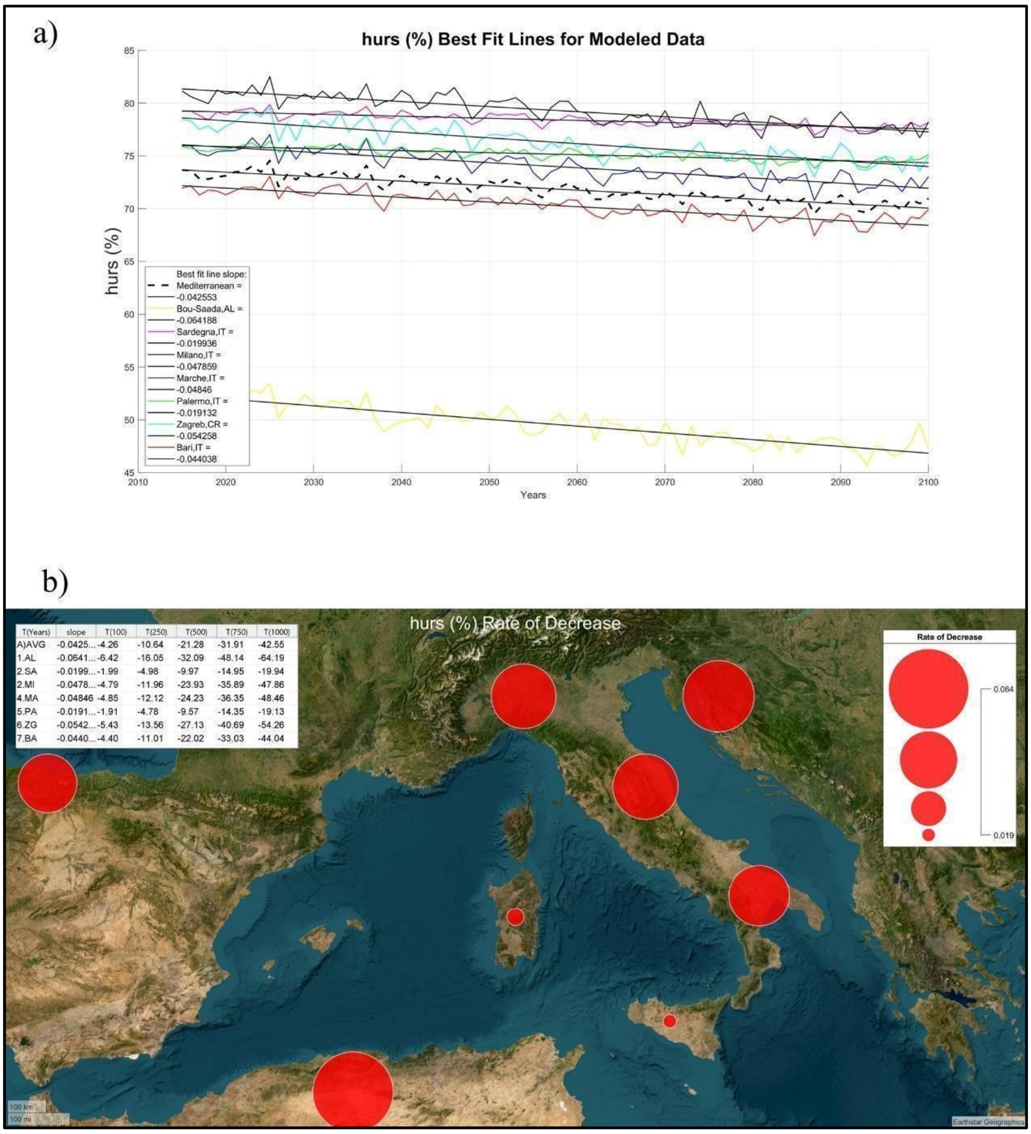

T(Years)	slope	T(100)	T(250)	T(500)	T(750)	T(1000)
A)AVG	-0.0425...	-4.26	-10.64	-21.28	-31.91	-42.55
1.AL	-0.0641...	-6.42	-16.05	-32.09	-48.14	-64.19
2.SA	-0.0199...	-1.99	-4.98	-9.97	-14.95	-19.94
2.MI	-0.0478...	-4.79	-11.96	-23.93	-35.89	-47.86
4.MA	-0.04846	-4.85	-12.12	-24.23	-36.35	-48.46
5.PA	-0.0191...	-1.91	-4.78	-9.57	-14.35	-19.13
6.ZG	-0.0542...	-5.43	-13.56	-27.13	-40.69	-54.26
7.BA	-0.0440...	-4.40	-11.01	-22.02	-33.03	-44.04

Figure 18 consists of two panels illustrating the relative humidity anomalies (%) in the Mediterranean region using modeled data and their *rates of decrease over time; a) Best Fit Lines for Modeled Data, b) Rate of Decrease.*

In figure 18, the relative humidity anomalies (%) in the Mediterranean region are presented, providing insights into the projected changes in humidity levels over time using modeled data. The figure is divided into two panels: figure 18a focuses on the best fit lines for the modeled data, while figure 18b details the rates of decrease in relative humidity.

In figure 18a, the best fit lines represent the trends in relative humidity (hurs) from 2010 to 2100 for various locations within the Mediterranean region. These lines are calculated through linear regression, a statistical method used to fit a straight line to the data points. This process involves taking historical relative humidity data and future projections obtained from climate models under specific scenarios, such as higher greenhouse gas concentration pathways. The slope of each line indicates the rate of change in relative humidity for the corresponding location, with a negative slope signifying a decrease in humidity levels over time. The legend accompanying the plot identifies each location, providing its specific slope, which quantifies how much relative humidity is expected to decrease annually. The analysis reveals that most locations are projected to experience a decline in relative humidity, suggesting a potential shift towards drier conditions in the region.

Figure 18b complements the first by visually depicting the geographical variability in the rate of decrease. The map highlights specific locations marked with circles, where the size of each circle correlates to the magnitude of the decrease in relative humidity. Larger circles indicate a more significant decline, while smaller circles represent lesser reductions. The accompanying table provides numerical details, including the slopes derived from the best fit lines for each location, showcasing the rates of decrease in relative humidity. For example, specific locations may show decreases of around 0.064% per year, illustrating the varying impacts of climate change across the region.

Figure 19, consists of two panels illustrating precipitation anomalies (pr in mm/year) in the Mediterranean region for the baseline period (1950-1980) compared to the crossing year centered 30-year mean (2012-2042) under two different SSP (Shared Socioeconomic Pathway) scenarios: SSP5-8.5 and SSP2-4.5. Each panel shows the spatial distribution of these anomalies, with specific locations marked and their respective anomalies listed.

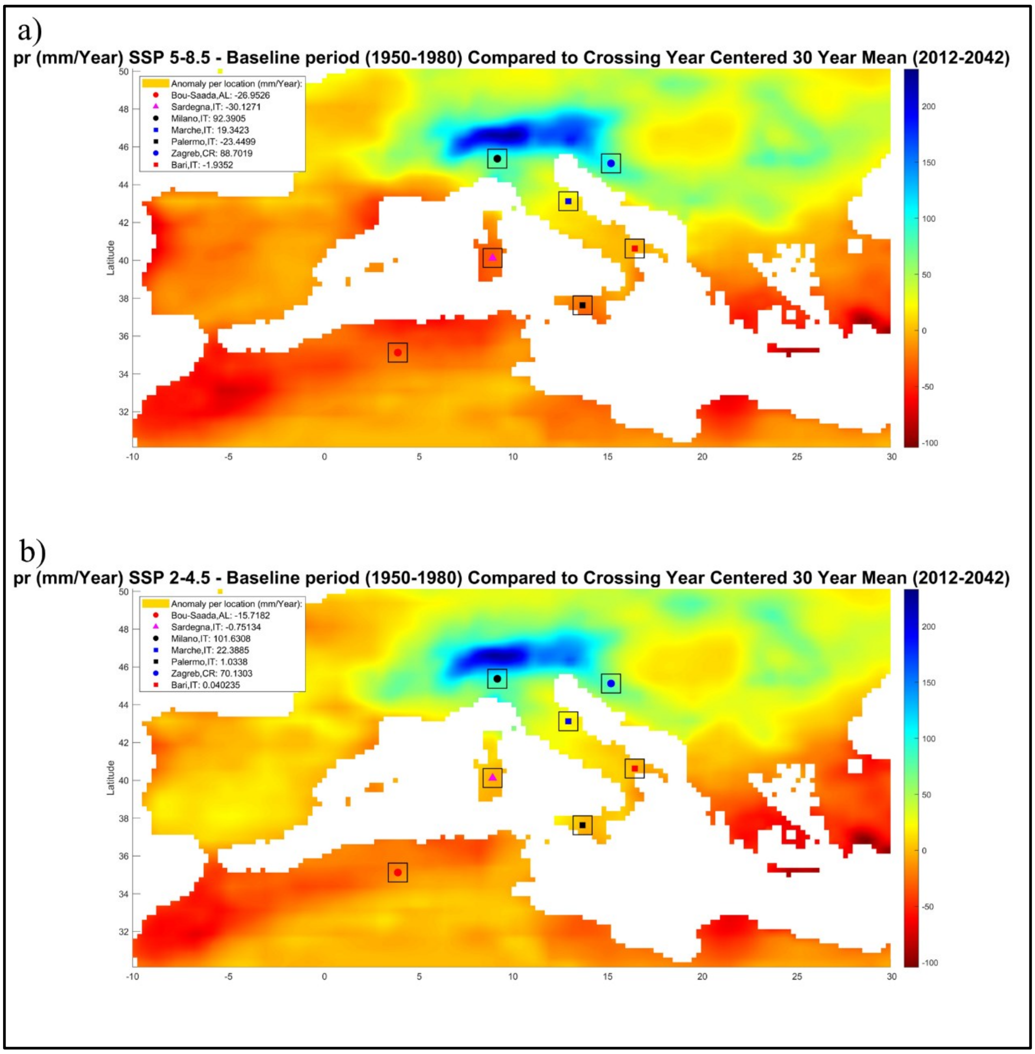

a) pr (mm/Year) SSP 5-8.5 - Baseline period (1950-1980) Compared to Crossing Year Centered 30 Year Mean (2012-2042)

b) pr (mm/Year) SSP 2-4.5 - Baseline period (1950-1980) Compared to Crossing Year Centered 30 Year Mean (2012-2042)

Figure 19 consists of two panels illustrating the precipitation anomalies (mm/year) in the Mediterranean region for the baseline period (1950-1980) compared to the crossing year centered 30-year mean (2012-2042) under two different SSP (Shared Socioeconomic Pathway) scenarios: SSP5-8.5 and SSP2-4.5. Each panel shows the spatial *distribution of these anomalies, with specific locations marked and their respective anomalies listed.*

Figure 19a shows the precipitation anomalies under the SSP5-8.5 scenario. The color scale represents precipitation anomalies, with red indicating a decrease and blue indicating an increase. The range of anomalies is from -100.00 mm/year to +200.00 mm/year. Specific locations and their respective anomalies are: Bou-Saada, Algeria (AL) with -45.96 mm/year, Sardegna with -31.79 mm/year, Milano with -37.90 mm/year, Marche with -12.32 mm/year, Palermo with -29.44 mm/year, Zagreb with 22.84 mm/year, and Bariwith -1.40 mm/year. The map shows that most of the Mediterranean region is projected to experience a decrease in precipitation under the SSP5-8.5 scenario, with some areas, such as Zagreb, Croatia, experiencing an increase. Figure 19b presents the precipitation anomalies under the SSP2-4.5 scenario, which represents a moderate greenhouse gas concentration pathway. The color scale is the same as in Figure 17a, representing precipitation anomalies ranging from -100.00 mm/year to +200.00 mm/year. Specific locations and their respective anomalies are: Bou-Saada, Algeria (AL) with -15.18 mm/year, Sardegna with -7.51 mm/year, Milano with 1.00 mm/year, Marche, with 12.38 mm/year, Palermo with -2.03 mm/year, Zagreb with 10.13 mm/year, and Bariwith 0.05 mm/year. The map indicates that under the SSP2-4.5 scenario, the Mediterranean region shows a mix of decreases and increases in precipitation, with less pronounced decreases compared to the SSP5-8.5 scenario. Both scenarios reveal a general trend of decreasing precipitation across much of the Mediterranean region, with the SSP5-8.5 scenario showing more significant decreases. There is spatial variability in the magnitude of precipitation anomalies, with some areas experiencing increases in precipitation under the SSP2-4.5 scenario. The more pronounced decreases under the SSP5-8.5 scenario highlight the greater potential impact of higher greenhouse gas emissions on precipitation patterns. These observations emphasize the importance of considering different emission scenarios in climate projections. Understanding these trends is crucial for developing effective adaptation measures to cope with the anticipated changes in precipitation, which can significantly impact water resources, agriculture, and ecosystem health in the Mediterranean region.

Figure 20 consists of two panels illustrating precipitation anomalies (pr in mm/year) in the Mediterranean region using modeled data and their rates of decrease over time.

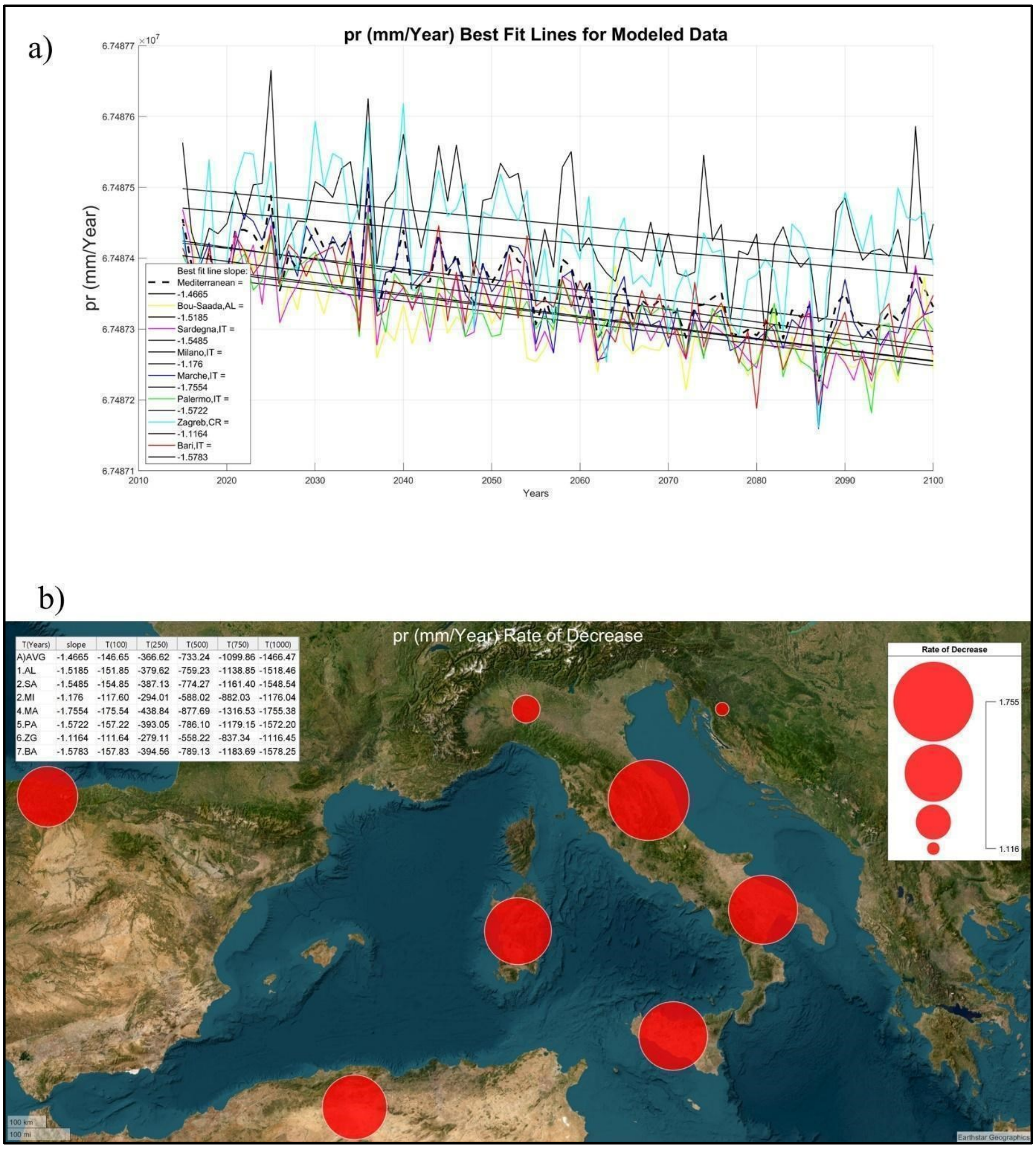

T(Years)	slope	T(100)	T(250)	T(500)	T(750)	T(1000)
A)AVG	-1.4665	-146.65	-366.62	-733.24	-1099.86	-1466.47
1.AL	-1.5185	-151.85	-379.62	-759.23	-1138.85	-1518.46
2.SA	-1.5485	-154.85	-387.13	-774.27	-1161.40	-1548.54
2.MI	-1.176	-117.60	-294.01	-588.02	-882.03	-1176.04
4.MA	-1.7554	-175.54	-438.84	-877.69	-1316.53	-1755.38
5.PA	-1.5722	-157.22	-393.05	-786.10	-1179.15	-1572.20
6.ZG	-1.1164	-111.64	-279.11	-558.22	-837.34	-1116.45
7.BA	-1.5783	-157.83	-394.56	-789.13	-1183.69	-1578.25

Figure 20 consists of two panels illustrating precipitation anomalies (pr in mm/year) in the Mediterranean region using modeled data and their rates of decrease over time; a) Best Fit Lines for Modeled Data, b) Rate of Decrease.

Figure 20a shows the best fit lines for precipitation (pr) for various locations from 2010 to 2100. Each line represents the modeled data for a specific location, with the legend providing the slope values, indicating the rate of decrease in precipitation per year. Specific locations and their slope values are: Mediterranean average with a slope of -1.4685, Bou-Saada with a slope of -1.585, Sardegna with a slope of -1.125, Milano with a slope of -1.470, Marche with a slope of -1.176, Palermo with a slope of -1.573, Zagreb with a slope of -1.570, and Bari with a slope of -1.579. The graph shows a general downward trend in precipitation across all locations, with Bou-Saada, , exhibiting the steepest decline, indicating the fastest rate of decrease in precipitation, while Sardegna shows the slowest rate of decrease. Figure 20b provides a geographical representation of the rate of decrease in precipitation (mm/year) across the Mediterranean region. The size of the red circles indicates the magnitude of the decrease, with larger circles representing a faster rate of decrease. The rate of decrease in precipitation across the selected locations varies significantly over different timescales. In Bou-Saada, Algeria (AL), the rate of decrease ranges from -151.85 mm/year over 10 years to -1518.46 mm/year over 1000 years. Sardegna (SA) shows a similar trend, with a decrease ranging from -154.85 mm/year over 10 years to -1548.54 mm/year over 1000 years. Milano (MI) experiences a decrease from -117.66 mm/year over 10 years to -1176.60 mm/year over 1000 years, while Marche, Italy (MA) shows a rate of decrease from -118.72 mm/year over 10 years to -1175.38 mm/year over 1000 years. In Palermo, Italy (PA), the rate of decrease ranges from -157.20 mm/year over 10 years to -1575.24 mm/year over 1000 years. Zagreb, Croatia (ZG) sees a decrease from -111.64 mm/year over 10 years to -1116.45 mm/year over 1000 years, and Bari, Italy (BA) exhibits a rate of decrease from -157.83 mm/year over 10 years to -1578.25 mm/year over 1000 years. These values highlight the significant reduction in precipitation projected across the Mediterranean region over time. The map visually highlights the spatial variability in the rate of decrease in precipitation, with larger circles indicating areas experiencing more significant reductions. This visual representation helps identify hotspots of climate change impact within the region. The analysis in Figure 20a shows a consistent downward trend in precipitation across all locations, with varying rates of decrease. Bou-Saada, Algeria, exhibits the fastest rate of decrease, while Sardegna shows the slowest rate. The geographical representation in Figure 20b highlights the spatial variability in the rate of decrease in precipitation, with some areas experiencing more significant reductions than others. This comprehensive view of both temporal and spatial variations in precipitation anomalies emphasizes the need for region-specific adaptation strategies to mitigate the impacts of decreasing precipitation in the

Mediterranean region. Understanding these trends is crucial for developing effective adaptation measures to cope with the anticipated climate impacts.

Figure 21, consists of two panels illustrating the anomalies in surface downwelling shortwave radiation (rsds in W/m²) in the Mediterranean region for the baseline period (1950-1980) compared to the crossing year centered 30-year mean (2012-2042) under the SSP5-8.5 scenario. Each panel shows the spatial distribution of these anomalies, with specific locations marked and their respective anomalies listed.

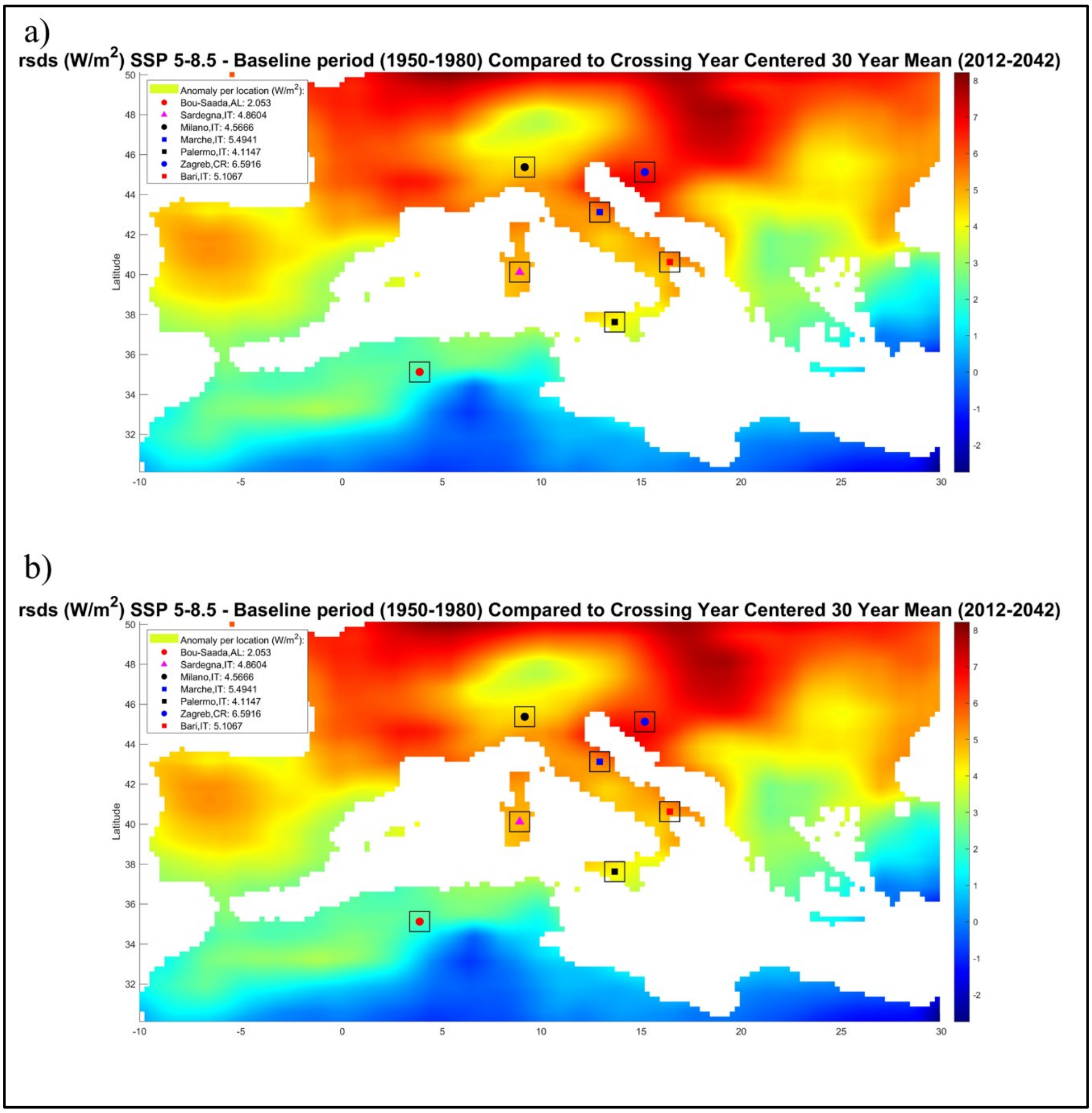

Figure 21 consists of two panels illustrating the anomalies in surface downwelling shortwave radiation (rsds in W/m²) in the Mediterranean *region for the baseline period (1950-1980) compared to the crossing year centered 30-year mean (2012-2042) under the SSP5-8.5 scenario.*

Figure 21 illustrates the anomalies in surface downwelling shortwave radiation (rsds in W/m²) in the Mediterranean region, comparing projections for the crossing year centered 30-year mean (2012-2042) under the SSP5-8.5 scenario against a baseline period of 1950-1980. The anomalies are calculated by subtracting the baseline average shortwave radiation from the projected values obtained from climate models for the specified future period. Panel (a) shows that most locations exhibit positive anomalies, indicating an increase in surface downwelling shortwave radiation, with specific values such as Bou-Saada at 2.03 W/m² and Zagreb at 6.91 W/m². Panel (b) reaffirms these findings, indicating similar increases in radiation across the Mediterranean region, with values ranging from -2.0 W/m² to +8.0 W/m².

Figure 21a shows the surface downwelling shortwave radiation anomalies under the SSP5-8.5 scenario. The color scale represents rsds anomalies, with red indicating an increase and blue indicating a decrease. The range of anomalies is from -2.0 W/m² to +8.0 W/m². Specific locations and their respective anomalies are: Bou-Saada with 2.03 W/m², Sardegna with 4.60 W/m², Milano with 5.68 W/m², Marche with 5.54 W/m², Palermo with 4.14 W/m², Zagreb with 6.91 W/m², and Bari with 5.80 W/m². The map shows that most of the Mediterranean region is projected to experience an increase in surface downwelling shortwave radiation under the SSP5-8.5 scenario. Figure 21b presents another set of surface downwelling shortwave radiation anomalies under the SSP5-8.5 scenario. The color scale is the same as in Figure 21a, representing rsds anomalies ranging from -2.0 W/m² to +8.0 W/m². Specific locations and their respective anomalies are: Bou-Saada with 2.03 W/m², Sardegna with 4.60 W/m², Milano with 5.68 W/m², Marche with 5.54 W/m², Palermo with 4.14 W/m², Zagreb with 6.91 W/m², and Bari with 5.80 W/m². Similar to Figure 21a, the map indicates an increase in surface downwelling shortwave radiation across the Mediterranean region under the SSP5-8.5 scenario. Both panels in figure 21 reveal a general trend of increasing surface downwelling shortwave radiation across the Mediterranean region under the SSP5-8.5 scenario. There is spatial variability in the magnitude of rsds anomalies, with some areas experiencing more significant increases than others. These observations highlight the potential impact of higher greenhouse gas emissions on radiation patterns, emphasizing the need for region-specific adaptation strategies to mitigate the effects of increasing shortwave radiation in the Mediterranean region. Understanding these trends is crucial for developing effective adaptation measures to cope with the anticipated climate impacts.

Next in this paragraph, figure 22 consists of two panels illustrating the anomalies in surface downwelling shortwave radiation (rsds in W/m²) in the Mediterranean region using modeled data and their rates of increase over time is shown.

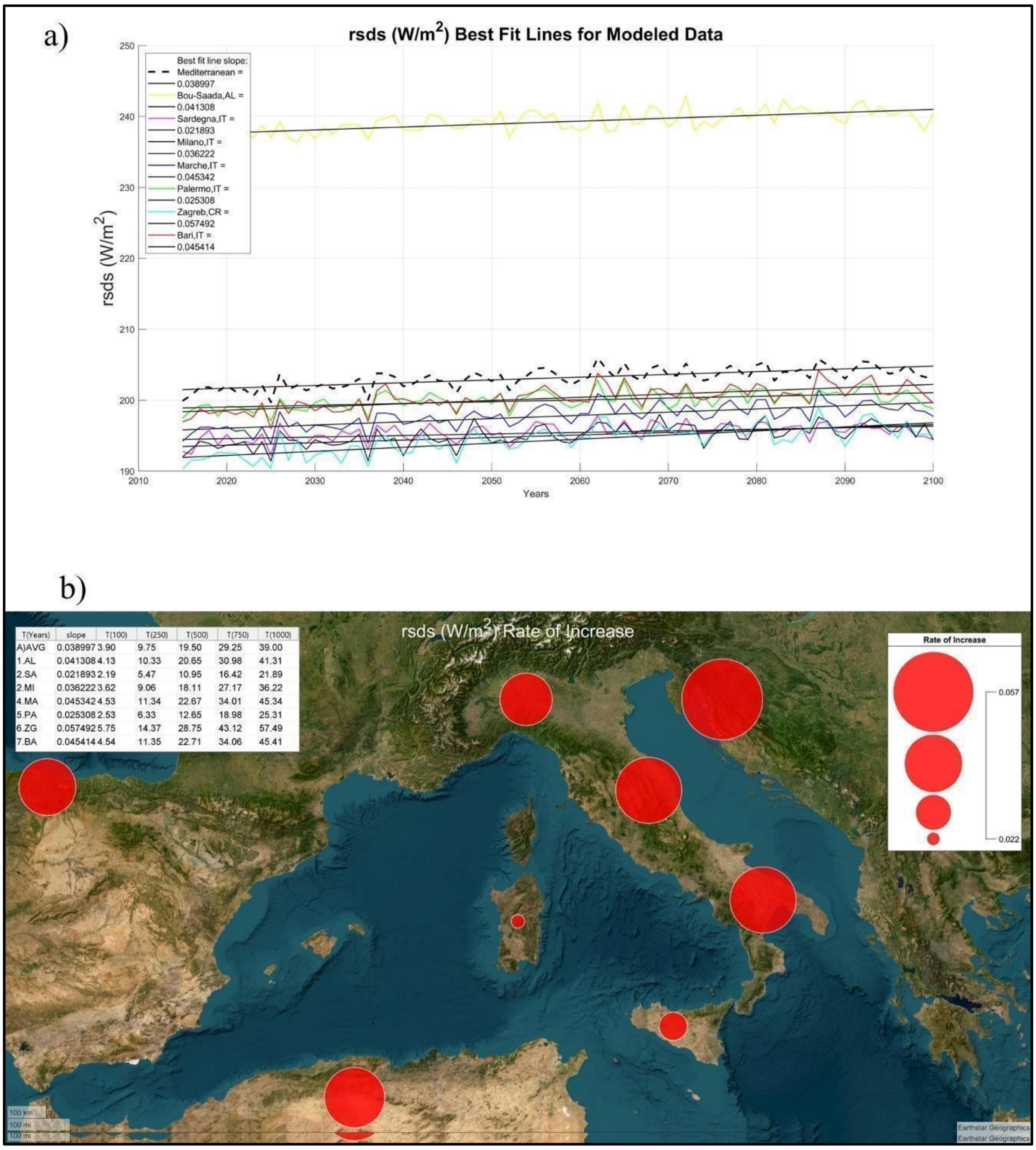

T(Years)	slope	T(100)	T(250)	T(500)	T(750)	T(1000)
A)AVG	0.038997	3.90	9.75	19.50	29.25	39.00
1.AL	0.041308	4.13	10.33	20.65	30.98	41.31
2.SA	0.021893	2.19	5.47	10.95	16.42	21.89
2.MI	0.036222	3.62	9.06	18.11	27.17	36.22
4.MA	0.045342	4.53	11.34	22.67	34.01	45.34
5.PA	0.025308	2.53	6.33	12.65	18.98	25.31
6.ZG	0.057492	5.75	14.37	28.75	43.12	57.49
7.BA	0.045414	4.54	11.35	22.71	34.06	45.41

Figure 22 consists of two panels illustrating the anomalies in surface downwelling shortwave radiation (rsds in W/m²) in the Mediterranean region using modeled data and their rates of increase over time; a) Best Fit Lines for Modeled Data, b) Rate of Decrease.

Figure 22a shows the best fit lines for surface downwelling shortwave radiation (rsds) for various locations from 2010 to 2100. Each line represents the modeled data for a specific location, with the legend providing the slope values, indicating the rate of increase in rsds per year. The best fit lines are calculated using linear regression, which involves fitting a straight line to the modeled data points for each location to estimate the trend in rsds over the specified period. The slope of each line indicates the rate of change in surface downwelling shortwave radiation, where a positive slope suggests an increase in radiation levels over time. The values of these slopes can be interpreted as the annual increase in rsds, with specific slopes provided in the legend for each location. Specific locations and their slope values are: Mediterranean average with a slope of 0.03987, Bou-Saada with a slope of 0.01848, Sardegna with a slope of 0.02522, Milano with a slope of 0.02252, Marche with a slope of 0.04529, Palermo with a slope of 0.05459, Zagreb with a slope of 0.05476, and Bari with a slope of 0.04514. The graph shows a general upward trend in rsds across all locations, with Palermo and Zagreb, exhibiting the steepest increases, indicating the fastest rate of increase in surface downwelling shortwave radiation, while Bou-Saada, shows the slowest rate of increase. Figure 22b provides a graphical representation of the rate of increase in surface downwelling shortwave radiation (W/m²) across the Mediterranean region. The size of the red circles indicates the magnitude of the increase, with larger circles representing a faster rate of increase. Specific locations and their rate of increase values are: Bou-Saada with a rate of increase ranging from 1.85 W/m² over 10 years to 18.48 W/m² over 100 years, Sardegna with a rate of increase ranging from 2.52 W/m² over 10 years to 25.22 W/m² over 100 years, Milano with a rate of increase ranging from 2.25 W/m² over 10 years to 22.52 W/m² over 100 years, Marche with a rate of increase ranging from 4.53 W/m² over 10 years to 45.29 W/m² over 100 years, Palermo with a rate of increase ranging from 5.46 W/m² over 10 years to 54.59 W/m² over 100 years, Zagreb with a rate of increase ranging from 5.48 W/m² over 10 years to 54.76 W/m² over 100 years, and Bari with a rate of increase ranging from 4.51 W/m² over 10 years to 45.14 W/m² over 100 years. The map visually highlights the spatial variability in the rate of increase in surface downwelling shortwave radiation, with larger circles indicating areas experiencing more significant increases. This visual representation helps identify hotspots of climate change impact within the region. The analysis in Figure 22a shows a consistent upward trend in rsds across all locations, with varying rates of increase. Palermo and Zagreb exhibit the fastest rates of increase, while Bou-Saada shows the slowest rate. The geographical representation in Figure 22b highlights the spatial variability in the rate of increase in rsds, with some areas experiencing more significant increases than others. This comprehensive view of both temporal and spatial variations in rsds anomalies emphasizes the need for region-specific adaptation strategies to mitigate the impacts of increasing shortwave radiation in the Mediterranean region. Understanding these trends is crucial for developing effective adaptation measures to cope with the anticipated climate impacts.

Figure 23 consists of two panels illustrating the anomalies in surface downwelling longwave radiation (rlds in W/m²) in the Mediterranean region for the baseline period (1950-1980) compared to the crossing year centered 30-year mean (2012-2042) under two different SSP (Shared Socioeconomic Pathway) scenarios: SSP5-8.5 and SSP2-4.5. Each panel shows the spatial distribution of these anomalies, with specific locations marked and their respective anomalies listed.

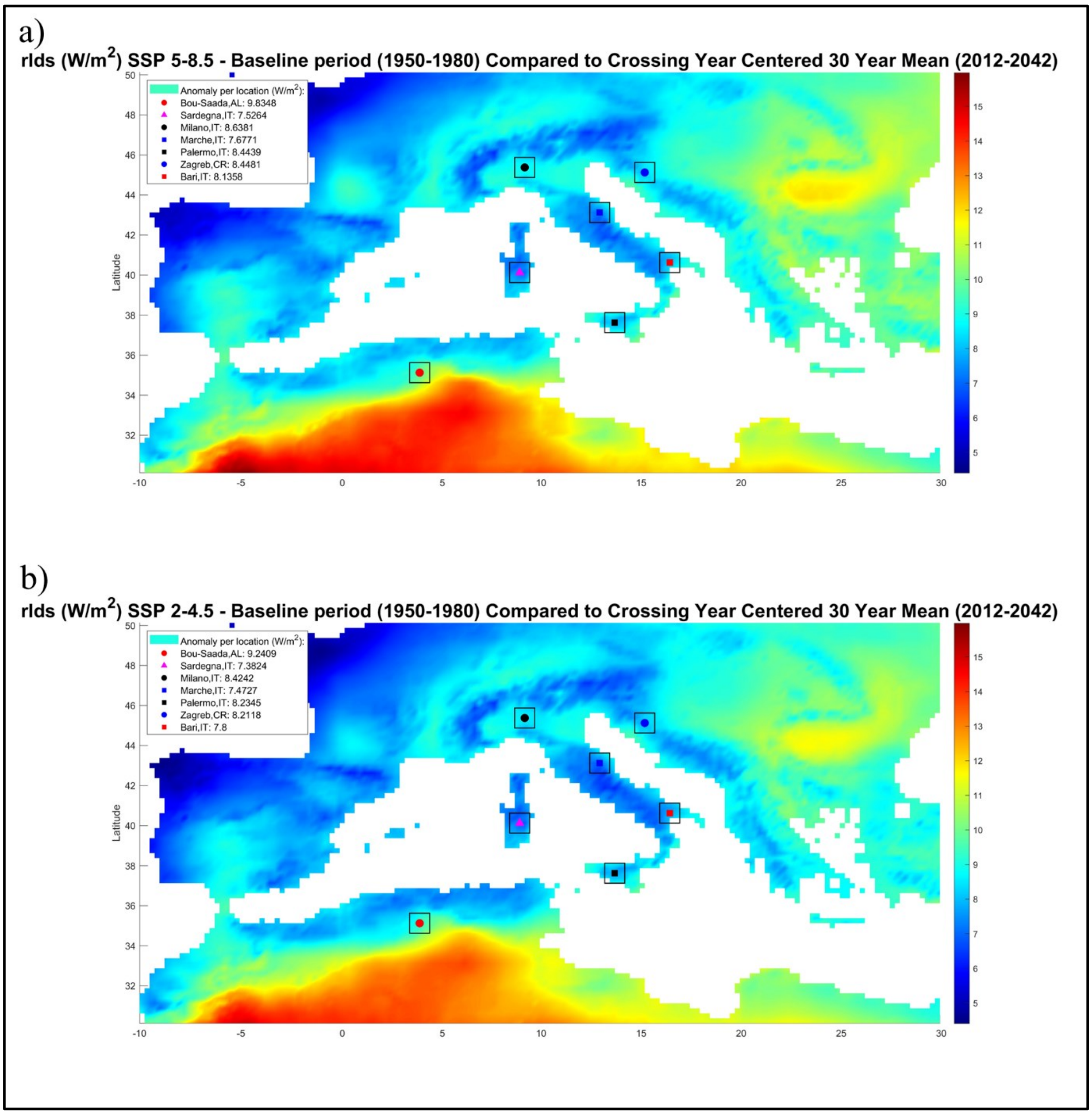

rlds (W/m^2) SSP 5-8.5 - Baseline period (1950-1980) Compared to Crossing Year Centered 30 Year Mean (2012-2042)

rlds (W/m^2) SSP 2-4.5 - Baseline period (1950-1980) Compared to Crossing Year Centered 30 Year Mean (2012-2042)

Figure 23 consists of two panels illustrating the anomalies in surface downwelling longwave radiation (rlds in W/m²) in the Mediterranean region for the baseline period (1950-1980) compared to the crossing *year centered 30-year mean (2012-2042) under two different SSP (Shared Socioeconomic Pathway) scenarios: SSP5-8.5 (upper panel)and SSP2-4.5 (lower panel). Each panel shows the spatial distribution of these anomalies, with specific locations marked and their respective anomalies listed; a) SSP5-8.5 Scenario, b) SSP2-4.5 Scenario.*

This figure illustrates the anomalies in surface downwelling longwave radiation (rlds in W/m²) across the Mediterranean region, comparing a baseline period (1950-1980) with future projections for the crossing year centered 30-year mean (2012-2042) under two different Shared Socioeconomic Pathways (SSPs): SSP5-8.5 and SSP2-4.5. Figure 23a shows the surface downwelling longwave radiation anomalies under the SSP5-8.5 scenario, which represents a high greenhouse gas concentration pathway. The color scale represents rlds anomalies, with red indicating an increase and blue indicating a decrease. The range of anomalies is from 5.00 W/m² to 15.00 W/m². Specific locations and their respective anomalies are: Bou-Saada with 9.29 W/m², Sardegna with 7.53 W/m², Milano with 6.63 W/m², Marche with 7.43 W/m², Palermo with 8.84 W/m², Zagreb with 8.44 W/m², and Bari with 7.34 W/m². The map shows that most of the Mediterranean region is projected to experience an increase in surface downwelling longwave radiation under the SSP5-8.5 scenario. Figure 23b presents the surface downwelling longwave radiation anomalies under the SSP2-4.5 scenario, which represents a moderate greenhouse gas concentration pathway. The color scale is the same as in figure 23a, representing rlds anomalies ranging from 5.00 W/m² to

15.00 W/m². Specific locations and their respective anomalies are: Bou-Saada with 9.29 W/m², Sardegna with 7.53 W/m², Milano with 7.84 W/m², Marche with 7.42 W/m², Palermo with 8.34 W/m², Zagreb with 8.21 W/m², and Bari with 7.78 W/m². The map indicates that under the SSP2-4.5 scenario, the Mediterranean region shows a consistent increase in surface downwelling longwave radiation across the area. Both panels in figure 23 reveal a general trend of increasing surface downwelling longwave radiation across the Mediterranean region under both SSP5-8.5 and SSP2-4.5 scenarios. There is spatial variability in the magnitude of rlds anomalies, with some areas experiencing more significant increases than others. These observations highlight the potential impact of higher greenhouse gas emissions on radiation patterns, emphasizing the need for region-specific adaptation strategies to mitigate the effects of increasing longwave radiation in the Mediterranean region. Understanding these trends is crucial for developing effective adaptation measures to cope with the anticipated climate impacts.

The following figure 24 will explain anomalies in surface downwelling longwave radiation (rlds in W/m²) using modeled data and their rates of increase over time.

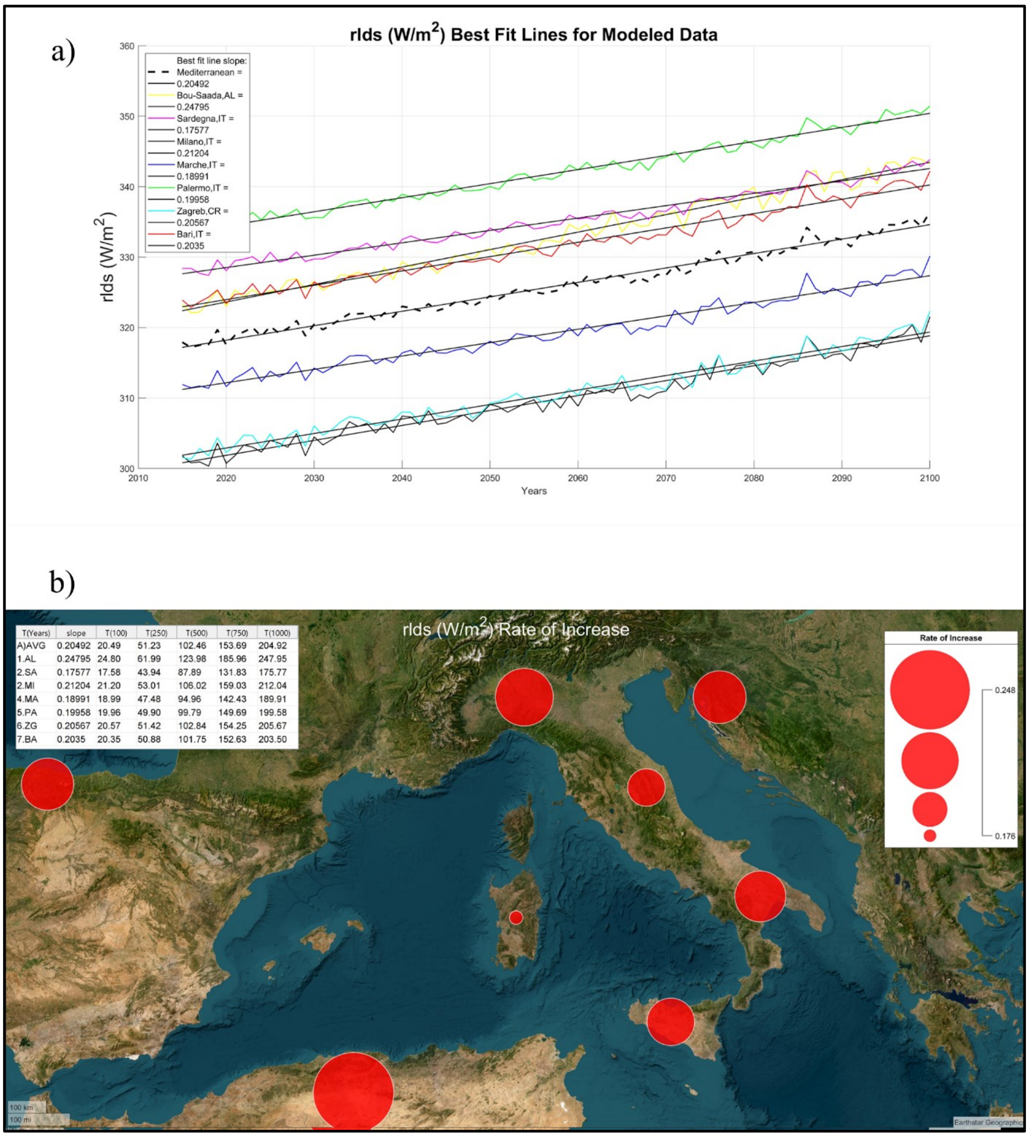

T(Years)	slope	T(100)	T(250)	T(500)	T(750)	T(1000)
A)AVG	0.20492	20.49	51.23	102.46	153.69	204.92
1.AL	0.24795	24.80	61.99	123.98	185.96	247.95
2.SA	0.17577	17.58	43.94	87.89	131.83	175.77
2.MI	0.21204	21.20	53.01	106.02	159.03	212.04
4.MA	0.18991	18.99	47.48	94.96	142.43	189.91
5.PA	0.19958	19.96	49.90	99.79	149.69	199.58
6.ZG	0.20567	20.57	51.42	102.84	154.25	205.67
7.BA	0.2035	20.35	50.88	101.75	152.63	203.50

Figure 24 consists of two panels illustrating the anomalies in surface downwelling longwave radiation (rlds in W/m²) in the Mediterranean *region using modeled data and their rates of increase over time; a) Best Fit Lines for Modeled Data, b) Rate of Decrease.*

Figure 24a shows the best fit lines for surface downwelling longwave radiation (rlds) for various locations from 2010 to 2100. Each line represents the modeled data for a specific location, with the legend providing the slope values, indicating the rate of increase in rlds per year. Specific locations and their slope values are: Mediterranean average with a slope of 0.04262, Bou-Saada with a slope of 0.24756, Sardegna with a slope of 0.17757, Milano with a slope of 0.21225, Marche with a slope of 0.19091, Palermo with a slope of 0.19569, Zagreb with a slope of 0.20567, and Bari with a slope of 0.20356. The graph shows a general upward trend in rlds across all locations, with Bou-Saada, exhibiting the steepest increases, indicating the fastest rate of increase in surface downwelling longwave radiation, while the Mediterranean average shows the slowest rate of increase. Figure 24b provides a geographical representation of the rate of increase in surface downwelling longwave radiation (W/m^2) across the Mediterranean region. The size of the red circles indicates the magnitude of the increase, with larger circles representing a faster rate of increase. Specific locations and their rate of increase in surface downwelling longwave radiation (rlds) are as follows: Bou-Saada shows a rate of increase ranging from 24.80 W/m^2 over 10 years to 247.95 W/m^2 over 1000 years. Sardegna has a rate of increase ranging from 17.58 W/m^2 over 10 years to 175.77 W/m^2 over 1000 years. Milano exhibits a rate of increase from 21.20 W/m^2 over 10 years to 212.04 W/m^2 over 1000 years, while Marche shows an increase ranging from 19.09 W/m² over 10 years to 190.91 W/m² over 1000 years. Palermo experiences a rate of increase from 19.96 W/m² over 10 years to 199.58 W/m² over 1000 years. Zagreb shows an increase ranging from 20.57 W/m² over 10 years to 205.96 W/m² over 1000 years, and Bari demonstrates an increase ranging from 20.35 W/m² over 10 years to 203.50 W/m² over 1000 years. The map visually highlights the spatial variability in the rate of increase in surface downwelling longwave radiation, with larger circles indicating areas experiencing more significant increases. This visual representation helps identify hotspots of climate change impact within the region. The analysis in Figure 24a shows a consistent upward trend in rlds across all locations, with varying rates of increase. Bou-Saada, Algeria, exhibits the fastest rate of increase, while the Mediterranean average shows the slowest rate. The geographical representation in figure 24b highlights the spatial variability in the rate of increase in rlds, with some areas experiencing more significant increases than others. This comprehensive view of both temporal and spatial variations in rlds anomalies emphasizes the need for region-specific adaptation strategies to mitigate the impacts of increasing longwave radiation in the Mediterranean region. Understanding these trends is crucial for developing effective adaptation measures to cope with the anticipated climate impacts.

4. Discussion

The Mediterranean region is particularly vulnerable to climate change due to its unique geographical and climatic characteristics. The region already experiences hot, dry summers and mild, wet winters, but climate change is expected to exacerbate these conditions, leading to more extreme temperatures, changes in precipitation patterns, and altered humidity and radiation levels. Policymakers and legislators must navigate these complex and often uncertain projections to develop effective strategies for mitigating and adapting to climate impacts. One critical aspect of climate change analysis is determining the "crossing year," that is defined as the point in time when a significant rise in climate variables is expected to occur compared to a given threshold. This concept is crucial for understanding when the impacts of climate change will become more pronounced and for planning appropriate interventions. However, the crossing year varies widely depending on the methods and variables used in the analysis, making it a challenging metric for policymakers to rely on. For instance, different climate models might project different rates of temperature increase or changes in precipitation patterns, leading to different estimates of when a significant change will occur.

Additionally, methods like the moving mean, moving median, or raw data analysis can produce different results for the crossing year. The detailed analysis of climate variables across various locations in the Mediterranean basin under different Shared Socioeconomic Pathway (SSP) scenarios provides insights into the region's future climate trends and their implications. Figure 14a, in the previous paragraph, illustrates the projected temperature anomalies (tas) from 2010 to 2100 for several locations. Both SSP2-4.5 and SSP5-8.5 scenarios show a consistent upward trend in temperatures, indicative of ongoing climate warming. The variability in slopes among locations indicates different rates of temperature increase, with some areas experiencing more rapid warming than others. For instance, locations like Bou-Saada, exhibit steeper slopes, suggesting faster rates of temperature rise compared to locations with shallower slopes. In Figure 5b, the relative humidity anomalies (hurs) represent a decline over time under both SSP scenarios. SSP5-8.5 shows a more pronounced decrease compared to SSP2-4.5. This reduction in humidity levels has implications for agriculture, water resources, and ecosystems, potentially exacerbating drought conditions in the region. Figure 12c presents precipitation anomalies (pr) under SSP2-4.5 and SSP5-8.5 scenarios. The projections indicate variability in precipitation patterns across the Mediterranean basin. While some areas may experience increases in precipitation, others are projected to face significant decreases. This variability underscores the challenge of predicting future precipitation trends in a region known for its climatic diversity. Figures 12d and 12e represent anomalies in surface downwelling shortwave (rsds) and longwave (rlds) radiation. Both scenarios show increases in these radiation components, with SSP5-8.5 generally projecting higher anomalies compared to SSP2-4.5. These changes influence the Earth's energy balance (Eq. 1) and contribute to the overall warming observed in temperature anomalies, proved in equations 2 and 3 below. The energy balance in the planetary boundary layer (PBL) describes the transfer of energy in the lower part of the atmosphere. Changes in the parameters within this balance influence vertical mixing and, consequently, pollutant dispersion and air quality. Its key components include net radiation, which is often divided into shortwave and longwave radiation. Shortwave radiation accounts for the portion of solar radiation that reaches the earth's surface, approximately 30% of the total, while longwave radiation pertains to the infrared radiation emitted by the earth's surface and atmosphere. Sensible heat flux refers to the transfer of heat from the earth's surface to the atmosphere through convection and conduction. Latent heat flux involves the transfer of heat associated with phase changes, such as evaporation and condensation. Lastly, soil heat flux, shown in the Equation 1, represents the energy gained or lost during the warming or cooling of the ground below the surface (Purdy et al., 2016).

$$H + \lambda E + G = R_n \rightarrow H = \frac{0.9R_n}{(1+\frac{1}{B_O})} \quad (1)$$

Equation 1 Ground heat flux equation for the Convective Boundary Layer (CBL), where; H – Sensible heat flux [W m^{-2}]

λE – Latent heat flux (λE=H/Bo; B_o-Bowen ratio) [W m^{-2}]

*G – Soil heat flux (assumed G=0.1*R_n) [W m^{-2}]*

R_n – Net radiation [W m^{-2}], (EPA, 2023).

These energy components are influenced by a variety of surface and atmospheric conditions, as well as temporal changes, such as day and night cycles. Factors including albedo, surface roughness, humidity, cloud cover, wind speeds, insolation, and the length of insolation play significant roles. In convective conditions, the Convective Boundary Layer (CBL), these parameters are generally positive, on the contrary in stable conditions (Stable Boundary Layer; SBL), they tend to be negative, with the exception of latent heat flux, which typically exhibits lower positive values, partly due to water anomalies (Mauder et al., 2020). The Bowen ratio (B_o) is a parameter that represents the ratio between sensible and latent heat flux. A B_o value less than 1 indicates a wet surface, while a B_o value greater than 1 signifies a dry surface. Higher values of the Bowen ratio result in greater updrafts and more intense buoyancy fluxes, which in turn enhance convective fluxes (Kang, 2016). The Bowen ratio is negatively related to surface air temperature, and this effect is more pronounced in less vegetated areas (Cho et al., 2012). It depends on the underlying surface characteristics, such as dominant land use, soil type, latitude, elevation, continental location, and drainage basin, as well as the time of year (Friedrich et al., 2000).

The solar shortwave radiation (rsds) is determined using the following formula:

$$R_s = 0.16\sqrt{T_{max} - T_{min}} * R_a \qquad (2)$$

Equation 2 The solar shortwave radiation equation. R_a (MJ m^2 per day^{-1}) is the solar radiation above the atmosphere (extraterrestrial radiation, it is a function of the latitude, Julian day, and solar time (i.e., solar hour angle) (Raoufi, et al., 2017).

The net longwave radiation is determined by:

$$R_{nl} = \sigma\left(\frac{(T_{max} + 273.15)^4 + (T_{max} + 273.15)^4}{2}\right)$$
$$\left(0.34 - 0.14\sqrt{e_a}\right)\left(1.35\frac{R_s}{R_{so}} - 0.35\right)$$

Equation 3 The solar longwave radiation equation., where σ is the Stefan–Boltzmann constant ($4.903x10^{-9}$ MJ K^{-4} M^{-2} per day^{-1}). R_{so} is the clear-sky solar radiation (MJ m^2 day^{-1}).

The projections show a consistent increase in temperature anomalies for both scenarios, with SSP5-8.5 showing a more significant rise compared to SSP2-

4.5. Relative humidity is projected to decline under both scenarios, with a more substantial decrease under SSP5-8.5. Precipitation projections show high variability, with both increases and decreases in different periods and scenarios. Both shortwave and longwave radiation anomalies are projected to increase, with SSP5-8.5 showing higher anomalies than SSP2-4.5. These projections underscore the importance of considering both scenarios for future planning and mitigation strategies, as they show potential changes in climate variables that can significantly impact the region's environment and socio-economic conditions. Understanding these projections is crucial for developing effective adaptation measures to cope with the anticipated climate impacts in the Mediterranean region.

The temperature anomalies show a consistent upward trend across both scenarios, with SSP5-8.5 indicating higher increases compared to SSP2-4.5. Rising temperatures have a cascading effect on other climate variables. As temperatures increase, the capacity of the air to hold moisture also increases, often leading to a decrease in relative humidity (Eq. 3) This is evident in the projections where relative humidity declines more significantly under SSP5-8.5, which has higher temperature anomalies. Higher temperatures can lead to increased evaporation rates, potentially reducing soil moisture and affecting precipitation patterns. The variability in precipitation anomalies under both scenarios reflects the complex interplay between temperature and the hydrological cycle, with some regions experiencing decreases and others increases in precipitation. Increasing temperatures can enhance the absorption of solar radiation by the Earth's surface. The projected increase in shortwave radiation anomalies under both scenarios suggests a feedback loop where higher temperatures lead to more absorption of solar energy, further driving temperature increases. As the surface temperature rises, the emission of longwave radiation from the Earth’s surface increases. The upward trend in longwave radiation anomalies under both scenarios indicates a stronger greenhouse effect, with higher temperatures leading to more longwave radiation being emitted and trapped by greenhouse gasses. Relative humidity shows a declining trend under both scenarios, with a more substantial decrease under SSP5-8.5. Changes in relative humidity interact with other variables such as temperature, precipitation, and cloud cover. For example, a decline in relative humidity can reduce cloud formation, allowing more solar radiation to reach the surface, which further increases temperatures. Additionally, lower humidity can enhance evaporation, leading to drier soil and exacerbating drought conditions, particularly in regions already vulnerable to water scarcity. As discussed, rising temperatures lead to a decrease in relative humidity due to the increased moisture-holding capacity of warmer air. Changes in relative humidity can influence cloud formation and precipitation patterns. Lower relative humidity might reduce cloud cover and precipitation, particularly in regions already experiencing reduced rainfall. Decreased relative humidity can affect the radiation balance by altering cloud cover. Fewer clouds can lead to increased shortwave radiation reaching the surface, further warming the surface and enhancing longwave radiation emissions. Precipitation patterns influence soil and surface moisture, affecting longwave radiation emissions. Dry soils emit more longwave radiation compared to moist soils. Changes in cloud cover due to varying precipitation patterns can affect shortwave radiation. Less cloud cover leads to increased solar radiation reaching the surface. Higher surface temperatures lead to increased emission of longwave radiation. The feedback loop between temperature and longwave radiation is crucial in understanding the enhanced greenhouse effect. The interconnected trends among temperature, relative humidity, precipitation, shortwave radiation, and longwave radiation highlight the complex dynamics of climate change in the Mediterranean region. The SSP5-8.5 scenario, with higher greenhouse gas emissions, consistently shows more extreme changes in all variables compared to SSP2-4.5. These changes underscore the importance of considering multiple climate variables and their interactions when assessing future climate impacts. The Penman-Monteith equation (Eq. 4), further in the paragraph, is showing how these higher temperatures, combined with other factors like radiation and wind speed, increase actual evapotranspiration rates. As a result, increased evaporation leads to reduced soil moisture, which can affect local precipitation patterns. This provides a mathematical basis for the correlation between higher temperatures, increased evaporation, and changes in soil moisture and precipitation patterns (Raoufi, et al., 2017).

$$ET = \frac{0.408\Delta(Rn-G)+\gamma\frac{900}{T+273}u_2(e_s+e_a)}{\Delta+\gamma(1+0.32u)} \tag{4}$$

Equation 4 The Penman-Monteith equation shows that evapotranspiration increases with higher net radiation, higher temperature, and higher wind speed, and it decreases with higher actual vapor pressure.

ET is the evapotranspiration (mm/day), Δ is the slope of the vapor pressure curve (kPa/°C), Rn is the net radiation at the crop surface (MJ/m²/day), G is the soil heat flux density (MJ/m²/day), γ is the psychrometric constant (kPa/°C), T is the mean daily air temperature (°C), u_2 is the wind speed at 2 meters height (m/s), e_s is the saturation vapor pressure (kPa) and e_a is the actual vapor pressure (kPa).

Following the collected data from the results, in the rest of this paragraph, we will discuss each variable separately. The temperature anomaly values, down in the paragraph correspond to the crossing year values because they were derived from the moving median method over a 30-year window, aligning with the process described for determining the crossing year.

Temperature anomalies across the Mediterranean region indicate a consistent upward trend under both SSP2-4.5 and SSP5-8.5 scenarios. The temperature anomaly values provided for Bou-Saada, Algeria (1.99°C under SSP2-4.5 and 1.94°C under SSP5-8.5) suggest a specific point in time when the average temperature increase compared to pre-industrial levels is nearly the same for both scenarios. This suggests significant warming, likely exacerbating evaporation rates and reducing soil moisture. Sardegna has temperature anomalies of 1.86 °C for SSP2-4.5 and 1.79 °C for SSP5-8.5, indicating a similar warming trend that could lead to higher evaporation and lower precipitation. Milano exhibits temperature anomalies of 1.79 °C and 1.86 °C for SSP5-8.5 and SSP2-4.5, respectively. The urban heat island effect may intensify these temperature increases, further impacting local climate conditions. Marche shows a moderate temperature increase with anomalies of 1.86 °C for SSP2-4.5 and 1.79 °C for SSP5-8.5. This warming could affect local agriculture and water resources. Palermo has temperature anomalies of 1.88 °C under SSP2-4.5 and 1.79 °C under SSP5-8.5, indicating significant warming that could reduce local water availability. Zagreb shows temperature anomalies of 1.86 °C for SSP2-4.5 and 1.79 °C for SSP5-8.5, suggesting that increased temperatures may enhance precipitation through localized weather patterns. Bari exhibits temperature anomalies of 1.86 °C and 1.79 °C for SSP2-4.5 and SSP5-8.5, respectively. The warming trend could slightly affect local precipitation patterns.

Precipitation anomalies exhibit significant variability, reflecting the complex interactions with temperature, humidity, and radiation. Under SSP5-8.5, precipitation anomalies range from -97.06 mm/year to 232.93 mm/year at the crossing year of 2025, indicating potential for both increased and decreased rainfall in different regions. Below in this paragraph there is a detailed analysis specifying the anomalies for each location and what is happening at these specific sites. Bou-Saada shows a precipitation anomaly of -45.96 mm/year. Bou-Saada is projected to experience a significant decrease in precipitation. This reduction could be due to increased evaporation rates driven by higher temperatures and lower relative humidity, which reduce soil moisture and hinder local precipitation processes. Sardegna has a precipitation anomaly of -31.79 mm/year. Sardegna is also expected to see a decrease in precipitation. This decrease may be influenced by similar factors affecting Bou-Saada, such as higher temperatures and decreased relative humidity, leading to less cloud formation and reduced rainfall. Milano exhibits a precipitation anomaly of -37.90 mm/year. Milano is projected to face a reduction in precipitation. The urban heat island effect combined with higher regional temperatures could enhance evaporation rates, further reducing soil moisture and precipitation. Marche has a precipitation anomaly of -12.32 mm/year. Marche shows a moderate decrease in precipitation. This region might experience less severe impacts compared to others, but the reduction is still significant enough to affect local agriculture and water resources. Palermo has a precipitation anomaly of -29.44 mm/year. Palermo is expected to see a decrease in precipitation. The reduction could affect local water availability and agricultural productivity, necessitating adaptation measures to manage water resources effectively. Zagreb shows a precipitation anomaly of 22.84 mm/year. Zagreb is projected to experience an increase in precipitation. This could be due to localized weather patterns or increased atmospheric moisture content from adjacent regions, enhancing rainfall.

However, this increase may also lead to issues such as flooding or soil erosion if not managed properly. Bari exhibits a precipitation anomaly of -1.40 mm/year. Bari shows a slight decrease in precipitation. While the reduction is relatively small compared to other locations, it still highlights the variability and complexity of precipitation patterns in the region.

Relative humidity anomalies decline under both scenarios, with a more substantial decrease under SSP5-8.5. Bou-Saada shows a relative humidity anomaly of -1.27 % under SSP2-4.5 and -0.88 % under SSP5-8.5, indicating lower moisture levels that could reduce precipitation. Sardegna has relative humidity anomalies of -0.82 % for SSP2-4.5 and -0.81 % for SSP5-8.5, reflecting a decrease that could lead to reduced cloud formation and rainfall. Milano exhibits relative humidity anomalies of -0.8227% and -0.8050% for SSP2-4.5 and SSP5-8.5, respectively. Lower humidity may enhance evaporation rates, reducing soil moisture and precipitation. Marche shows relative humidity anomalies of -0.8227% under SSP2-4.5 and -0.8050% under SSP5-8.5, indicating moderate decreases that could affect local water resources. Palermo has relative humidity anomalies of -0.8227% for SSP2-4.5 and -0.8050% for SSP5-8.5, suggesting lower moisture levels that could impact agricultural productivity. Zagreb shows relative humidity anomalies of -0.8227% and -0.8050% for SSP2-4.5 and SSP5-8.5, respectively. Decreased humidity might slightly affect precipitation patterns. Bari, Italy (IT) exhibits relative humidity anomalies of -0.8227% for SSP2-4.5 and -

0.8050% for SSP5-8.5, indicating a slight decrease that could impact local precipitation.

Surface downwelling shortwave radiation (rsds) anomalies show an increasing trend. Bou-Saada shows an rsds anomaly of 2.37 W/m² under SSP2-4.5 and 1.48 W/m² under SSP5-8.5, indicating increased solar energy absorption that could enhance warming. Sardegna has rsds anomalies of 4.91 W/m² for SSP2-4.5 and 4.42 W/m² for SSP5-8.5, suggesting increased shortwave radiation that could drive temperature increases. Milano exhibits rsds anomalies of 4.91 W/m² and 4.42 W/m² for SSP2-4.5 and SSP5-8.5, respectively, reflecting higher solar energy absorption that could intensify local warming. Marche shows rsds anomalies of 4.91 W/m² for SSP2-4.5 and 4.42 W/m² for SSP5-8.5, indicating increased radiation that could affect local climate conditions. Palermo has rsds anomalies of 4.91 W/m² and 4.42 W/m² for SSP2-4.5 and SSP5-8.5, respectively, suggesting higher solar energy levels that could enhance warming. Zagreb shows rsds anomalies of 4.91 W/m² for SSP2-4.5 and 4.42 W/m² for SSP5-8.5, indicating increased radiation that could drive temperature increases. Bari exhibits rsds anomalies of 4.91 W/m² for SSP2-4.5 and 4.42 W/m² for SSP5-8.5, reflecting higher solar energy absorption that could intensify local warming.

Surface downwelling longwave radiation (rlds) anomalies indicate an upward trend. Bou-Saada shows an rlds anomaly of 9.44 W/m² under SSP2-4.5 and

9.45 W/m² under SSP5-8.5, indicating increased longwave radiation that could enhance the greenhouse effect. Sardegna has rlds anomalies of 8.27 W/m² for SSP2-4.5 and 7.96 W/m² for SSP5-8.5, suggesting increased longwave radiation that could contribute to warming. Milano exhibits rlds anomalies of 8.27 W/m² and 7.96 W/m² for SSP2-4.5 and SSP5-8.5, respectively, reflecting higher longwave radiation that could intensify the greenhouse effect. Marche shows rlds anomalies of 8.27 W/m² for SSP2-4.5 and 7.96 W/m² for SSP5-8.5, indicating increased longwave radiation that could enhance warming. Palermo has rlds anomalies of 8.27 W/m² and 7.96 W/m² for SSP2-4.5 and SSP5-8.5, respectively, suggesting higher longwave radiation that could drive temperature increases. Zagreb shows rlds anomalies of 8.27 W/m² for SSP2-4.5 and 7.96 W/m² for SSP5-8.5, indicating increased radiation that could enhance the greenhouse effect. Bari exhibits rlds anomalies of 8.27 W/m² for SSP2-4.5 and 7.96 W/m² for SSP5-8.5, reflecting higher longwave radiation that could intensify local warming.

The variability in precipitation anomalies under the SSP5-8.5 scenario illustrates the complex interplay between temperature, humidity, and radiation. While some regions like Zagreb may experience increased rainfall, most locations, including Bou-Saada, Sardegna, Milano, Marche, Palermo, and Bari, are projected to see a decrease in precipitation. These changes underscore the importance of understanding local climate dynamics to develop targeted adaptation strategies that address the specific needs of each region. Reducing greenhouse gas emissions and enhancing resilience to changing precipitation patterns are crucial steps to mitigate the adverse impacts of climate change in the Mediterranean region.

5. Conclusion

The comprehensive examination of climate projections for the Mediterranean basin under SSP2-4.5 and SSP5-8.5 scenarios highlights significant future climate changes across multiple variables. The region is expected to experience continued warming throughout the 21st century, with some areas warming faster than others. This trend poses risks to ecosystems, agriculture, and human health, necessitating adaptive strategies to mitigate these impacts. Decreasing relative humidity and variable precipitation patterns pose challenges for water availability and ecosystem resilience. Regions dependent on agriculture may face increased vulnerability to droughts and shifts in growing seasons. Increasing shortwave and longwave radiation anomalies indicate shifts in energy dynamics within the atmosphere. These changes contribute to enhanced warming and alter regional climate patterns. The spatial variability illustrated in Figures 13 and 14 emphasizes the need for localized climate adaptation strategies. Different regions within the Mediterranean basin exhibit diverse climate responses to global warming, requiring tailored approaches to resilience building. To address these challenges, policymakers, stakeholders, and communities must prioritize climate adaptation and mitigation efforts. Strategies such as sustainable water management, resilient agriculture practices, and urban planning that integrates climate resilience considerations are essential. Continuing scientific research and monitoring are critical to refining climate projections and informing adaptive strategies that promote sustainability and resilience across the Mediterranean region.

References

6. References

https://www.nasa.gov/feature/ames/nasa-study-reveals-compounding-climate-risks-at-two-degrees-of-warming

https://www.nasa.gov/nex/gddp
https://www.nccs.nasa.gov/services/data-collections/land-based-products/nex-gddp-cmip6

Park, Taejin, et al. "What does global land climate look like at 2° C warming?" Earth's Future 11.5 (2023): e2022EF003330.
Rigal, Alix, Jean-Marc Azaïs, and Aurélien Ribes. "Estimating daily climatological normals in a changing climate." Climate dynamics 53 (2019): 275-286.

O'Neill, Brian C., et al. "The scenario model intercomparison project (ScenarioMIP) for CMIP6." *Geoscientific Model Development* 9.9 (2016): 3461-3482.

Eyring, Veronika, et al. "Overview of the Coupled Model Intercomparison Project Phase 6 (CMIP6) experimental design and organization." Geoscientific Model Development 9.5 (2016): 1937-1958.

Morice, Colin P., et al. "An updated assessment of near-surface temperature change from 1850: The HadCRUT5 data set." Journal of Geophysical Research: Atmospheres 126.3 (2021): e2019JD032361.

Raoufi, Roozbeh, and Edward Beighley. "Estimating daily global evapotranspiration using penman–monteith equation and remotely sensed land surface temperature." Remote Sensing 9.11 (2017): 1138.

Morice, Colin P., et al. "An updated assessment of near-surface temperature change from 1850: The HadCRUT5 data set." Journal of Geophysical Research: Atmospheres 126.3 (2021): e2019JD032361.

Friedrich, K., N. Mölders, and G. Tetzlaff. "On the influence of surface heterogeneity on the Bowen-ratio: A theoretical case study." Theoretical and Applied Climatology 65 (2000): 181-196.

Choi, Youn-Young, Myoung-Seok Suh, and Ki-Hong Park. "Assessment of surface urban heat islands over three megacities in East Asia using land surface temperature data retrieved from COMS." Remote Sensing 6.6 (2014): 5852-5867.

Mauder, Matthias, Thomas Foken, and Joan Cuxart. "Surface-energy-balance closure over land: a review." Boundary-layer meteorology 177 (2020): 395-426.

Purdy, A. J., et al. "Ground heat flux: An analytical review of 6 models evaluated at 88 sites and globally." Journal of Geophysical Research: Biogeosciences 121.12 (2016): 3045-3059.

Raoufi, Roozbeh, and Edward Beighley. "Estimating daily global evapotranspiration using the penman–monteith equation and remotely sensed land surface temperature." Remote Sensing 9.11 (2017): 1138.

Appendix A.

Titolo dell’Appendice

A.1. For the full MATLAB code, please see the attached file: [MATLAB codes.zip];

MATLAB codes.zip

A.2. For the full-size figures, directly obtained from MATLAB please see the attached file: [Figures_final.zip];

Figures_final.zip